Structural Analysis of Alba Patera, Mars

From deep-seated to shallow events

Dissertation zur Erlangung des Doktorgrades
der Mathematisch-Naturwissenschaftlichen Fakultät
der Christian-Albrechts-Universität zu Kiel

vorgelegt von
Béatrice Cailleau
geboren in Bressuire, Frankreich

Kiel, 2002

Referent: Prof. Dr. Peter Janle.....

Korreferent: Prof. Dr. Jason Phipps Morgan.....

Tag der mündlichen Prüfung: 18.02.2003.....

Zum Druck genehmigt: 19.02.2003.....

Der Dekan: Prof. Dr. W. Depmeier

Hiermit erkläre ich an Eides statt, dass die vorliegende Abhandlung, abgesehen der Beratung durch meine akademischen Lehrer, nach Inhalt und Form meine eigene Arbeit darstellt. Ferner habe ich weder diese noch eine ähnlich Arbeit an einer anderen Abteilung oder Hochschule im Rahmen eines Prüfungsverfahrens vorgelegt.

Béatrice Cailleau

Table of contents

Abstract

Today, the planet Mars is in a phase of volcanic and tectonic quiescence. However, the 11.000 m high and 8000 km wide volcanic dome of the Tharsis region, transected by giant tectonic features, bears witness to past intense activity on the red planet. At the northernmost boundary of the Tharsis dome, the volcanic edifice of Alba Patera forms a widespread shield of 2700 km diameter and 7.000 m maximum elevation. The tectonics on Alba Patera has been the particular object of attention. The volcano and its environment are intensely breached by lineaments, which are interpreted as being fault-type structures. The orientation of those faults is in general north-south, radial to the Tharsis dome. On the flanks of Alba Patera, however, the faults curve around and are arranged in concentric pattern, encircling the summit of the edifice.

In this thesis, the structural information of Alba Patera was reviewed and newly analysed based on Viking Mosaic data. Due to the high resolution of 60 m pro pixel, details about the fault development on Alba Patera are observable. Based on cross-cutting relationships of the observed lineaments, it becomes obvious that concentric fracturing of Alba Patera formed progressively, after radial fracturing. The further focus of this thesis is to study the implications of observed structures for hidden subvolcanic processes and to infer coupled genetic mechanisms that generate tension within the crust and the volcanic edifice. It is demonstrated that the lineaments record the dynamic past of Alba Patera, enlightening that this region of the red planet suffered a multifaceted history of crustal and volcanic evolution.

Modelling the observed structures is used as a crucial key to understand their formation. Two modelling methods were used. Most of the analysis was performed by numerical models using the Finite Element code TEKTON. Semi-automatic Fortran subroutines were programmed to accelerate Finite Element data input and allow modelling with a large variety of unknown mechanical parameters. The numerically predicted surface deformation and fault arrangements are compared to the Viking Mosaic lineaments, and finally reproduced qualitatively by analogue experiments in a sand-box.

Variations of subsurface source characteristics have been investigated specifically their interplay with the volcanic loading, and their superposition with a regional extension representative of the Tharsis doming. This study shows that the observed radial structures, i.e. the Tantalus Fossae, that extend from the flanks of Alba Patera toward large northern distance, reflect the extensional surface effect of local uplift. This supports the idea that Alba Patera was an autonomous hotspot and structural dome. The following tectonic phase on

Alba Patera is dominated by the formation of concentric grabens on the western and eastern mid and upper flanks of the volcano. The orientation and position of these grabens are found to be best reproduced by local crustal subsidence, superposed with a regional extensional stress field. Simulating these mechanisms in analogue sand-box models also produced surface-structures of arrangements that almost perfectly mimic the observed lineaments on Alba Patera. As seen from the mosaic image analysis, the formation of the circumferential grabens was incrementally and increasingly pronounced towards the final stages of volcanic shield construction. Since this spans a time period probably on the order of a billion years, this suggests long-term geodynamic processes to be responsible for subsidence of the central Alba Patera area. The progressive change toward higher concentricity likely resulted from an increase of density by cooling and accumulation of intrusive material during the construction of the volcano – and thus subsidence of the region above this volcanic root.

The reader will find within various parts of the thesis implications for the potential mechanical properties of Alba Patera and the Martian crust. Also the absence of lineaments can be used, to infer new information about the mechanical properties of the planet's upper lithosphere. For instance, the absence of bending signatures surrounding the Martian volcano provides information about the mechanical properties of the lithosphere. The methodical work presented in the second part of this thesis is devoted to the modelling of lithospheric flexure under the load of Alba Patera. It is shown that the lithospheric viscosity together with the load emplacement, the planet curvature and the crustal strength are primordial parameters to reduce the flexural stresses, and thus explaining the absence of flexural fractures surrounding the volcano.

Summary and perspective: Due to the minor crustal plate movement and erosion, a very long-term creation history of Alba Patera is reconstructable. The formation of lineaments, as analysed by Viking photo-mosaics, was simulated by numerical and analogue methods to elucidate the dynamic history of this volcanic edifice. The proposed vertical tectonic processes may have been not only of importance on Alba Patera, probably on Earth similar mechanisms exist on similar dimensions that are however obscured by plate tectonics.

Zusammenfassung

Der Mars ist aus unserer heutigen Sicht in einem vulkanisch und tektonisch ruhigen Zustand. Trotzdem sind die Zeugen eines geologisch einst äußerst aktiven Planeten noch heute deutlich sichtbar, so z.B. der 11.000 m hohe und 8000 km weite vulkanische Domkomplex der Thasis-Region, welcher durch gewaltige tektonische Gräben und Störungen durchzogen ist. An der Nordgrenze der Region von Tharsis bildet Alba Patera ein Vulkanschild von ungewöhnlichem Relief mit einem Durchmesser von 2700 km und einer Höhe von 7.000 m. Der tektonischen Entwicklung von Alba Patera wird hier besondere Aufmerksamkeit geschenkt. Schon auf Photographien zeigt das Vulkangebäude mitsamt seiner Umgebung unzählige lineare Strukturen, die als Ausbisslinien von Verwerfungen interpretiert werden. Die Orientierung dieser Verwerfungen ist hauptsächlich Nord-Süd, d.h. radial von Tharsis nach Norden. An den Flanken Alba Pateras schwenken diese jedoch um in ein deutlich konzentrisches Streichen, um das Vulkanzentrum herum.

Im Rahmen dieser Dissertation wurden Mosaikdaten der Viking-Mission strukturgeologisch ausgewertet. Aufgrund der hohen visuellen Auflösung von 60 m pro Pixel sind Detailinformationen zu einzelnen Verwerfungen untersucht worden. Die relative Altersabfolge einzelner Lineamente zeigt, dass sich konzentrische Verwerfungen an Alba Patera erst allmählich über ein älteres radiales System durchsetzten. Ein wichtiger Punkt dieser Arbeit ist aufgrund derartiger Beobachtungen mehr über subvulkanische Prozesse zu erfahren und abzuschätzen, inwieweit komplexe und interagierende Mechanismen für ein derartiges Zerbrechen der Kruste verantwortlich sein können. Die Lineamente erst zeigen die sehr dynamischen Ereignisse Alba Pateras und die vielseitige Geschichte der krustalen und vulkanischen Geschichte auf.

Die Modellierung der erkennbaren Strukturen ist ein wichtiger Schritt um deren Entwicklung zu verstehen. In dieser Arbeit wurden zwei Modellierungsmethodiken verwendet. Der Hauptteil der Analysen erfolgte durch numerische Berechnungen mittels der TEKTON Finite Elemente Methode. Die ergänzende Programmierung von halbautomatischen Fortran Unterprogrammen beschleunigte maßgeblich die Dateneingabe, sowie dadurch die Berechnung zahlreicher Modelle mit leicht abgeänderten mechanischen Parametern. Für verschiedene Eingabeparameter werden die numerisch simulierten Oberflächendeformationen und potentiellen Störungsorientierungen mit den Stellungen der analysierten Lineamente der Viking Mosaic Daten verglichen, und schließlich durch Sandbox Analogexperimente reproduziert.

Im Speziellen erfolgt eine Gewichtung von tiefliegenden Deformationsmechanismen sowie deren Zusammenspiel mit gravitativen Auflasteffekten und regionalen Spannungen durch die Tharsis Aufdomung. Diese Studie zeigt, dass die beobachteten radialen Strukturen von Tantalus Fossae, die sich von der Vulkanflanke Alba Pateras bis weit nach Norden erstrecken, ihre Ursache in einem lokalen Hebungsereignis haben. Dies untermauert die Idee, dass Alba Patera einst ein selbständiger Hotspot und struktureller Dom war. Spätere tektonische Phasen von Alba Patera waren durch konzentrische Gräben dominiert, die zumeist an den westlichen und östlichen, mittleren bis oberen Flankenbereichen des Vulkanes entstanden. Die Lage und die Orientierung dieser Gräben wurden bei allen Modellen am besten durch örtliche krustale Subsidenz simuliert, überlagert von einem regionalen Dehnungsfeld. Die Simulation dieser Mechanismen durch Analogmodelle ergab ebenfalls Oberflächenstrukturen die beinahe perfekt die Photolineamente von Alba Patera nachstellen. Wie am Photomosaik erkennbar, waren entstehende Gräben gegen Ende des Schildvulkanismus deutlich stärker konzentrisch gebogen als in früheren Zeiten. Da der Schildaufbau von Alba Patera insgesamt ca. 1.5 Ga dauerte, scheinen auch die geodynamischen Prozesse welche für die Grabenbildung durch Subsidenz verantwortlich sind, äußerst langandauernd zu sein. Ein allmählicher Dichtezuwachs an der Vulkanwurzel, möglicherweise verursacht durch Intrusionen und deren Erkaltung, kann die zunehmende Subsidenz und somit den zunehmenden Wechsel hin zu stärker konzentrischen Strukturen erklären.

Der Leser wird in verschiedenen Teilen dieser Arbeit Implikationen für mögliche mechanische Eigenschaften von Alba Patera und der Planetenkruste finden. Auch die Abwesenheit von Strukturen birgt dabei Informationen. Der methodische Teil in dem zweiten Teil der Arbeit beispielsweise behandelt die Modellierung von lithosphärischen Ausgleichbewegungen unter der Last von Alba Patera. Es wird gezeigt, inwiefern die Viskosität der Lithosphäre gemeinsam mit der Auflast, der Oberflächenkrümmung und der krustalen Elastizität die Hauptfaktoren sind, um die Flexurspannungen derart zu reduzieren, dass keine einhergehenden Verwerfungen um die Basis des Vulkans auftreten können.

Resümee und Perspektive: Aufgrund der geringen Plattenbewegung und Erosion ist eine lange Entwicklungsgeschichte von Alba Patera rekonstruierbar. Vergleichend zu den erkennbaren Photomosaik-Lineamenten, konnte die Verwerfungsentstehung in numerischen und analogen Modellen simuliert und somit die dynamische Geschichte des Vulkangebäudes etwas geklärt werden. Die hierin für Alba Patera vorgeschlagenen vertikaltektonischen Prozesse sind womöglich in ähnlicher Form auf die Erde übertragbar, hier jedoch oftmals aufgrund plattentektonischer und einhergehender festverankerter Konzepte nicht erkennbar.

Introduction

1. Preface

Since the observations of canals on Mars (Fig. 1) related to handiwork of intelligent Martians by Lowell at the end of the 19th century, our view of Mars has been strongly improved thanks to spacecraft data acquisition. The Viking mission between 1976-1980 provided high resolution images of the surface (Fig. 2). Volcanoes, lava plains, immense canyons, cratered areas, wind-formed features, and evidence of surface water are apparent in the Viking images. The most recent Mars Global Surveyor mission was launched in 1996 to study the surface, atmosphere and interior. The new accurate data, competitive in resolution to non-military satellite observations of Earth, facilitate scientific analyses and have considerably increased our knowledge of the red planet.

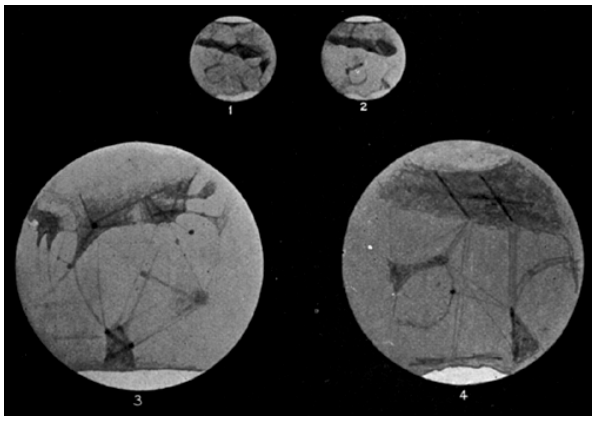

Figure 1 – Drawing by Lowell showing "canals" based on telescope observation and thought to be handiwork of intelligent Martians. The Mariner and Viking images showed no sign of “canals” and little correspondence between albedo markings, i.e. dark or light markings on the surface, and topographic features.

Studies of Mars serve the ultimate goal of planetary research, i.e. to understand the origin and evolution of the planets. Besides the detailed observations, Mars has the advantage to share many similarities with the Earth, i.e. chemical composition, relative size, distance to the sun. There is evidence for recent geological activity during the past 10 million to 100 million years on Mars (Hartmann and Neukum, 2001) but because of its smaller size, its history is older and the signatures of early geological events are well preserved. Finally, identification and interpretation of physical processes are simplified on Mars thanks the limited erosion and the absence of present-day plate tectonics.

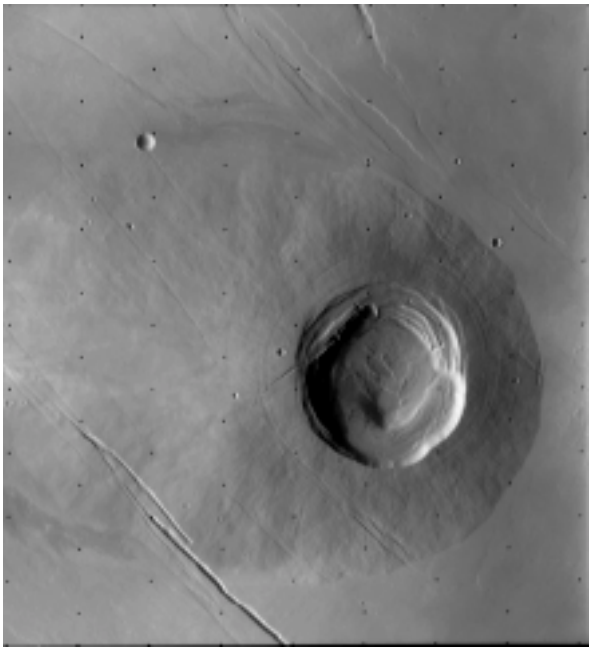

Figure 2 - The small Martian volcano Biblis Patera is shown in this Viking Orbiter 2 image. The diameter of the exposed portion is about 100 km. Truncation of the flow features on the volcano's flanks by surrounding plains material indicates that part of the edifice is buried. Note the circular faults surrounding the caldera. North is at ~11:30 in this image, which is about 200 km across. (Viking Orbiter 044B50)

The red Planet is characterised by multiple landscapes that provide geological information about the atmospheric, surface and deep processes. This thesis concerns the tectonics associated with volcanoes on Mars and focuses on the case of Alba Patera. Alba Patera is one of the most peculiar and outstretched volcanoes known in the Planetary System, measuring up to 2700 km across and 7 km high, thus well comparable in size with mountain ranges on Earth. In contrast, the summit of the main shield volcanoes on Tharsis - that is the Tharsis Montes and Olympus Mons - rises up to 27 km height while the diameters do not exceed 600 km. The main shield edifice of Alba Patera measures 1300 km across with flat apex of about 5 km elevation on which formed a younger 2 km high central cone (Fig. 3). As reported from the Viking images, Alba Patera is characterised by sets of numerous fractures (Fig. 3). These have a predominantly north-south trend likely influenced by the location of the volcano on the northern boundary of the Tharsis bulge (Fig. 5). The fractures have apparently been diverted around the central part of Alba Patera.

The main purpose of this thesis is to understand the origins of these striking radial and concentric lineaments. Another aspect of Alba Patera has been also studied, i.e. the absence of signatures around the volcano from lithosphere bending. This work is based on numerical and analogue modelling to reconstruct the deformation under different simulated volcanic processes. Image analysis is used for the comparison between the theoretical results and the observations on Alba Patera. It allows us to gain a general comprehension of the

tectonic and volcanic characteristics of Alba Patera, as well as the geodynamic processes that are responsible for these features.

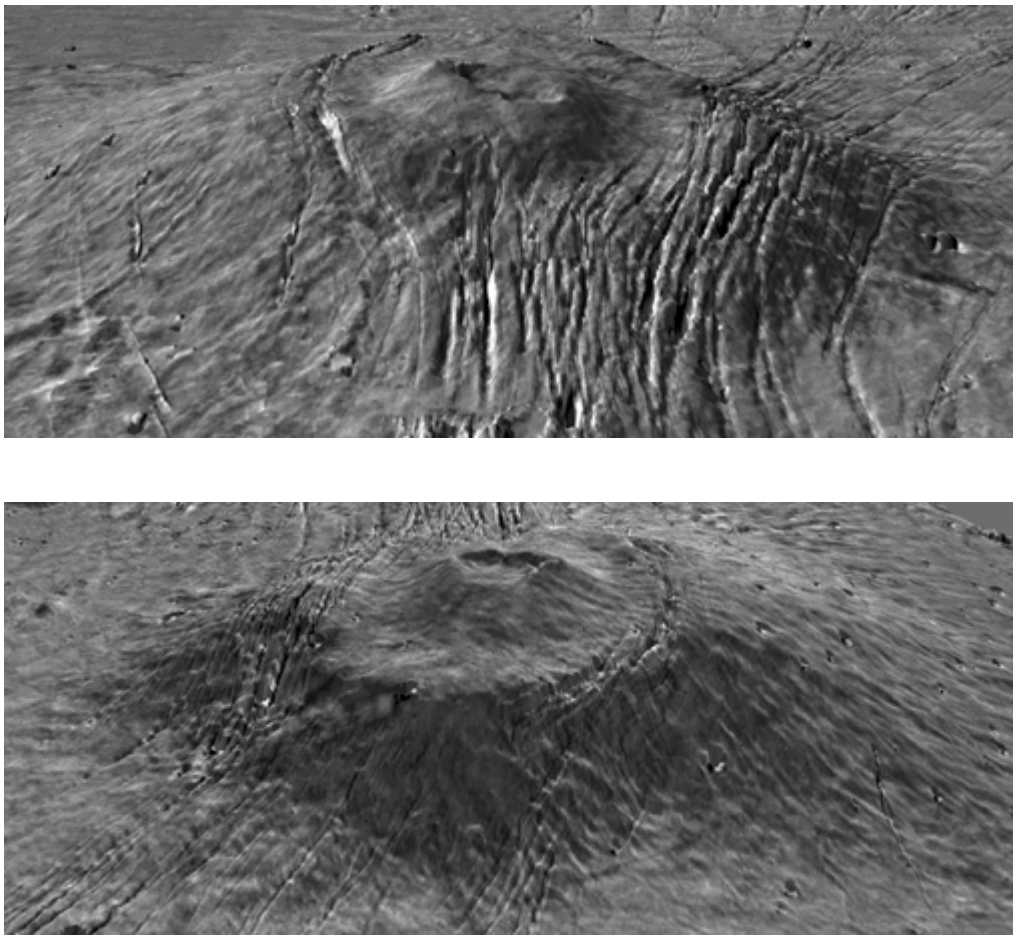

Figure 3 - Two views of Alba Patera (north-south and south-north) with topography draped over a Viking image mosaic. MOLA data have clarified the relationship between fault location and topography on and surrounding the Alba construct, providing insight into the volcanological and geophysical processes that shaped the edifice. The vertical exaggeration is 10:1. (Credit: MOLA Science Team)

The starting point for modelling is the knowledge that has been so far acquired on the volcanoes on Earth. Figure 4 illustrates situations to which a terrestrial volcano may be subjected. Subsurface processes are first described, from deep-seated to shallow ones. Second, the deformation that arises from surface events is presented. A hot spot forms above a deep plume of hot mantle material that is rising up and heating the upper layer of the Earth. Above a hot spot the crust may bulge up, a process that is found for example beneath Iceland or the Hawaiian Islands. Under sufficient heat, the lower part of the crust can melt partially. Such underplating has been detected by seismic velocities intermediate

between lower oceanic crust and upper mantle along the Hawaiian-emperor seamount chain (Watts et al., 1985). In shallower levels, the brittle crust may present multiple fractures that are filled by magma giving rise to a dike complex. A magma chamber forms when magma stagnates and accumulates at specific depth weakening further the crust. The Skaergaard complex in Groenland is an example of magma chamber in crystallised state that has outcropped by erosion (McBirney, 1984). The presence of a magma chamber can be detected by the surface uplift that arises from the arrival of new magma. Magma from the chamber can erupt through the central conduit or laterally on the flanks depending on the most favourable stress field within the edifice. Draining of the magma chamber during eruption leads to the subsidence of the overlying crust and the formation of calderas on the summit (McBirney, 1990). These are craters with relative flat floor bounded by steep normal faults.

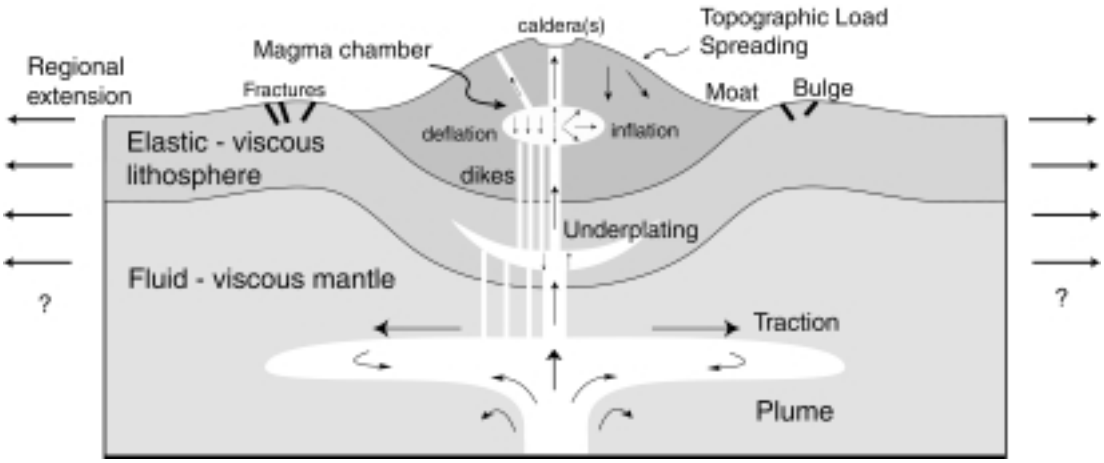

Figure 4 - General situation of a volcano. The volcano may be subjected to gravitational spreading, plate flexure, subsurface forces and regional stress. The elastic lithosphere overlying a fluid or viscous mantle flexes under the weight of the volcano. This leaves a moat filled by volcanic flows or landslide materials under the edifice and a bulge at its surrounding with possible formation of tensile fractures. The subsurface forces can be of four types: the inflation and deflation of a magma chamber, dike complexes, magma underplating at the crust-mantle boundary or at depth a mantle plume. Lithosphere-plume interaction may exist in the form of traction. Regional stresses could be tensile or compressive but are generally unknown at depth.

The volcanoes may also deform by surface processes. Gravitational spreading on Etna has been evidenced toward the east and south and by the formation of the 7 km long depression Valle del Bove (Borgia et al., 1992). The locations of feeding dikes are affected by such near-surface stresses, as recently seen by the October 2002 eruptions.

As the outer layers of a planet, i.e. the lithosphere, are rigid and overly a weak mantle, the load of the volcano induces lithospheric flexure. This is characterised by a depression under the volcano followed at further distance by uplift or bulge as observed around the Hawaiian islands (see the detailed study of Watts, 2001). The viscous nature of the mantle has been demonstrated from the delayed rebound of the lithosphere after release of its ice load in North America or Fennoscandia (Cahtles, 1975). Finally, to understand the processes that occur on a volcano, it must be resituated in its regional context, which may influence the pattern of the tectonic structures.

Most of the processes presented above are studied in this thesis devoted to Alba Patera. However, due to its low aspect ratio (height/diameter), gravitational spreading is unlikely on Alba Patera (Thomas et al., 1990). Horizontal traction from a mantle plume is also ruled out because it must be accommodated by significant compression at the periphery which is however not observed around Alba Patera. The following section details the organisation of this work. The striking concentric and radial grabens of Alba Patera probably originate from deep endogenous processes. At the base of the volcano on the surface, there is neither a bulge, nor moat, nor any significant grabens that need to be explained in context of plate flexure caused by the volcanic loading. On the summit of the volcano, multiple calderas indicate instabilities of magma chamber caused by shallow or even surface effects.

2. Organisation of this thesis

In the part I of this thesis, the lineaments of Alba Patera and their time relationship have been re-examined using satellite images of the Viking mission. Based on 60 m resolution data, the chronology of fracturing was studied. Numerical and analogue methods are used to simulate the effects of doming or subsidence exerted by subsurface forces. The estimated deformation and stress fields serve to discriminate the processes responsible for the observed features on Alba Patera. These are compared with similar structures on Earth and Venus.

While part I describes the effects of endogeneous processes and forces, part II is devoted to the lithospheric deformation caused by the gravitational load of Alba Patera. Numerical models are used for a quantitative analysis of the flexure exerted by the volcano. The effects of geometric and mechanical parameters, regional extension, planet curvature and viscosity are studied. Alba Patera lacks the topographic and tectonic signatures of lithospheric

bending that are observed on other Martian volcanoes. This key “non-observation” provides constraints on the mechanical properties of the Martian lithosphere.

Each part contains its own specific introduction, discussion and conclusion as each has different thematic and methodical concerns. In the following section, the characteristics of the Tharsis region are summarised, in order to better understand the regional framework of the study area “Alba Patera”.

3. Tharsis, the regional setting of Alba Patera

Tharsis is a 8000 km wide and 11 km high dome which covers one sixth of the planet’s surface (Wise et al., 1979). It is characterised by six major volcanic centres: Olympus Mons, the three Tharsis Montes (Arsia, Pavonis and Ascraeus), Alba Patera and Uranius Patera (Fig. 5). A giant system of radial grabens and rifts formed by extensional stresses transects the surface: Memnonia, Sirenum, Thaumasia, Icaria, Claritas Fossae, Valles Marineris, Tantalus Fossae, Tempe Terra (Fig. 5). Not only is horizontal extension preserved, concentric wrinkle ridges due to compressive regime are also observed e.g. in Lunae Planum, Solis Planum, Sirenum and Acidalia (Golombek et al., 2001). The elevation of Tharsis is attributed to both volcanic extrusion and crustal intrusion (Solomon and Head, 1982; Banerdt et al., 1992; Smith et al., 2001). Wide uplift from a rising plume may also contribute to the present topography (Harder, 2000).

Tanaka et al. (1991) presented the first detailed regional tectonic study of the Tharsis region. The Mars Global Surveyor mission led to new studies on a regional scale (Banerdt and Golombek, 2000; Anderson et al., 2001) or local scale, i.e. Tempe Terra (Hauber and Kronberg, 2001), Valles Marineris (Tanaka and MacKinnon, 2000), Pavonis Mons (Montesi, 1999), Alba Patera (McGovern et al, 2001). Table 1 indicates the Martian epochs and corresponding ages as inferred recently by Hartman and Neukum (2001). The main tectonic activity is dated in Noachian, i.e. the early history of Mars, when approximately half of the structures formed (Anderson et al., 2001). The intensity of this activity decreased until middle-late Amazonian. In general, features are centred on the elevated region of Syria Planum, but multiple secondary centres associated to intrusive activity are also inferred (Scott and Tanaka, 1980; Plescia and Saunders, 1982; Anderson et al., 2001). Anderson et al. (2001) found that the tectonic history of Tharsis is composed of five main stages (Fig. 5).
Stage 1. In early Noachian, the extensional structures of Syria Planum and Thaumasia region extended radially to the Claritas Fossae. The formation of radial rifts on the northern

side of Tharsis, such as Tempe Terra, Uranius, Archeron Fossae and Ceraunius Fossae also happened during this period. The appearance of Memonia Fossae and Sirenum Fossae is not well known. They may begin in this stage or later in the next two periods (Anderson et al., 2001).

Martian periods
Age
Late Amazonian
0.3 by-present
Middle Amazonian
1.4-0.6 by
Early Amazonian
2.9-2.1 by
Late Hesperian
3.6-3.1 by
Early Hesperian
3.7-3.6 by
Late Noachian
3.8-3.7 by
Middle Noachian
3.92-3.8 by
Early Noachian
Before 3.92 billion years ago

Table 1. Martian epochs derived from crater counts, the estimated cratering flux and studies of Martian meteorites. The model is proposed by Hartman and Neukum (2001). Intervals between two epochs correspond to uncertainties.

Stage 2. The canyon system of Valles Marineris developed to the east mainly during this second phase i.e. late Noachian and early Hesperian, under a local extensional regime influenced by the regional stress due to Tharsis doming (Tanaka et al., 1991; Anderson and Dohm, 2000). Associated fractures appeared also in the Thaumasia region.

Stage 3. The Noctis Labyrinthus is composed of multiple blocs delimited by short canyons. It is very similar to the surface structures developed above a pressurised reservoir during analogue experiments (Walter and Troll, 2001). This corresponds to the Syria Planum centre activity dominating the Early Hesperian. New fractures formed in this period in Pavonis, Ulysses and Tempe Terra. At the edge of the Tharsis bulge, the structural pattern is characterised by concentric wrinkle ridges which are compressive in nature (Tanaka et al., 1991).

Stage 4. Anderson et al. (2001) situated this phase in Late Hesperian. Intense centralised volcanic and tectonic activity occurred on Alba Patera and also Olympus Mons, the Tharsis Montes and Syria Planum and modified the regional stress conditions (Tanaka et al., 1991; Anderson and Dohm, 2000). Concentric grabens around the Tharsis Montes, Syria Planum and Alba Patera formed in response of volcanic loading (Comer et al., 1985) or subsidence above a draining magma chamber (Tanaka and Davis, 1988).

Stage 5. The final tectonic phase in the Amazonian period is related to the volcanic construction of Olympus Mons and Tharsis Montes. The structures are radial to a centre south of Ascreaus Mons.

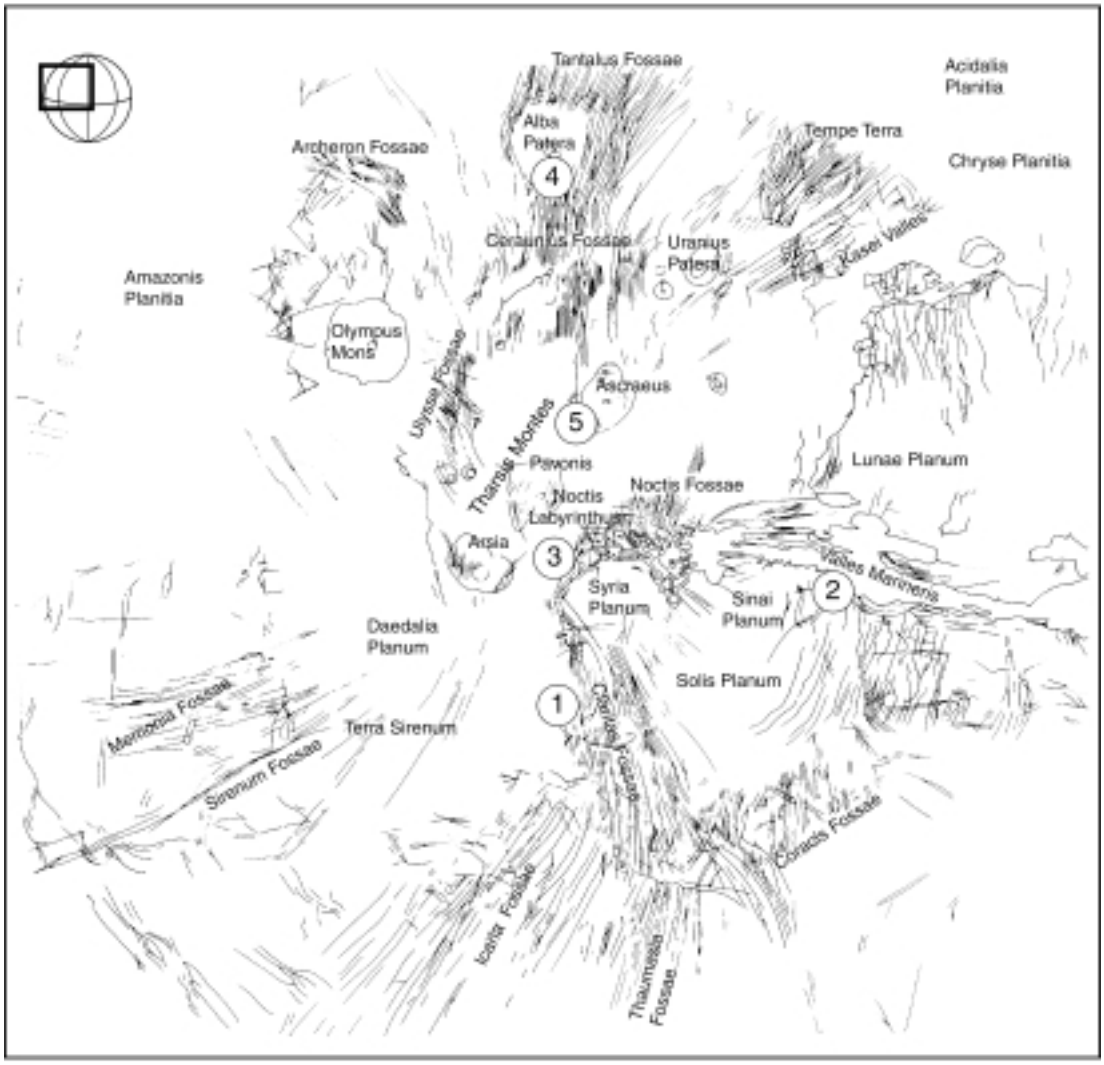

Figure 5 - Fractures, grabens, ridges of Tharsis region with associated volcano-tectonic centres. Modified after Hamblin and Christiansen (1990). The numbers represent the tectonic centres or phases identified by Anderson et al. (2001) and briefly described in the text.

Different origins of these structures have been proposed. A combination of isostatic stresses on the rise and flexural stresses at the periphery of the Tharsis dome was suggested for the formation of the grabens and wrinkle ridges (Tanaka et al., 1991; Banerdt et al., 1991). In term of stress, the surface loading of Tharsis would create radial compression within the province surrounded by a ring of concentric extension. Isostasy in response of the volcanic intrusion and extrusion and the consequent thickening would give concentric extension (radial grabens) on the edifice and radial compression at the periphery (Banerdt et al., 1991). Recent work from Banerdt et al. (2001) using the new MOLA data indicates that a

unique process of regional surface loading interacted with local uplift centres. Using analytic spherical modelling with top and bottom loading and a laterally varying crustal thickness, Banerdt et al., (2001) found that the estimated uplift surrounding Tharsis correlates with the structural evolution of Memnonia, Sirenum, Thaumasia and southern Claritas Fossae, Valles Marineris and Tempe Terra and the central compression with the belt of wrinkle ridges. This coincides with most of the structures except those on the top of the rise around the Tharsis Montes and Syria planum and those at Alba Patera. Flexural loading from Tharsis is clearly shown by an oval ring of gravity and topography anomaly (Phillips et al., 2001). Alternatively, several authors relate the extensive radial grabens to the surface expression of giant dike swarms from a plume (Ernst et al., 2001; Wilson and Head, 2002). The wrinkle ridges could be well caused by the peripheric effects of plume (Mege and Ernst, 2001).

Whereas most of the tectonic structures (radial, circumferential, compressive or tensile) in the Tharsis area develop in groups of faults of uniform orientation, distribution and dimension (Tanaka et al., 1991) under regional or local stresses, the Valles Marineris underwent significant erosion. This huge canyon system is 4500 km long, 7 km deep and reaches a maximum width of 600 km in its central part (Cattermole, 1992). It extends along the equator, from Noctis Labyrinthus on the west to chaotic terrain on the east. This latter area formed by eroding water rather than faulting and was source of outflow channels (Hamblin and Christiansen, 1990). Radial to the Tharsis bulge, the Valles Marineris likely initiated by tectonic activity and the formation of shallow grabens (Barnedt et al., 1982; Plescia and Saunders, 1982) in Late Noachian or early Hesperian (Cattermole, 1992; Anderson et al., 2001). These were subsequently widened and deepened by fracturing, collapse from magma withdrawal from neighboured volcanic centres, and sapping by groundwater fluidised ice (Cattermole, 1992; Tanaka and MacKinnon, 2000).

These studies showed that the Tharsis dome-type deformation structures form the dominant volcanic architecture of Mars. However, local tectonic processes and volcanic or erosive foci change the picture on a small-scale view. Likewise, the structures on Alba Patera may have been biased - or even generated - by local deformation mechanisms and Tharsis regional tectonism.

Part I

Lineament Analysis of Alba Patera

Implications for subvolcanic processes

Lineament analysis on Alba Patera, Mars

Implications for subvolcanic processes

1. Introduction

Alba Patera is one of the most peculiar and widespread volcanoes known in the Planetary System, measuring up to 2700 km across and 7 km high. The bulk edifice is constituted by a large shield volcano with flat apex of about 5 km elevation on which formed a younger and steeper 2 km high central cone. As reported from the Viking images, Alba Patera is characterised by numerous extensional fractures in predominantly north-south direction (Fig. 1.1). These are geometrically and chronologically divided into diverse lineament sets. The old Tantalus Fossae extend from the north-eastern side of the volcano toward the pole in a radial orientation. In the south, the Ceraunius Fossae are north-south lineaments. After the 5 km high and 1300 km diameter main shield was built, new grabens arose on the flanks of Alba Patera with a general concentric orientation. The volcanic field of Alba Patera is composed of three main units (Scott and Tanaka, 1986) which differ in age and aspect ratio (height/radius) (Fig. 1.2). The first stage of Alba Patera consists of a widespread plateau dated in the late Hesperian epoch (Table 1 of introduction). Centralised volcanism in the early Amazonian epoch gave rise to the main shield. The construction of the summit cone occurred in the third stage, when volcanic products probably covered most of the concentric tectonic structures in the central region of Alba Patera.

Until Mars Global Surveyor (MGS) was launched in 1996, the topographic characteristics of Alba Patera were poorly constrained. The maximum elevation was found 3-5 km above the surrounding terrain. Concentric lineaments were seen at the base of the main shield and found to be roughly symmetric around the centre of the edifice (Turtle and Melosh, 1997). The main accepted explanation for the formation of the concentric fractures was the flexure of the lithosphere under the topographic load (Wise, 1976; Comer et al., 1985; Turtle and Melosh, 1997; Heller and Janle, 2000). New topographic data from MGS, now with a vertical precision of 37 cm and a spatial resolution of 230 m, redefined the position of the lineaments to be much higher, on the flanks of the edifice (Fig. 1.1). These are not centred about the topographic summit but instead shifted toward the east. Thus, the previous

hypothesis for the origin of the grabens has been replaced by the combination of surface loading and subsurface forces. Alba Patera may have been formed by an autonomous hot spot responsible for local uplift (Janle and Erkul, 1991; Mège and Masson, 1996; Banerdt et al., 2000). As proposed by McGovern et al. (2001), concentric normal faulting may form by sill complexes combined with a growing surface loading. This model is similar to the piston effect with minimum or zero deformation above the indent and maximum tensile stresses at its edge. Topographically, this corresponds respectively to an upward translation and a notch on the flanks that was correlated by the authors to the flat zone surrounding the summit cone. Scott (2000) suggested that the fractures do not result from upward movement but from crustal subsidence and spreading after the rebound due to detachment of Alba Patera's root. This process would induce strong compression at the margin of the volcano which is however not observed (Scott, 2000). Although several studies have been devoted to understand the concentric fractures on Alba Patera, no consensus has been found yet.
Furthermore, the question arises how the radial trends north and south of Alba Patera developed and how they interacted with the concentric grabens. In previous works, the radial structures are generally attributed to an east-west extension caused by the Tharsis doming. This may explain the Ceraunius Fossae radial to the Tharsis centre. However, the Tantalus Fossae diverge from Alba Patera toward the north pole and extend beyond the uplifted Tharsis region into regions where the stress field should be compressive.

Here is proposed a new evolutionary model based on the presence of a hotspot local to Alba Patera in conjunction with subsequent rifting and intrusive processes. Predominantly vertical directed processes, such as wide doming followed by topographic subsidence of shorter extent, can reconcile the various stages of tectonics on the Martian volcano. Based on the Viking images, the time sequences in the graben formations are re-examined. To discriminate the processes responsible for the observed structures, deformation and stress fields induced by uplift or subsidence with a regional extension are reconstructed in analogue experiments and finite element models. A combination with surface loading due to the volcano is also studied numerically. The two methods give similar results, so that the effects of the main forces, i.e. uplift, subsidence, regional stress and surface loading, and their interactions can be outlined with confidence. Comparison of these theoretical cases, Alba Patera and similar structures known on Earth provides additional information on the geodynamic processes that prevailed on the Martian volcano.

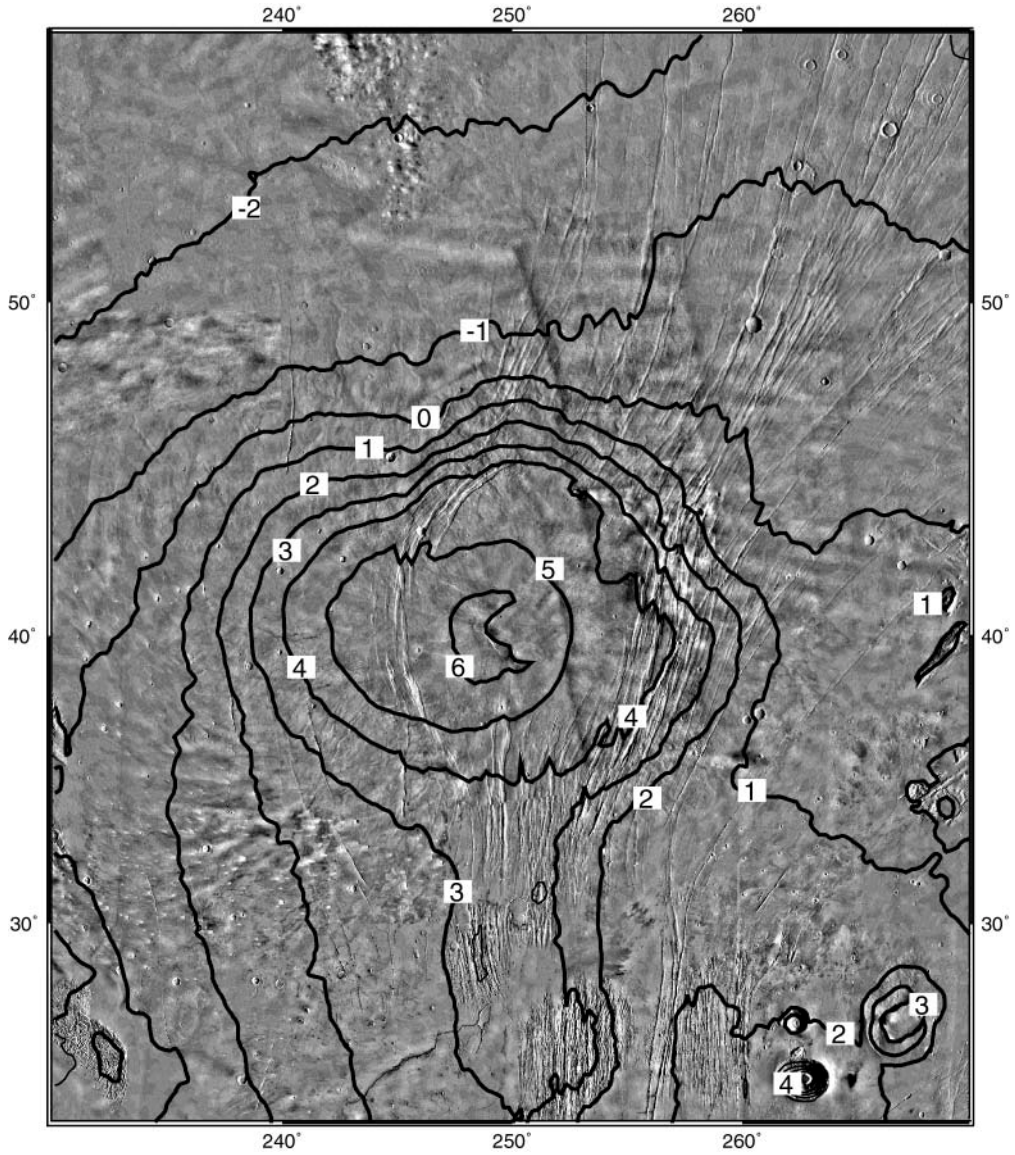

Figure 1.1 - Mars Digital Image model for Alba Patera with superposed MOLA topographic contours (in km). The Viking images have here a resolution of (1/256°)/pixel (about 230m). Alba Patera is characterised by sets of grabens N-S to the south (Ceraunius Fossae), radial to the north (Tantalus Fossae), and concentric around the summit (Alba Fossae to the west and Tantalus Fossae to the east) (location of Fossae, see Fig 1.3). The concentric grabens are not centred to the summit but shifted toward the eastern side. There is a topographic assymetry with a more elevated eastern flank than western side. To the southern side of Alba Patera begins the topographic effect of the Tharsis bulge.

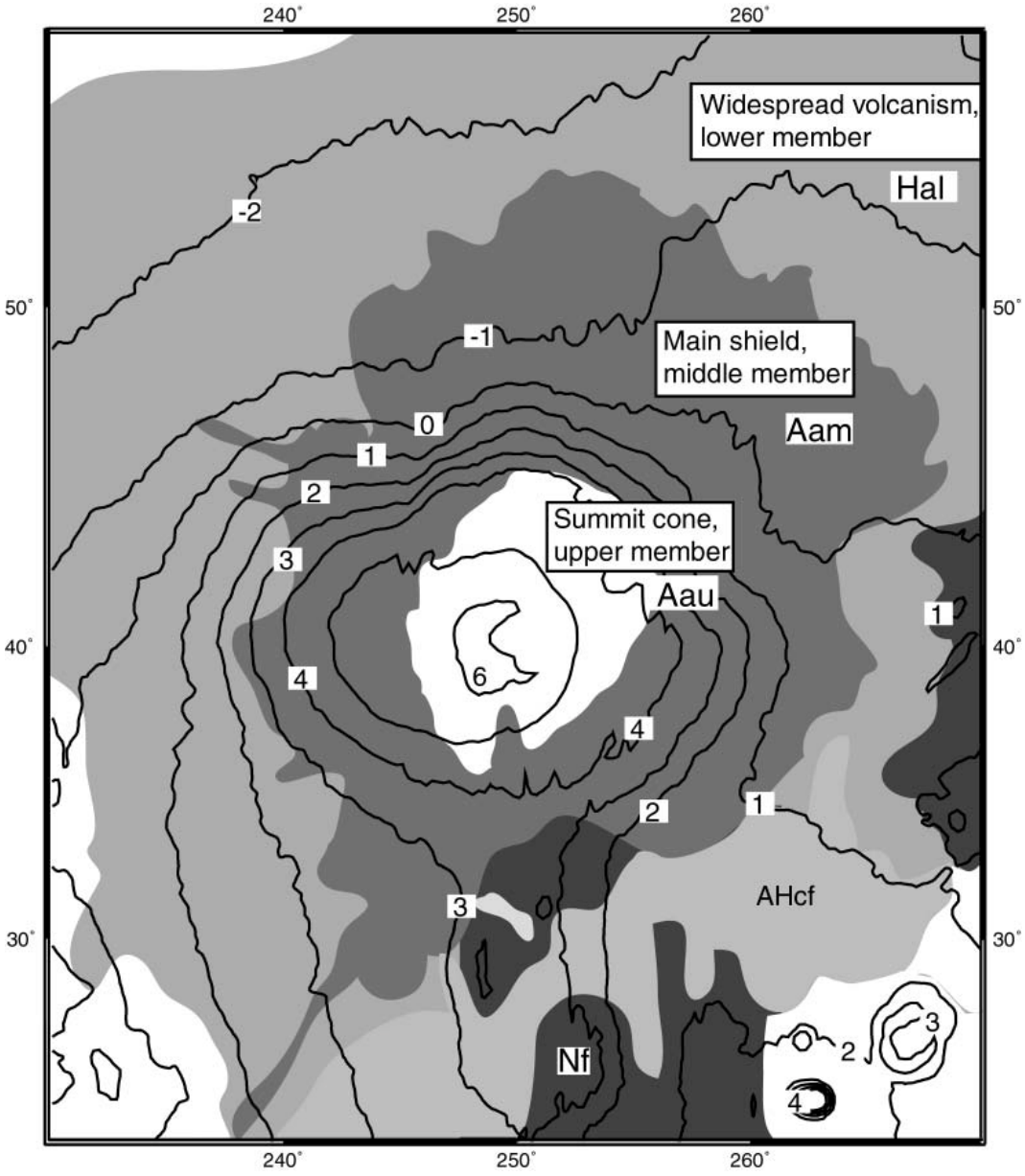

Figure 1.2 - MOLA topography superposed with volcanic units (Scott and Tanaka, 1986). The first letters N,H,A indicate the Martian epochs Noachian, Hesperian and Amazonian. Hal, Aam, Aau are the upper, middle and lower members of Alba Patera. There is a change from widespread to centralised volcanism with increasing slope between each unit.

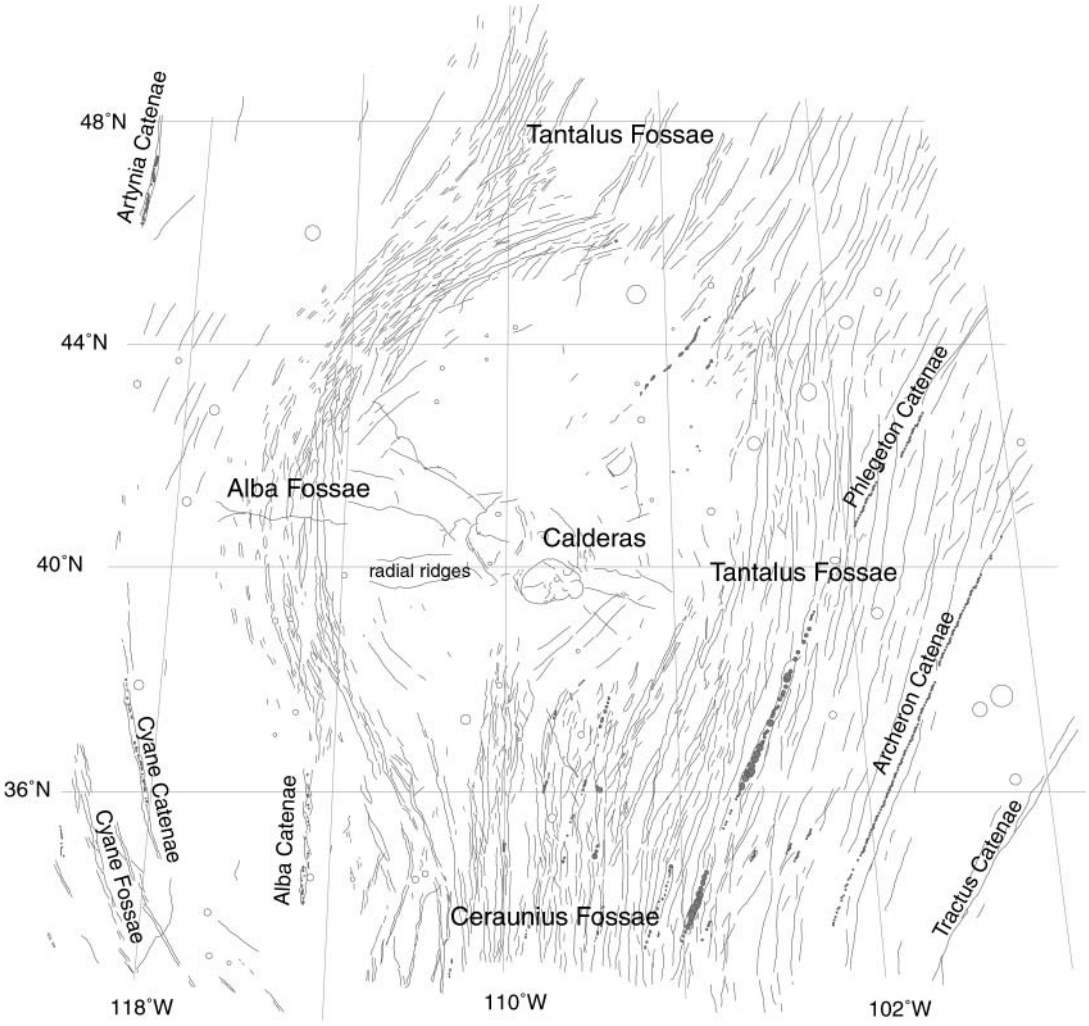

Figure 1.3 - Lineaments on the main shield of Alba Patera. This map has been constructed from a Viking mosaic with a resolution of about 60m/pixel. Cross-cutting indicates that the Ceraunius Fossae are the oldest structures. In intermediate stages, the northern radial Tantalus Fossae and the Catenae sppeared. Then the concentric grabens on the upper and mid-flanks formed. Late summit volcanism recovered numerous flank grabens. The final tectonic activity focused on the summit part with formations of ridges thought to be compressive in nature and concentric fractures. Two calderas are also observed on the top. The Alba Fossae and concentric Tantalus Fossae display generally an increase in concentricity from the mid-flanks to the upper ones. Note the numerous small concentric segments on the northern side of Alba Fossae that cut older and less concentric grabens. In the northern side, the concentric structures transect radial ones. On the south, however, the features are continuous with the linear Ceraunius Fossae. The Catenae are grabens characterised by pit craters on their floors, thus thought to be volcanic in origin. The eastern Catenae display a NE-SW trend that contrasts with the concentric grabens while the western Catenae are relatively concentric.

2. Tectonics and volcanism on Alba Patera

The structures described in the literature are generally grouped into three to five main groups associated with different phases of volcanism (Scott and Tanaka, 1986; Schneeberger and Pieri, 1991; Heller and Janle, 2000; McGovern et al., 2001). In age order, there are the oldest N-S Ceraunius Fossae in the south, the Catenae on the eastern sides of the volcano and the radial Tantalus Fossae in the north, and finally the concentric Alba Fossae and Tantalus Fossae (Fig 1.3). "Fossa" defines the linear depression or long and narrow valley and "Catena" means chain of craters.

Tectonic structures	**Volcanic unit**	**Epoch**
Ceraunius Fossae	Noachian crust	Noachian (before 3.7by)
Radial Tantalus Fossae Eastern Catenae (Phlegeton, Archeron, Tractus)	Lower member (widespread volcanic unit) / middle member (main shield)	Late Hesperian / Early Amazonian (3.6-2.1 by)
Western Catenae Concentric Tantalus Fossae Alba Fossae	Middle member (main shield) / upper member (summit cone)	Late Hesperian / Early Amazonian (3.6-2.1by)

Table 1.1 – Main tectonic structures of Alba Patera and the volcanic units on which they are observed. See text for details. The Ceraunius Fossae belong to the linear construction south of Alba Patera that was little affected by later activities of Alba Patera. The radial Tantalus Fossae are seen continuously on both the main shield of Alba Patera (middle member) and on the widespread volcanic unit (lower member). This indicates either a graben formation related to the main shield or permanent rifting during the constructions of the two volcanic units. The concentric structures formed mostly before the summit cone, but some of these grabens cut lava flows from the late edifice. The Catenae originated from the Tharsis region but were influenced by stress field local to Alba Patera, the eastern Catenae present similarity with the radial Tantalus Fossae, the western Catenae with the concentric Alba Fossae. However, the western Catenae could be dated earlier (see partII, section 11). The ages for the epochs are from Hartman and Neukum (2001).

The radial grabens

Figure 1.3 presents the different sequences of graben formation on the main shield of Alba Patera. Two mosaics of Alba Patera of different resolution and coverage have been used. A mosaic has been constructed with 160 individual Viking images with a resolution of about 60 m pro pixel. Earlier mosaic images used by Heller and Janle (2000) with a 230 m/px resolution, cover larger regions around Alba Patera (Fig. 1.1). The Martian epochs and the corresponding ages are indicated in the table 1 of the introduction.

In the south of Alba Patera, the oldest N-S structures Ceraunius Fossae cut the crust of Noachian age and are of radial arrangement relative to the Tharsis bulge (Plescia and Saunders, 1982; Plescia, 1991; Schneeberger and Pieri, 1991). They have been partially covered by lava flows of the younger units of Alba Patera (Heller and Janle, 2000) and were themselves the locus of lava flows by late reactivated extensional fractures (Jager et al., 2000). In the northern side, the Tantalus Fossae are radial to Alba Patera and extend northward up to 1000 km into the polar plains of Vastitas Borealis (Heller and Janle, 2000). The northernmost part of the radial Tantalus Fossae cut a region of widespread volcanism of late Hesperian while the southern part is observed on the more recent and centralised unit of Alba Patera (Scott and Tanaka, 1986; Anderson et al., 2001).

The Catenae

The Catenae represent a particular group of extensional structures around Alba Patera. These features are defined as graben with aligned pit craters (Schneeberger and Pieri, 1991). The crater chains lying on the floors of the grabens are thought to have formed by subsidence after a) permafrost heating and removal of overlying crust (Mège and Masson, 1996), b) collapse due to withdrawal of magma or volatile in subsurface dikes (Mège et al., 2000; Scott and Wilson, 2002) or c) collapsed material slumped into a tension crack at depth (Tanaka et al., 1989). Morphologically very similar are for instance the chain of pit craters of Hawaii´s Big Island that formed by extensional stresses above shallow dike intrusions.

The main Catenae - Tractus, Archeron, Phlegethon - trend linearly from a NE-SW direction on the eastern side of Alba Patera. Tractus Catenae prolong to a N-S direction in the southern part of Alba Patera. In the north, these structures are parallel to the radial Tantalus Fossae and the Mareotis Fossae in Tempe Terra region. In the middle part of the volcano, they are cut by the concentric grabens but sever the Ceraunius Fossae. Thus they have an intermediate age between the Ceraunius Fossae and the concentric grabens and are contemporaneous to the radial Tantalus Fossae. On the western side of Alba Patera, the Cyane Catenae and the associated Cyane Fossae display a concentric trend similar to the Alba Fossae. On the contrary, Alba Catenae and Artynia Catenae are oriented in linear N-S direction. The Catenae are related to formation of a giant dike swarm, with a source that has been apparently situated within the northern flanks of Ascraeus Mons (Tanaka and Golombek, 1989) or farther south within the Tharsis Province (Mege and Masson, 1997; Scott et al., 2002).

The concentric grabens

The younger concentric Alba Fossae and Tantalus Fossae formed on the upper and mid-flanks of the more centralised unit of Alba Patera situated in Early Amazonian (Scott and

Tanaka, 1986). This unit represents the main shield of Alba Patera since Mars Global Surveyor has provided better topographic data (Fig. 1.2). The southern branch of both sets of grabens changes toward a N-S linear trend that cross-cut, follow or reactivate the Ceraunius Fossae. In the north of Alba Patera, the continuity between the two fractions of the Tantalus Fossae is not obvious, i.e. there are numerous overlapping of radial and concentric trends. In contrast, the fractures of Alba Fossae are strongly concentric there. Continuity or cutting have been attributed to the effect of a growing load (Turtle and Melosh, 1997) or regional stresses in the different areas (McGovern et al, 2001).
Differences concern also the distribution of the two sets of concentric fractures. While the Alba Fossae are confined to the upper flanks, the concentric Tantalus Fossae cover much of the eastern flanks of the volcano (Fig. 1.1). This particularity is often described as “eccentricity”. The grabens are on the summit mostly recovered by the last volcanic unit of early Amazonian time, termed here summit cone regarding its steeper slope. The MOLA data revealed also eccentricity in the relief. The summit cone is surrounded by a flat zone, morphologically and structurally asymmetrically in east-west sections. On the west side, the plateau at about 5 km elevation is the locus of the concentric Alba Fossae. In contrast, the eastern flat zone is situated at about 4 km elevation and the concentric Tantalus Fossae are much more widespread down to the lower flanks of the underlying shield. This eccentricity may be essentially volcanic because the Alba Fossae on the western side of Alba Patera and the Cyane Catenae seem to belong to a unique system which has been covered in its central part by more recent lava flows (also suggested by Mouginis-Mark et al.; 1988). This would explain both the apparent confined distribution of the Alba Fossae and the higher elevation of the western part of Alba Patera.

There were numerous discussions on the time relationships between the concentric grabens and the formation of the summit cone. Scott and Tanaka (1986) classified the concentric graben formation after the late Hesperian periods and before the upper member formation, while several authors favoured a final appearance much later during the evolution of Alba Patera (Comer et al, 1985; Mouginis-Mark et al, 1988). One important criterion for invoking models of surface loading to explain concentric grabens is the occurrence of faulting after the major construction of the edifice. Comer et al. (1985) based their models on such observations mainly to the west and northwest of the volcano. The last flow unit corresponds to the upper member of Scott and Tanaka (1986) but extends beyond the Alba Fossae. According to Mouginis et al. (1988), the grabens appeared after the summit lava flows which are liable for volatile liberation, water sapping in the ash deposits and the observed fluvial channels. New data obtained by MGS clarified the relationship between the topography of Alba Patera and the volcanic units (Jager et al, 2000; McGovern et al., 2001;

Ivanov and Head, 2002). Topographically, the middle and upper parts correspond respectively to the 5 km high and 1300 km wide shield and the overlying 2 km high and 200 km radius summit cone. In general there is now a consensus that appearance of the summit cone on top of the wide shield volcano occurred mainly after formation of the fracture rings. A slight contemporaneous formation of grabens and summit cone at least at the earlier stage of cone formation is indicated since these fractures cut also early flows at the base of the summit cone (Comer et al., 1985; Schneeberger and Pieri 1991; Ivanov and Head, 2002).

Several sub-sequences in the graben formation have been added to the general tectonic phases described previously (Fig. 1.3). Graben formation was active (or reactive) during the main stages of Alba Patera, with an extreme longevity compared to similar rift zones on Earth. On Alba Patera rifting had a pronounced relevance for more than 1-2 byrs, being generally oriented N-S in early times and trending concentrically in late stages (see Fig. 1.1). Older grabens are crosscut and displaced by younger grabens that deviate even more from the initial radial orientation and surround the summit plateau of the main shield. On the northern side of Alba Fossae, e.g. N40° trending fractures are overprinted by numerous N60° lineaments of smaller length. Some of these younger structures present an en-echelon pattern that may indicate strike-slip faulting. The orientations of the tectonic structures overall tend toward stronger concentricity still after summit cone formation (see e.g. in NW flank of summit cone, Fig. 1.3). Individual episodes of sudden widespread concentricity increase can not be distinguished on the mosaic, supporting more the concept of a gradual change from radial to concentric lineament arrangement. This all implies a mechanism responsible for concentric fractures that becomes more important with succeeding volcanic activity.

Summit cone

The last tectonic and volcanic activity of Alba Patera focused on the summit part and formed the so-called upper member of Scott and Tanaka (1986). Abrupt morphometric and structural changes define the summit cone. It is characterised by reduction of length and number of flows with time (Schneeberger and Pieri, 1991), a relatively steep flank inclination, and an apical caldera complex. Structurally, the lower and middle member volcanic unit of Alba Patera were both strongly transected by grabens, whereas most of the flanks of the upper member are relatively free from these pairs of large normal faults, except the few grabens that cut the lowermost flows of the cone cited previously. The summit cone is however surrounded by arcuate structures thought to be extensional in origin (Fig 1.3). On various places at about 100-150 km radial distance from the caldera

complex, minor developed fine concentric lineaments are observed on the mosaic. Positioned on the lower and mid-flanks of the summit cone, they postdate its oldest lava flows. A few radial wrinkle ridges, surface expression of thrust faulting, have been also mapped on the summit of Alba Patera (Scott and Tanaka, 1986), alternatively defined as lava ridges by Cattermole (1987) (Fig. 1.3).

In all those various morphological observations and genetic implications, it remains unclear whether flank eruptions and flank deformation really occurred on the summit cone and how those were associated to the incisively fractured volcanic shield below. Spatter ridges have been evidenced on the summit cone, these are magma flows spreading over fissure rims (Cattermole, 1986). The orientation is generally concentric around the summit. Cattermole (1986) evokes a "regional" trend for both the grabens and the spatter ridges. Schneeberger and Pieri (1991) proposed a shift of activity from the summit to the volcano's flanks in waning stages. These source vents may have also taken place contemporaneously with the caldera-fed eruptions (Cattermole, 1987). There is the question whether the mechanism that gave rise to the concentric grabens was also responsible for the formation of these fine features. Similar fine concentric fissures are however also observable on other volcanoes (Mouginis-Mark and Rowland, 2001). Fissures vents, i.e. surface expression of dikes, may imply other processes that redirect the magma toward the flanks. Caldera formation, for example, reorient the dikes in arcuate pattern vents (Munro and Rowland 1993).

The summit cone is truncated at its top by a large depression 140 km in diameter that encompasses two main calderas of 50-100 km diameter and up to 400 m deep (Cattermole, 1984; Ivanov and Head, 2002). The caldera scarp of the older basin is partially preserved on its western boundary, whereas in the region of its likely eastern ring fault position the younger caldera complex of Alba Patera formed. Most of the older caldera trace is covered and obscured by subsequent eruptions. Wrinkle ridges within caldera indicate post-collapse subsidence and contraction of the caldera floor that was partially filled (Cattermole and Reid, 1984). These quasi circular structures on the top of a volcano relate to the collapse above a decompressed or drained magma chamber (Smith and Bailey, 1968; Lipman, 1997). Scalloped walls of the calderas of Alba Patera suggest that collapse occur incrementally (Mouginis-Mars and Rowland, 2001). A mechanism for multiple caldera formations on Mars was proposed by Zuber and Mouginis-Mark (1992), where the change of stress conditions within the edifice destabilises the initial reservoir and favours migration of magma, facilitating the formation of annexe reservoirs. Most (if not all) calderas on Earth are likewise nested caldera complexes, where much more complex dynamics are discussed to destabilise a reservoir (such as crystallisation and degassing effects, magma replenishment, or abrupt viscosity change).

In overall, concentric lineaments occurred on Alba Patera in various stages of volcano evolution. The caldera-related faults represent a late, short and presumably shallow deformation type. Considering the entire Alba Patera, it was subjected to a one and a half billion-year long period of graben growth. Understanding the transition from radial north-south lineaments in pre- or early stages of Alba Patera that incrementally developed into to concentric orientation, is the goal of the following numerical models. From these models we hope to get an idea of the deep volcanic and crustal constitution and the implications of surface features for subvolcanic processes.

3. Numerical models

Doming and subsidence exerted by deep forces are numerically simulated to estimate the surface displacements and stress fields, using the Finite Element program TEKTON (Melosh and Raefsky, 1983). Other types of force are also investigated (Fig. 1.4). The subsidence (or uplift) was combined with volcanic loading or added with an east-west regional extension representing the stress field from the Tharsis bulge.

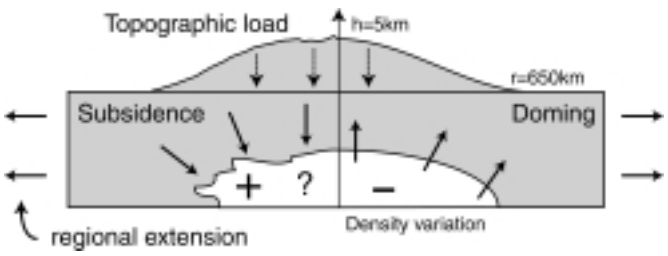

Figure 1.4 – Model of topography and subvolcanic core. The source of deep forces is unknown and ideally modelled by an elliptic area that has a density different from the surrounding rock. A higher density (+) simulates any crustal subsidence by cooling, withdrawal of magma, dying support from below or rifting. Inversely, a lower density (-) induces doming. Effect of regional extension and surface load are also tested.

3.1 Methods

An elastic half-space is used to estimate the full elastic response of the crust to subsurface loading. The density of the crustal rocks is taken to be 2900kg/m³ (Zuber, 2001), the Young's Modulus to be 50 GPa and the Poisson ratio to be 0.25 (Turcotte and Schubert, 1982). Gravitational acceleration on Mars' surface is 3.7067m/s². When specified, the topography of Alba Patera was also meshed. The dimensions are a 650 km radius, 5km

height and a cosine form which better reproduces the approximate shape of the volcano. The mechanical parameters of the volcano are assumed to be those of the crust.

Subsurface loading is simulated by changes of density at depth relative to the surrounding rocks (Fig. 1.4). The region of density difference is modelled to be elliptic form and will be termed for simplification the “reservoir” or “core”. The physical meaning of this region, i.e. plume, underplating, magma chamber or intrusive complex can be determined a posteriori from the characteristics of the model that best correlate with the observed structures. This will be discussed further below. A smaller density relative to the surrounding induces uplift or doming and is representative of a higher temperature, lighter material, and/or input of magma. Inversely, higher density simulates any crustal subsidence, i.e. cooling magma, decrease of pre-existing support or change of crustal strength.

Subroutines were developed to automate the mesh construction for Finite Element modelling and vary the dimensions and depth of the reservoir within the half-space. The grid is finer around the modelled reservoir and near the surface to assure sufficient accuracy in the results, and larger at high horizontal and vertical distances of the studied area to limit the number of elements and processing time. The bottom and lateral sides are enough far to avoid boundary effects. The model is axisymmetric and only half of the grid needs to be meshed. There is no horizontal displacement at either the axis of symmetry, or on the far side. These boundaries are free to move vertically. The bottom of the grid is fixed.

The effects of an unidirectional, horizontal and tensile regional stress with various magnitudes are considered. Stresses from the axisymmetric models of subsurface loading are previously transformed into a Cartesian coordinate system before addition to the regional extension. The area on which stresses apply must be also projected by the mean of Mohr’s circle. Thanks to symmetries in the problem, only a quarter of the surface is plotted. East describes the horizontal line from the summit to the eastern direction and north the vertical line from the summit to the northern direction.

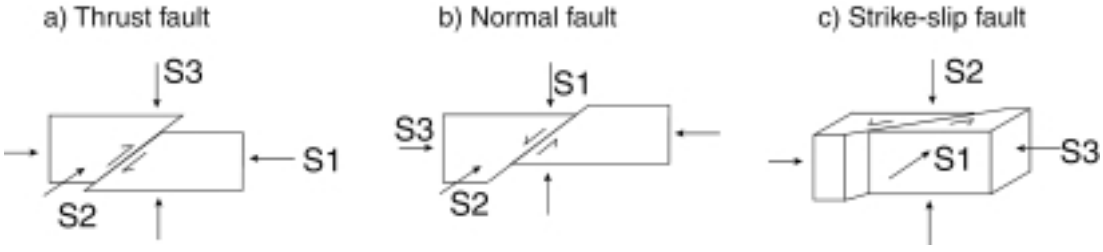

Figure 1.5 - Type of faulting depending of the orientations of the principal stresses. a) Thrust faults form when the the minimum compressive stress S3 is vertical. b) Normal faults are expected if the maximum compressive stress S1 is vertical. c) A vertical intermediate principal stress leads to strike-slip faulting.

The different regions of faulting predicted are determined using Anderson's theory (1951), modified to suit the convention of a positive stress for extension. This theory states that when the vertical stress is greater than the radial and hoop stresses, thrust faults form (Fig. 1.5). If the vertical stress has an intermediate value, then strike-slip faults form. Finally, if the vertical stress is minimum, then normal faults form. Fracture experiments have shown that the initiation of fracturing depends on the differential stress ($\sigma1$-$\sigma3$) (e.g. Twiss and Moores, 1992). Thus, the difference between the maximum and minimum stresses has been calculated. This gives information on the position and type of presumable failure(s), when the position of maximum stress difference is correlated to the different regions of faulting. Alternatively, the fractures near the surface may simply depend on the maximum tensile stress whose position is close to that of the maximum differential stress.

3.2 Results

The stress field and corresponding regions of faulting are presented for three types of loading: a) doming, b) subsidence and c) topographic load. The effect of varying the dimensions and depth of the reservoir are studied (d). The following part e) shows how the surface stresses caused by the reservoir interact with the topographic loading. f) Finally, the diverse types of loading are combined with the regional stress.

a) Doming

In the following, the stresses that may form by increase of the rock volume within a volcanic core are described. Doming is characterised by maximum tensile radial and hoop stresses at and near the axis of symmetry (Fig. 1.6a). Radial orientation of normal faulting is predicted, the hoop stress being the greatest. At further radial distance, strike-slip faults are expected followed outward by thrust faults, because the hoop stress tends toward zero while the radial one becomes significantly compressive.

b) Subsidence

A volcanic core at depth subjected to a density increase sinks. Likewise, a cooling magma body shrinks. For both processes, on the surface, strong compression involving thrust faults is obtained along a radial distance similar to the horizontal radius of the reservoir (Fig. 1.6b). Around its distal edge, there is a high tensile radial component generally associated with negative hoop stress leading to strike-slip faulting regarding the position of maximum differential stress.

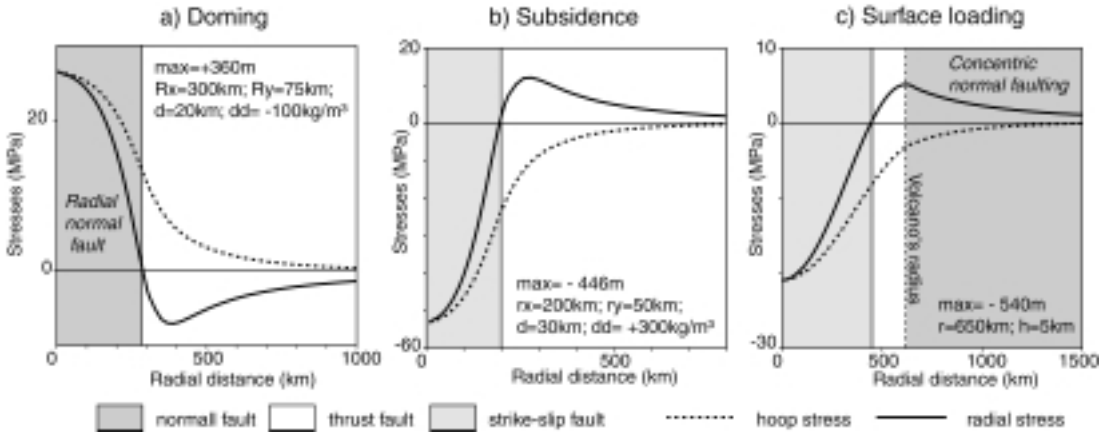

Figure 1.6 - Axisymmetric surface stresses for three type of forces, i.e doming or subsidence due to the volcanic core and surface loading. The horizontal and vertical radii of the reservoir are Rx and Ry. d is the depth to its top, dd the difference of density relative to the surroundings, the sign + indicates a higher density, the sign - a lower density. Max is the maximum value of displacements observed in all cases at the axis of symmetry. The radius of the volcano is r, the height is h. For surface loading or subsidence, when the tensile radial stresses are much more higher than the negative hoop stresses, normal faulting is more likely outside the volcanic construct.

c) Topography

Crustal subsidence can be also created by the volcanic topographic load. Variations of stresses induced by the topography alone are thus similar to the previously described effect of subsidence. A third region of concentric normal faulting following the strike-slip faulting area is expected (Fig. 1.6c), the negative hoop stress being very low relative to the radial positive stress. Knowing that the minimum stress level for normal failure is approximately a half of those required for strike-slip faulting (Weijermars, 1997), only normal faults might form and no strike-slip faults in the whole immediate surrounding of the volcano or above the distal edge of the subsidence source.

d) Variations of reservoir characteristics

The effects of varying the reservoir characteristics are shown in figure 1.7 only for subsidence, but these are similar to doming. Widening the horizontal or the vertical size of the reservoir or increasing its depth enlarges the regions of faulting on the free surface. Higher density difference between the reservoir and surrounding rocks augments the magnitude of the stresses but doesn't modify the horizontal extent of the deformation on the surface. Greater stresses are also obtained for shallower reservoirs. The surface stresses for a wider reservoir are also larger, its upper walls being closer to the surface.

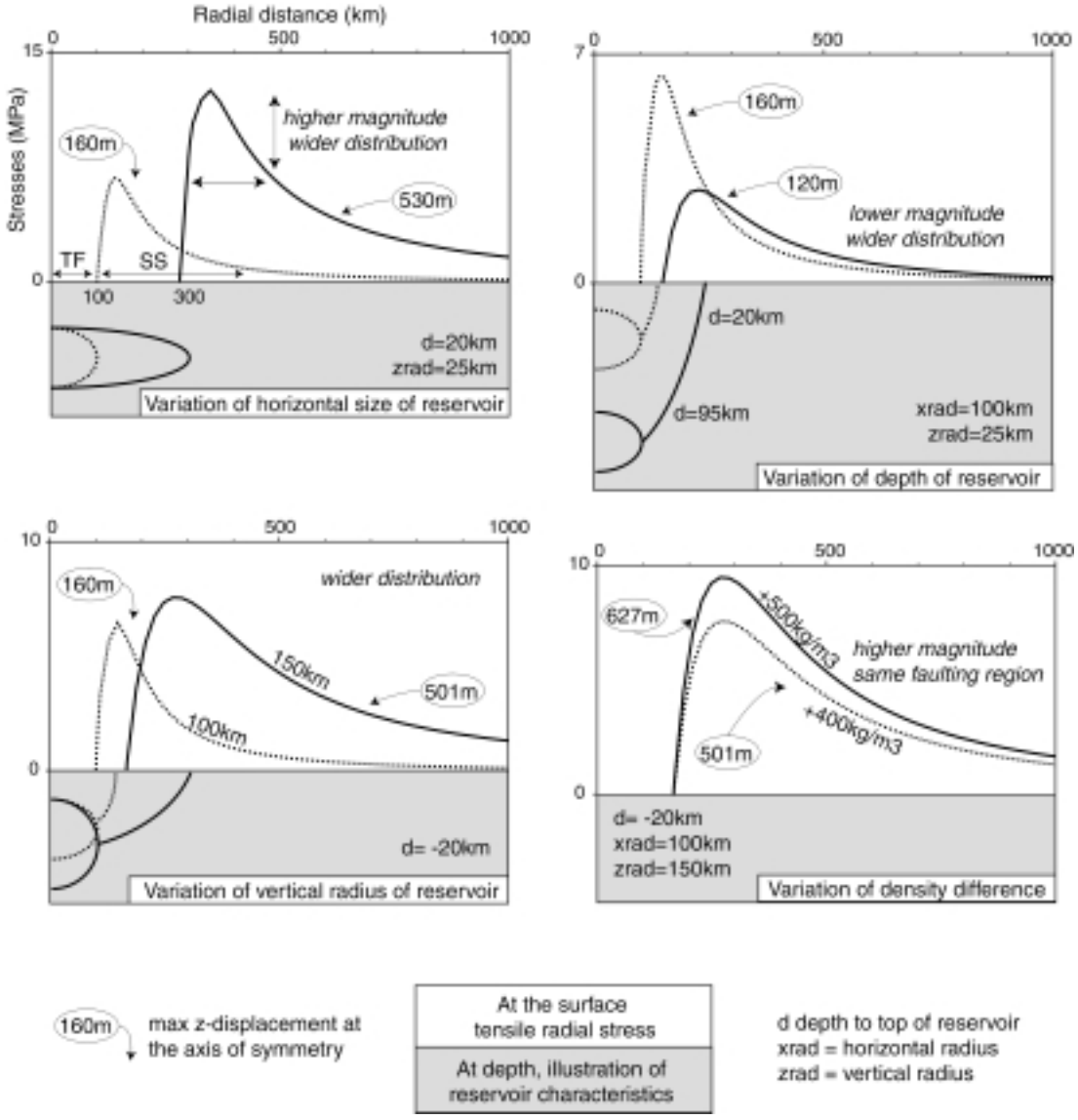

Figure 1.7 - Tensile radial stresses on the surface for various characteristics of the reservoir illustrated below each plot. The process between the core and the surrounding rocks is subsidence simulated by higher density of reservoir relative to the surrounding. The density difference is generally taken arbitrarily to be +400kg/m³ when not otherwise specified. The region of thrust fault (TF) begins at the axis of symmetry where the hoop and radial stresses - not indicated here - are both negative. It continues until the radial stress passes to a positive value, following which faulting is strike-slip (SS) as the hoop stress remains negative. The maximum downward displacements found at the summit are shown in meters.

For subsidence only, the position of maximum tensile stresses is presented for various depth and radii of the reservoir (Fig. 1.8). In principle, to obtain this position between 200 and 300 km radial distances from the axis of symmetry, the horizontal half-length of a shrinking core must be in the range of 150-250 km, if its vertical half-thickness is low (<25 km) and at 30 km depth from its top. The reservoir is then oblong, similar to a sill. For a deeper

reservoir, the horizontal half-size is shorter by 20-50 km for 50 and 80 km depth respectively. For long vertical radius of 50-100km, the reservoir needs to have a more circular shape to obtain similar regions of deformation on the surface. This shows the non-uniqueness of solutions for the shape and depth of the subsurface load for this type of model.

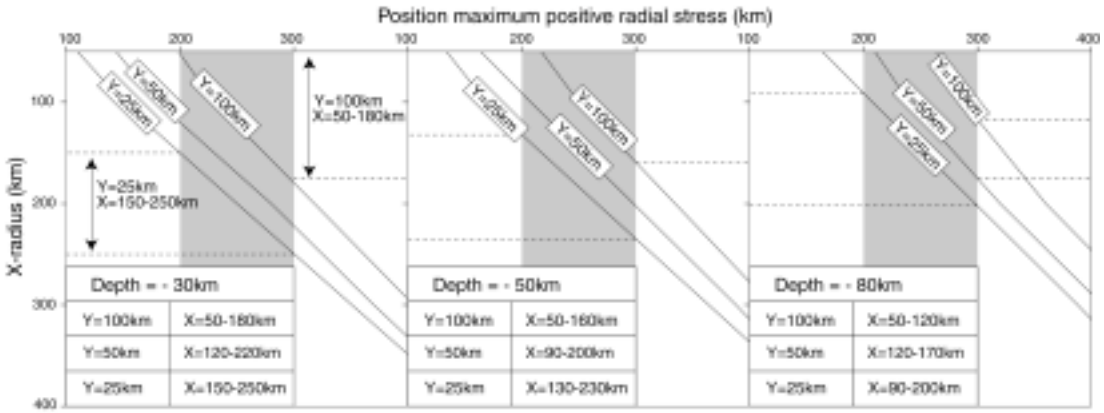

Figure 1.8 – Position of maximum tensile radial stress due to subsidence caused by density increase. The depth to the top of the reservoir and the horizontal and vertical radii X and Y respectively are varied. The tables indicate the model of reservoir that lead to maximum tensile stresses between 200 and 300km (the black area). This range corresponds to the radial distance of the observed concentric fractures.

e) Combination of doming or subsidence with surface loading

In the following, the combined mechanisms of vertical upward forces (doming) plus loading forces are simulated, to determine their coupled influence on normal faulting. Uplift of horizontal extent much smaller than the volcano size has only minor effects at the foot and surroundings of the volcano. The stresses remain approximately those created by the volcanic load. The previously described case-examples show that the horizontal extent of uplift is the primary factor to control the type and position of faulting. Maximum differential stresses are observed around 550km radial distance in the region of predicted strike-slip faulting. Compression on the flanks is observed at 150-200km radial distances. No maxima of extensional stress formed on the edifice flanks. Near the summit, the area of normal faulting has a small extent, being less than 100km.

Uplift alone affecting half the volcano's radius induced compressive stresses at the base of the volcano. As a consequence, the tensile effect of the surface loading decreases (Fig. 1.9a). The most striking result is the compressive area with the peak stress difference on the

mid-flanks around 300km radial distance over 200km. Near the summit up to 200 km radial distance, radial normal faulting is predicted. This example clearly does not match the structural patterns observed on Alba Patera.

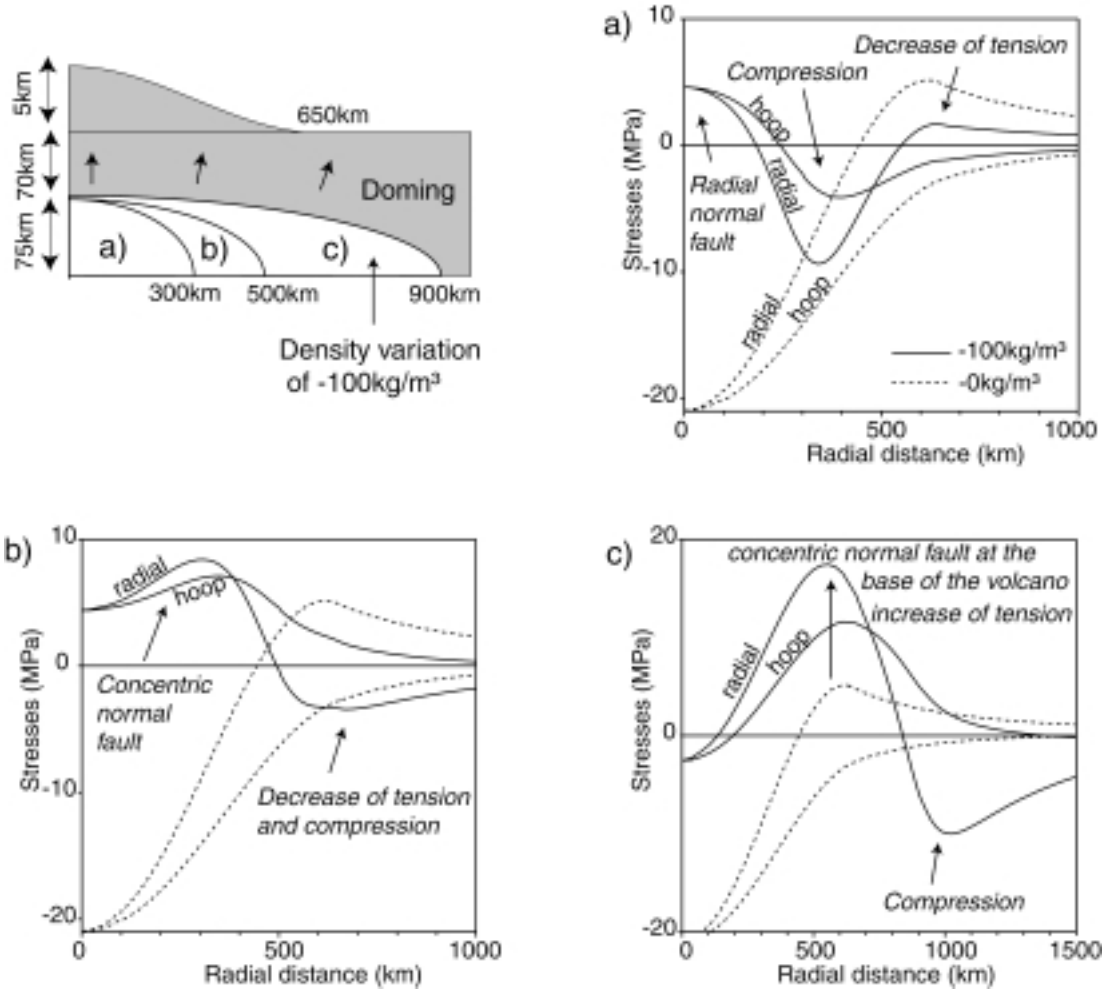

Figure 1.9 - Effect of doming on the stresses caused by the load of the volcano (black line). Dotted lines show the stresses without reservoir inflation. Doming is simulated by a decrease of 100kg/m³ density in the "reservoir" relative to its surroundings. The horizontal radius of the reservoir is respectively a) 300km; b) 500km; c) 900km. The vertical radius is fixed arbitrarily to 75km. The depth to the top of the reservoir is 70km. The surface load is that of a 650km radius and 5km high volcano that has the same density as the crust, i.e. 2900kg/m³.

Concentric orientations of normal faulting on the mid-flanks are found only for doming of an extent similar to the wideness of the volcano load (Fig. 1.9b). In models that only include surface loads, the area of normal faulting is, at the surface, confined to the lower flanks. By increasing the magnitude of subsurface pressures within the core, this area shifts and extends toward the summit. The regions of thrust faulting and strike-slip faulting on the

upper and mid-flanks thus diminish. When the doming mechanism is dominant, the maximum tensile stresses are found at the summit, the faulting becomes radial. However, the net upward displacements, i.e. after the emplacement of the volcano, need to greatly exceed known realistic values to overcome the compression caused by surface loading, i.e. of the order of 5 km vertical surface uplift for a reservoir of a horizontal dimension of 500 km in diameter.

Large uplift, wider than the volcano, augments the possibility of concentric normal faulting at the base and surrounding of the volcano (Fig. 1.9c) whereas strike-slip faulting is easiest to generate without subsurface forces. On the upper and mid-flanks, the regions of thrust faults and strike-slip faults decrease, replaced by normal faulting that remains confined to the base of the volcano. Strong compression is observed at a radial distance equivalent to the size of the reservoir.

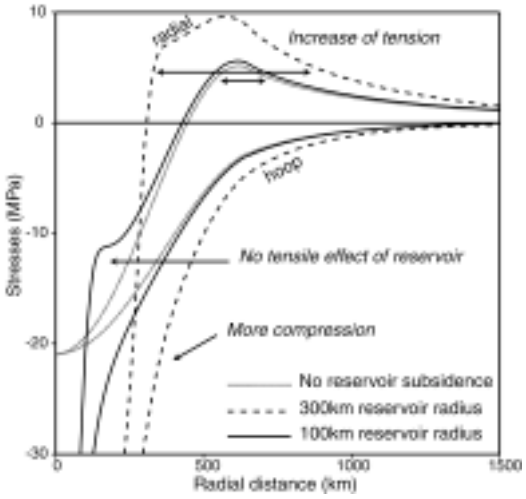

Figure 1.10 - Effects of subsidence on the stresses caused by the load of a volcano. The volcano has a 650km radius and 5km height. Subsidence is simulated by a density increase of 400kg/m³ in an elliptic reservoir of horizontal radius 300km or 100km and fixed vertical radius of 25km. The depth to the top of the reservoir is 20km. Here the radial stress is always greater than the hoop stress.

What happens if surface loading is combined with subsidence?. Around the summit, while doming decreases the compression due to the surface loading, subsidence of the volcanic core augments this effect. A subsidence of small extent relative to the size of the volcano and of realistic magnitude has its tensile effect swept out by the compression induced by the volcano, thus the latter stresses must either be low or relaxed to produce fractures on the flanks (Fig. 1.10). Subsidence confined to the flanks increases the tension at the base of the volcano. For a reservoir of 300km x-radius and 25km z-radius at 20km depth to its top, the tension affects the whole mid to lower flanks.

f) Regional stress combined with doming, subsidence or surface loading

The effects of a regional east-west extension have been combined with the above described mechanisms of subsidence or doming. Where the regional stress is dominant in a E-W rifting environment, the orientation of likely faulting or dyke propagation is north-south perpendicular to the least compressive stress direction. Thus, regional stress can contribute solely to the N-S directed grabens on Alba Patera. For a combination of regional extension and local doming of Alba Patera, the radial normal faults do not change to a concentric orientation. However, if the root of Alba Patera contracts or subsides slightly, concentric fractures can form on the volcano flanks. Structures must present previously concentric orientation under other forces to be still visible after addition with a regional stress.

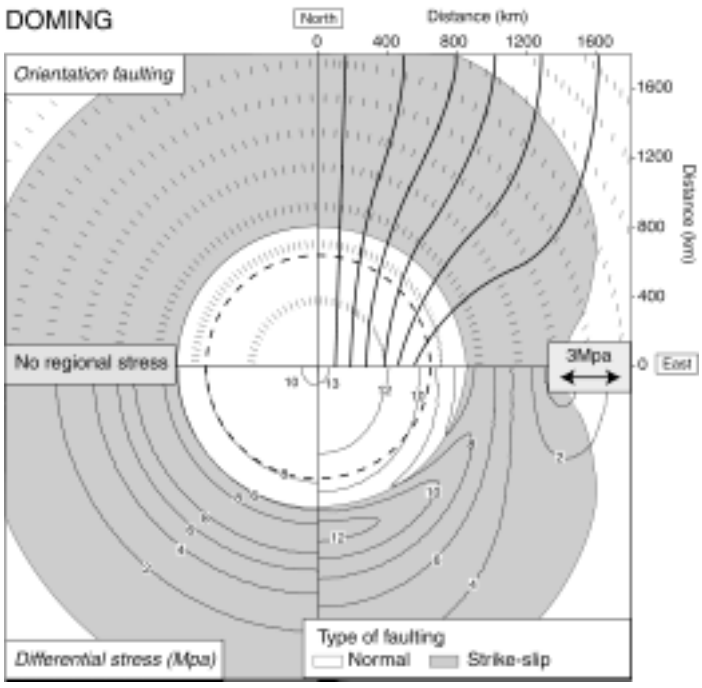

Figure 1.11 - Doming (left) and combination with regional stress (right). Surface view of the orientation of maximum compressive stress σ1 (top), Anderson's faulting types and the differential stress σ1-σ3 (bottom) that maximum indicates position of likely failure. The inflation or buoyancy-driven upward magma migration is simulated by a density decrease of 200kg/m³ relative to the surrounding in a reservoir 1000km and 25km horizontal and vertical radii at 120km depth to its top. The black dashed circle indicates the contour of a volcano 1300 km across representative of Alba Patera. Modelled in a halfspace.

Regional stresses give rise to two typical forms of faulting. Whenever doming or local subsidence accomplishes extension, the resultant fracture types can be discriminated descriptively. A change from concentric near the summit of the volcano to linear or radial at the lower flanks and surroundings is termed a "wristwatch" shape (Fig. 1.12) while an "hourglass" shape characterises a change from linear near the summit to radial orientation at further distance (Fig. 1.11) (Van Wyk de Vries and Merle, 1996). Regional extension may also widen or shorten one region of faulting in disfavour or in favour to another one. The combination of regional stresses with surface loading augments the chance for normal faulting in the whole immediate surroundings of the volcano (Fig. 1.13).

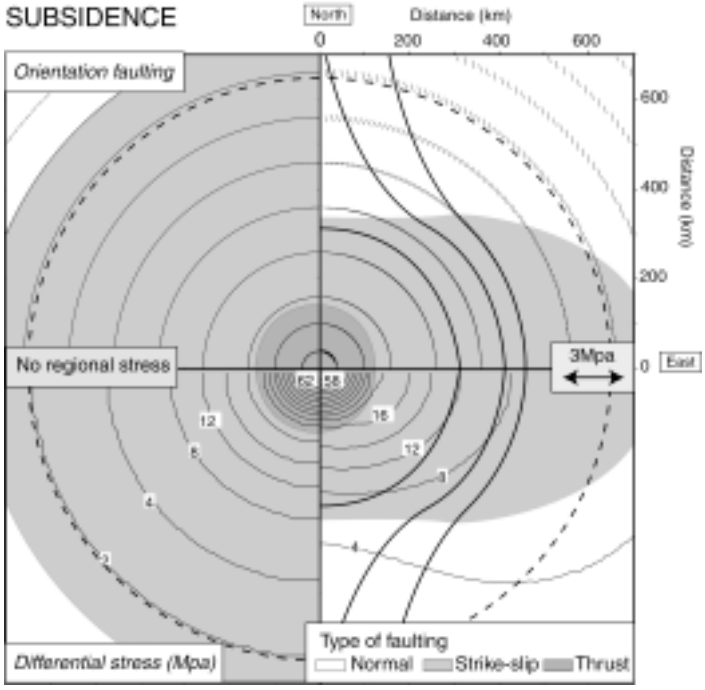

Figure 1.12 - Subsidence (left) and combination with regional stress (right). According to a magma body that contracts on cooling by about 10%, subsidence is herein simulated by a density increase of 10% or 300kg/m³ relative to the surrounding in a reservoir 100km horizontal and vertical radii at 30km depth to its top. The dashed circle indicates the contour of a volcano 1300km across representative of Alba Patera. Modelled in a halfspace.

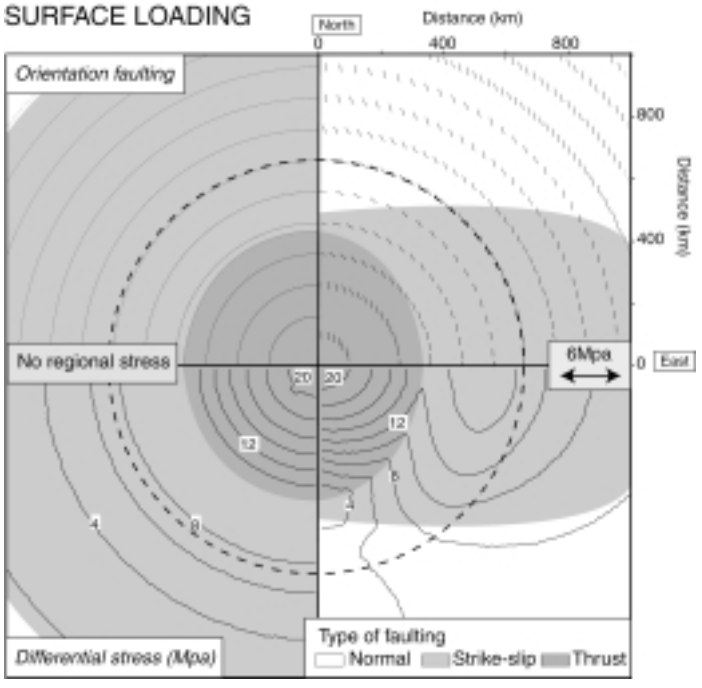

Figure 1.13 - Volcano loading (left) and combination with regional stress (right). The topography has 5km height and 650km radius indicated by the dashed circle. The regional stress has been taken twice the value of the precedent model of subsidence to show that the maximum differential stress is still situated at the margin of the volcano on the east side and the concentric orientation changes quicker to north-south direction around the load (650km here, around 100km distance in Fig.1.12).

Finally, the positions of the peaks of differential stress vary from one point to another one, the stress field is no longer axisymmetric, so that fractures may not contour the whole volcano. The differential stresses for a combination of subsidence and regional stress, for example, are higher on the eastern side than on the northern one having implications for the

appearance of the first fracturing (Fig. 1.12). With increasing subsidence, the eastern part should fail before the northern one.

The above numerical models showed that concentric normal faulting on the upper and mid-flanks of Alba Patera is best simulated if an extended part of the volcanic core is shrinking or subsiding. The mechanism to drain this magma reservoir seems elusive, since the geometric dimensions of the order of hundreds of kilometres do not seem realistic. However a high density intrusive core may account for such relevant subsidence rates and fault migration toward concentric orientations on Alba Patera's flanks. This mechanism was also tested in physical models summarised in the following section.

4. Physical models

The aim of the following sand-box models was to reconstruct the structural patterns caused by uplift or subsidence combined with rifting. Physical models help to understand qualitatively geologic processes and have advantages in illustrating the effects of progressive deformation and showing a plane view of the structures that could arise on the surface (e.g. Ramberg, 1981). The mechanism of local subsidence was simulated by deflation of a sill-shaped rubber balloon filled with air that quantity is controlled by a valve (Fig. 1.14). Circular and elliptic plan-view forms of the balloon have been tested. Such reservoirs were placed in a sand box deformation rig. The box was constructed in a way to produce a regional linear extension (regional stress field). The bottom of the box is an elastic layer that is fixed to two moving piston walls. Moving the walls in opposite sides stretches the bottom layer and the extension is transmitted to the overlying sand. The flat surface of the infilled sand is covered by a fine layer of flour for visualising small-scale fractures.

Since the physical models aimed to reproduce natural-scale dimensions of the order of several hundreds of kilometres, geometric and mechanical scaling to smaller dimensions was necessary. To model in cm or dm size, the material properties must be of orders weaker than the prototype rocks. To obtain similar orientations of fractures, the internal friction coefficient of the analogue material must be constant. Moreover, to simulate natural rocks of strength ratios between 10e6-10e7Pa (Schultz, 1996) in laboratory scale, low cohesive granular materials best fulfil mechanical scaling (Ramberg, 1981). In the previous analogue experimental studies, dry eolian sand has been commonly used as analogue materials, and mechanically tested for analogue scaling purposes (Cobbold and Castro, 1999).

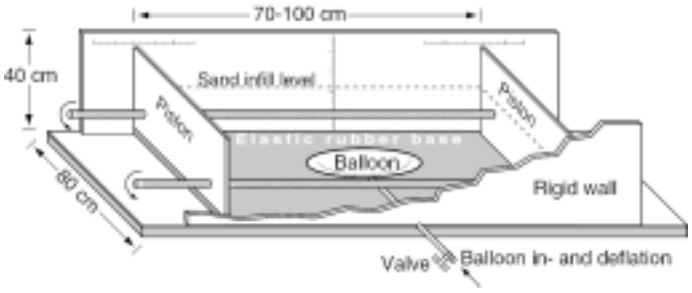

Figure 1.14 - Experimental set-up for physical models. See text for description

In these experiments, a 0.4mm grained quartz sand, for which the mechanical values were determined in direct shear tests. Cohesion was ~50Pa, with a coefficient of internal friction of $\mu s=0.6$, obtaining fault inclinations of 33° relative the maximum compressive principal stress $\sigma 1$. As in all physical models some simplifications were necessary, e.g. the gravity acceleration was not scaled and the deflated balloon was considered as an analogue to any subsidence mechanism produced within a volcanic core. The regional extension of the sand box was measurable as a bulk widening per time unit, however accurate values for Alba Patera are unknown. During balloon deflation, an overall bulk extension of 10% was chosen to be appropriate. Prior to balloon inflation or contraction, a regional stress field was built up by 4% extension of the pistons. Subsequently reservoir deformation and regional extension was simulated simultaneously. Surface deformation was measured and photographed, afterwards compared to the numerical models and the prototype Alba Patera.

Linear extension with doming leads to structures on the surface parallel to the regional trend at far distance from the reservoir. Approaching the reservoir, they converge toward the summit. On the doming centre, multiple blocks form. The general arrangement strongly mismatches the observed structures on Alba Patera and thus will not be further discussed.
With the deflation of the balloon, two sequences of fracturing have been observed. With increasing subsidence, fracturing first appears following the modelled regional trend, i.e. mostly linear in north-south direction (Fig. 1.15). Near the reservoir, fractures are concentric to the reservoir. Continuity between concentric to linear structures are found for those which are farther from the reservoir centre. In further steps, new fracturing occurs in directions that are not favoured by the regional stress field, transecting the linear structures. Multiple linear fractures are seen all around at the periphery. The regional stress affects the timing of fractures formation above the reservoir but doesn't modify the general orientation of these fractures. Explicit concentricity is obtained all around the circular reservoir while the structures are more elongated for the deflation of an elliptic reservoir whose longer radius is perpendicular to the extension.

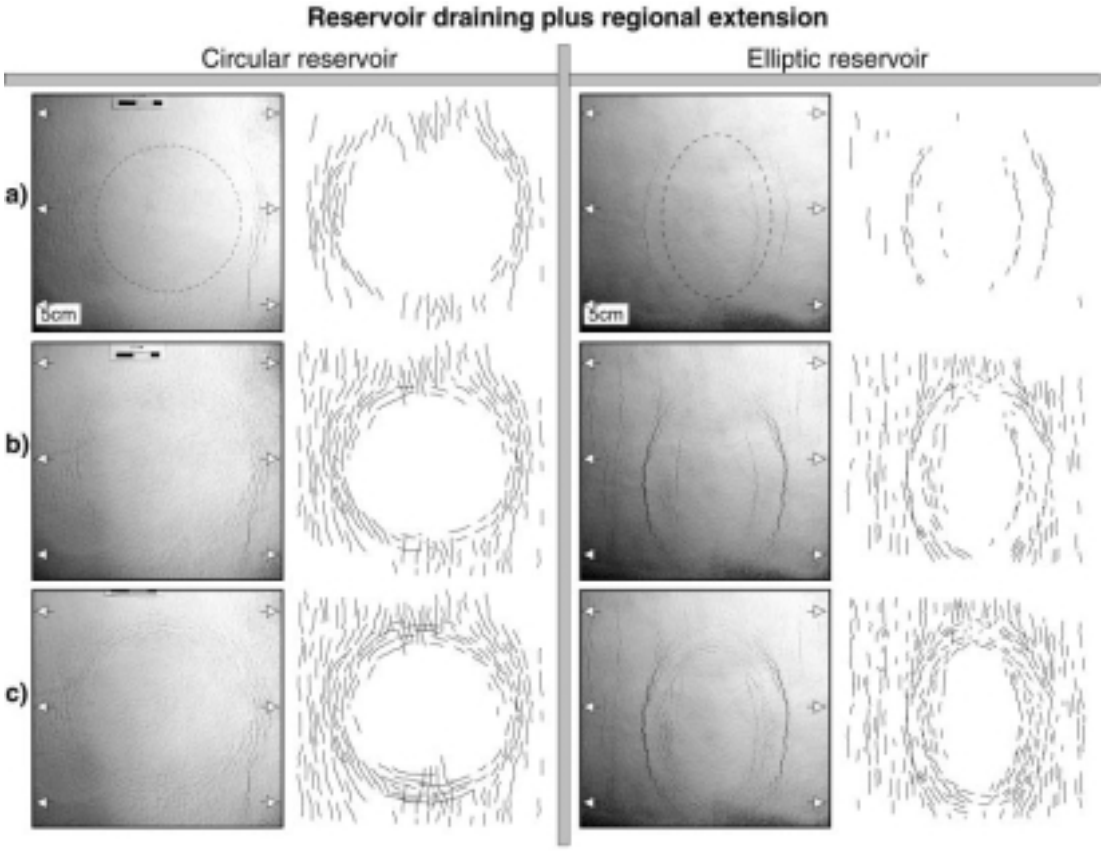

Figure 1.15 - Physical models of reservoir draining plus regional extension. A circular (left) and elliptic (right) plan-view shape of the balloon have been tested. This shows the changes from linear trends to increasing concentricity with time.

For the oblong reservoir, two sets of concentric fractures are observed (Fig. 1.15). The radius of the reservoir is situated within this range. The outward set is composed of unique long and large fractures which become more marked with increasing subsidence. The characteristics of the set closer to the summit do not change, but new small and numerous similar fractures appear at further radial distances to join with the other set of fractures.

5. Discussion, model comparisons to Alba Patera

A comparison between the regions of faulting predicted by the numerical models and the visual arrangement of lineaments seen on Alba Patera can lead to a better understanding of this remote volcano. The stress field associated to the volcanic loads is well constrained as the topography has been accurately known since the Mars Global Surveyor mission. In contrast, in the absence of information about the processes at depth and the characteristics of the magma reservoir, it is possible to vary the dimensions of uplift or subsidence associated to deep or shallow events in order to generate correlations with the observed structures.

The early stage of Alba Patera: a local hotspot-generated dome?

The Tantalus Fossae and Ceraunius Fossae have a general N-S trend that was related to the regional stress field from the Tharsis bulge (Turtle and Melosh, 1996; Heller and Janle, 2000; McGovern et al., 2001). The combination of doming with a regional east-west extension gives an hourglass pattern of faulting (Fig. 1.11). Increasing the regional stress changes the orientation to N-S and augments the differential stresses. This could explain the set of linear and numerous grabens of the Ceraunius Fossae in the south of Alba Patera which are closer to the Tharsis bulge and are thus subjected to higher E-W extension. However, doming local to Alba Patera can not be discriminated by these structures. The Ceraunius Fossae appeared contemporaneously with the Archeron Fossae on the western side and Tempe Terra on the eastern side, associated with regional tectonic activity centred on the Claritas area (Plescia and Saunders, 1982; Plescia, 1991; Schneeberger and Pieri, 1991; Anderson et al., 2001). The Ceraunius Fossae could be thus solely attributed to the regional stress field.

The Tantalus Fossae formed much later than the southern counterpart (Anderson et al., 2001). Their particular length is in the order of 1000km, genetically interpreted by underlying dike intrusions (McKenzie and McKenzie, 1992; Wilson and Head, 2002). In such cases, a tensile tectonic stress field is not necessarily indicated, since the surface extension above a dike is a local phenomenon.

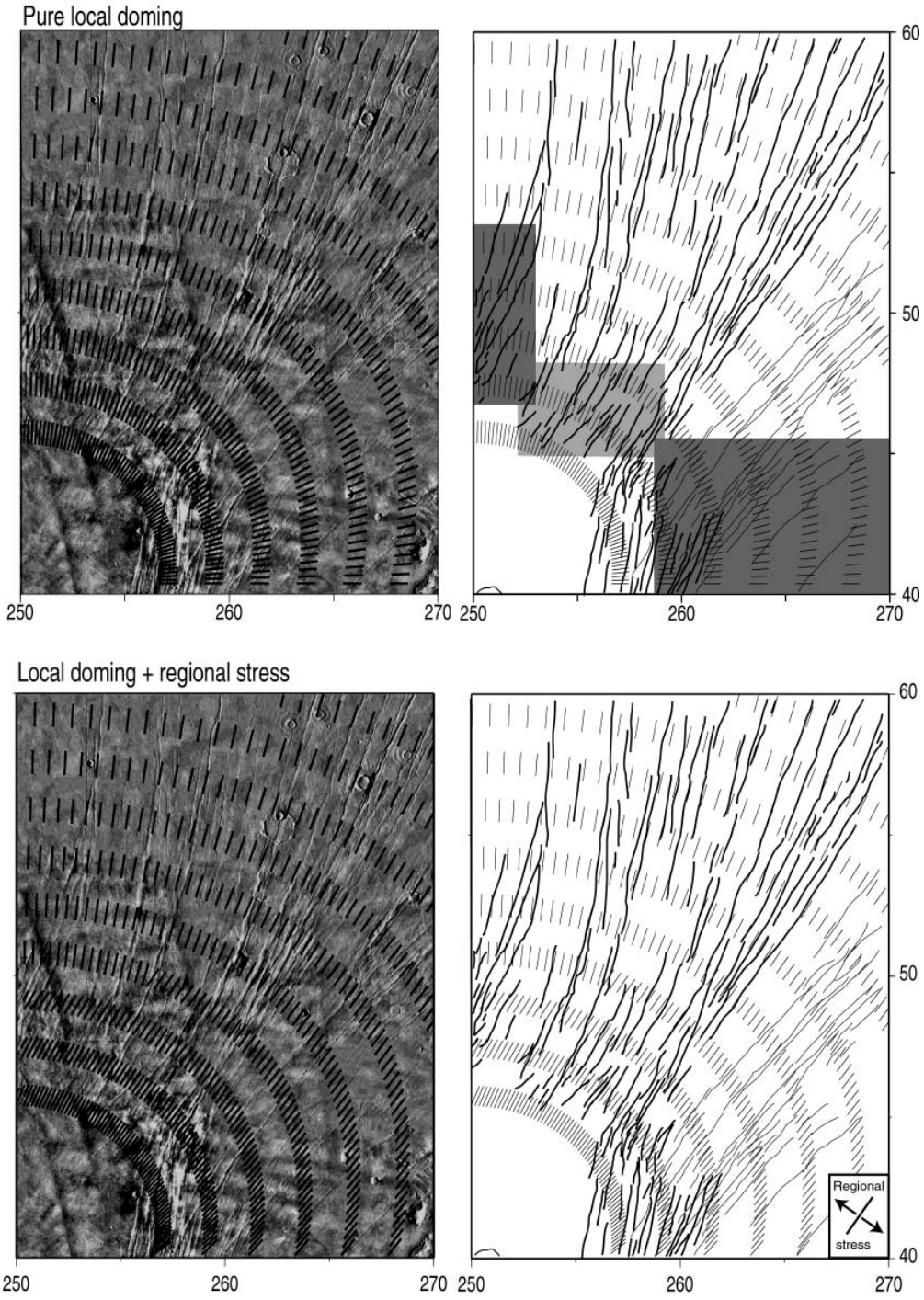

Figure 1.16 - Predicted faulting by doming superposed with Alba Patera Viking mosaic. The gray areas indicate the regions of poor fit between the models and observation. The thin lines are faulting that are related to regional structures. Below, the local doming is combined with an SW-NE regional extension south of 50° latitude. In order to compare the numerical results with the observed structures, the coordinates (x-y) of the models have been changed in units from kms to degree and from aerocentric to areographic system (the planetographic system). The GMT plot is in Mercator projection. See figure 1.17 for the orientation of regional extension.

Dikes are elongate emplacements of magma into the crust following the direction of least compressive stresses or weak zones (Anderson, 1951). The dimensions and distributions of grabens and dykes are both controlled by the magma source pressure (Anderson, 1936; Smith and Bailey, 1968; McKenzie and McKenzie, 1992). Small viscosity and small thermal conductivity of the melt and wall rock may trigger a considerable extension before cooling of the radial dikes from their source (McKenzie and McKenzie, 1992). At a sufficient distance to the centre, the trend of the radial dikes follows the direction of the regional stress (McKenzie and McKenzie, 1992; Glen and Ponce, 2002). This is also shown by the numerical models (Fig. 1.11). However, in the case of Alba Patera, the Tantalus Fossae present a trend strictly radial to the volcano at far distance which can not be resolved with an added extension related to the broad Tharsis centre. This is however well explained by pure local doming (Fig. 1.16). The regional stress must have been of negligible importance relative to the local doming in these northernmost areas.

Pure doming produces however a poor fit to the structures on the northern side of Alba Fossae and on the eastern side (Fig. 1.16). These later structures belong to the neighbouring Tempe Terra and the Tharsis central area (Tanaka and Golombek, 1989; Scott et al., 2002; Mege and Masson, 1997) (see also Fig. 5 in the introduction). Similarly to the formation of the Ceraunius Fossae, the more recent structures of Alba Patera must be resituated in their regional context at the time of their formation. Figure 1.17 illustrates the regional stress field in a stage contemporaneous with the radial Tantalus Fossae, that could be responsible for the eastern Catenae and the multiple fractures of the Mareotis Fossae from the near Tempe Terra region (Mege and Masson, 1997a). There is a mutual influence of the local doming of Alba Patera and the regional stress. The regional extension was likely a consequence of the Tharsis Megaplume and associated surface deformation. Towards the centre of the Tharsis dome, extension was favoured in radial directions.

In the periphery of the Tharsis dome, i.e. in the region where Alba Patera formed, a Tharsis-circumferential extensional stress field dominated. As seen by radial lineaments of the structural dome of Tharsis, the influence of this regional extension decreases towards the northern Alba Patera region. Adding a NW-SE regional extension to the local doming in the areas below 50° latitude, where it is thought to be significant, thus significantly improves the correlation between the numerical models and the radial northern features (Fig. 1.16).

This can explain the confinement of the Tantalus Fossae to the eastern side, the curvature of the structures on the northern mid-flanks of the main shield and finally the Catenae and multiple fractures on the eastern side. The structures on the northern side of Alba Fossae present also similarity with the wrist-watch shape predicted to form by combination of subsidence and E-W extension (Fig. 1.3). This would moreover indicate a progressive

change of stress field from doming (hourglass pattern) to subsidence (wrist-watch shape), which will be further discussed in the section devoted to the models of subsidence.

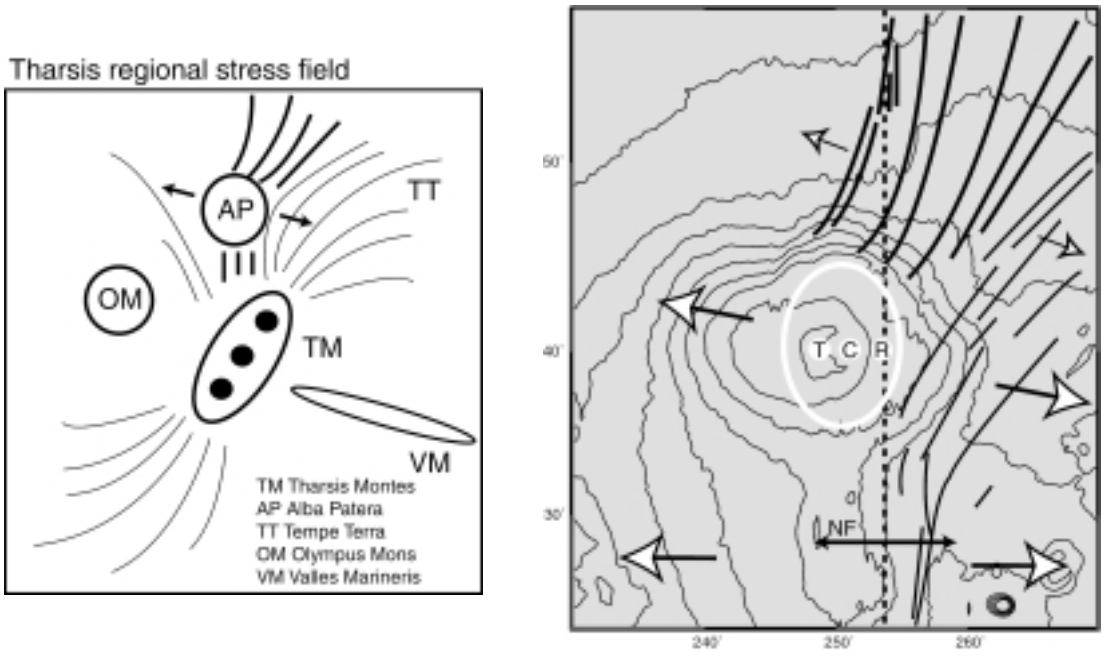

Figure 1.17 – Regional Tharsis stress field. (a) Left, the regional stress is centred on the rift that gave rise in later stage to the linear Tharsis Montes (TM) and in earlier stage to numerous radial structures in the regions of Alba Patera (AP) and Tempe Terra (modified after Mege and Masson, 1997). There is an interplay between the local stress field of Alba Patera and the regional deformation. The structures on the north of Alba Patera (thick lines) do not follow properly the regional trend, i.e. they are strictly radial to Alba Patera, implying a local doming of AP. However, the grabens are oriented and confined to the east that indicates a regional effect. The trend of the long radial structures (fine lines) that extend from the Tharsis region to the eastern side of Alba Patera is modified by the local situation of Alba Patera. (b) Right, the regional stress is reproduced on Alba Patera. The black arrow indicates the orientation of the east-west previous regional extension in Noachian epoch and the extent of the subsequent Ceraunius Fossae. The regional centre is thought to lie in the Claritas region (Fig. 5 of the introduction). The white arrows indicate the younger regional extension presented on the right. Toward the north, the regional stress wanes shown by the northernmost grabens radial to Alba Patera (smaller arrows). Different centres are found on Alba Patera. T is the topographic summit. R corresponds to the regional centre indicated by the middle line that cut the Ceraunius Fossae, and the linear northernmost grabens of Alba Patera (dotted line), C is the centre of the concentric grabens outlined by the white ellipse, i.e. the summit area surrounded by the concentric grabens, supposing that many grabens of the Alba Fossae on the western side were covered by lava flows.

Relation of the radial Tantalus Fossae to the volcanism of Alba Patera.

Radial structures reinforce the idea that Alba Patera was the centre of an autonomous hotspot (Janle and Erkul, 1991; Mège and Masson, 1996; Banerdt et al., 2000; Anderson et

al., 2001). A general understanding of the initial processes that gave rise to Alba Patera can be outlined from the forms of volcanism observed in relation to the tectonic structures and from natural examples on the Earth. Long linear dikes are often curved near a volcanic centre e.g. Alpha Regio on Venus (McKenzie and McKenzie, 1992), in the Spanish Peaks region of south central Colorado (Muller and Pollard, 1977), the MacKenzie Dyke swarms in western Canada (Fahrig, 1987) or the Northern Nevada rifts associated to the Yellowstone hotspot in western north America (Glen and Ponce, 2002). The widespread volcanism of the earliest phase of Alba Patera may be comparable to the flood basalt provinces commonly associated with an initial hot-spot and continental rifting episodes (Richards et al., 1989; Glen and Ponce, 2002). The actual dimensions of the flood basalts beneath Alba Patera are unknown. Concerning their widespread distribution, they surely represent the beginning stage and highly productive event of a billion-year active volcanic field. Probably coupled to the eruptivity, giant dike swarms formed above the dome, presumably trapping large volumes of magma as intrusives disclosing the fractures in the stressed crust. Since the effects of mantle upwelling are well visible on the surface, the question arises of the nature of the “Alba Patera Hotspot”. Geographically, the vicinity to the Tharsis Bulge can not be neglected, indicating a genetic interaction to be plausible. The Tharsis mega-plume formed a wide uplift and extension, affecting the area of Alba Patera prior to its first growth episodes. An interesting but puzzling question is, whether the Alba Patera hotspot rooted deep in the mantle as a small or parasitic blob of the Tharsis Plume, or instead was a consequence of crustal deformations and shallow vertical tectonics in the crust and uppermost mantle. For a less coupled, individual origin of a local hotspot beneath Alba Patera various principles and mechanisms could perhaps be (jointly) responsible, such as a detached lower crustal segment sweating in the upper mantle, or decompressional effects beneath a thinning crust.

Although the adjacent Alba Patera has been the locus of high volcanic and tectonic activity, the Ceraunius Fossae were surprisingly stable except for some reactivated faulting (Plescia, 1991). This suggests an increase of crustal strength in this area. Since intrusives are mechanically more resistant than eruptive products, the relative permanence of the Ceraunius Fossae could be explained. It is possible that this pre-existing construction influenced the location of Alba Patera to its northern portion. The formation of Alba Patera on the northernmost side of the Tharsis bulge is probably not a coincidence. A relative tectonic symmetry is found between the north and south of Tharsis (Fig. 1.17). However, thicker crust toward the south (Zuber et al., 2000) might preclude significant eruptions associated with southern giant grabens supposed to be related to dike swarms from the Tharsis superplume (Wilson and Head, 2002).

The middle stage of Alba Patera: local subsidence due to an intrusive core?

The best correlation for the younger concentric Alba Fossae and Tantalus Fossae has been found with models of subsidence. The general behaviours inferred for subsidence combined with a regional extension were reproduced with two different methods. Linear extension with subsidence leads to structures similar to the wrist-watch shape that characterises the concentric to linear grabens of Alba Patera. The two time sequences obtained with increasing subsidence in the analogue models correlate strikingly to the observations on the northern side of Alba Fossae with concentric grabens, frequently in en-echelon fashion, that overlap older more linear structures (Fig. 1.18). Great concentricity is obtained all around the circular reservoir. An even better correlation has been found with the deflation of the elliptic reservoir. By simultaneously increasing both the subsidence and the regional extension, concentricity augments, i.e. younger fractures are more concentric than older ones. A similar relation is seen on Alba Patera.

In numerical models that use Anderson's theory of faulting as their basis, strike-slip faulting is predicted instead of normal faulting. Analogue models show that the crust would likely fail in normal faulting. Since dikes follow the direction of minimum compressive stress their actual orientation correlates well with the observed structures. The absence of strike-slip faulting has been predicted in other works of surface loading (Tanaka et al., 1991; McGovern and Solomon, 1993; Williams and Zuber, 1995; Roger and Zuber, 1998). They might have been inhibited by the initial formation of tension cracks or normal cracks which reactivate (Tanaka et al., 1991; McGovern and Solomon, 1993) when for example the volcano radius was smaller or also may be buried by younger lava flows (McGovern and Solomon, 1993). The presence of a highly fractured upper layer 1-3km thick or megaregolith on the Moon where the fault may initiate reduces significantly the prediction for strike-slip faulting (Golombek, 1985). Here such lower strength was considered by taking a Young Modulus of 50 GPa. The most probable explanation has been proposed by Freed et al. (2001), who suggested that the Anderson theory of faulting doesn't take into account the regions of mixed mode of faulting which would lead to a region of pure strike-slip faulting of half the width predicted by Anderson (1951).

The best-fit model: Sinking of the crust can be caused by magma retreat from a magma chamber between eruptive stages or by an increase of density during the cooling of magma or surrounding warm area (Walker, 1987, 1992; Stofan et al., 1991). Volcanic rift zones on ocean island volcanoes are thought to subside due to their incremental density increase, restricted relative to the regions were dominantly less-dense eruptive products accumulate (Walker 1992). Solidifying magma bodies contract since crystallisation processes are

accompanied by crystal contraction and the release of gas species, which depends on the amount of crystallisation as a function of time (Tait et al., 1989).

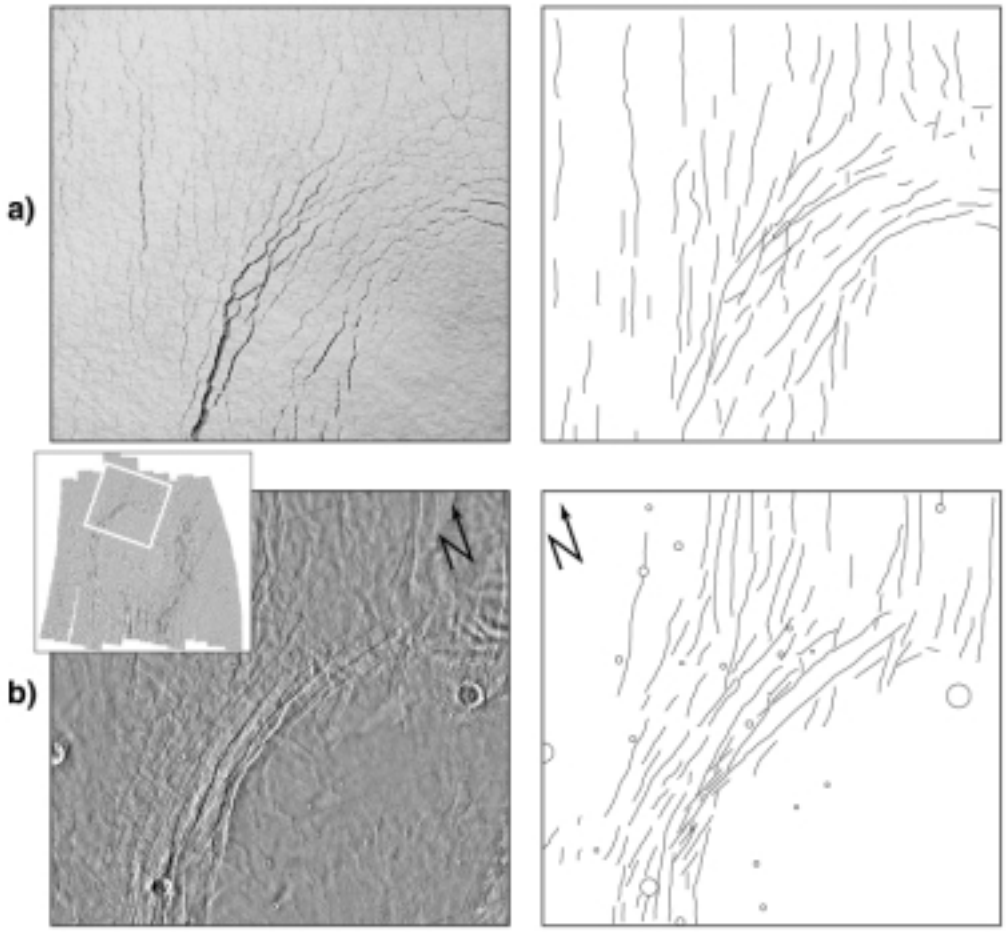

Figure 1.18 – Subsidence a) simulated in physical models and b) observed on Alba Patera. The northern part of Alba Fossae on the western side of Alba Patera. Subsidence simulated in physical models

Density changes within cooling magma bodies are typically within a range of 50-200kg/m³ (Williams and McBirney 1979). Cooling of an intrusion complex may cause significant volume decrease and thus density increase in the core – a process that is proposed to be realistic for this specific case because Alba Patera was the locus of strong intrusive activity (see above the discussion with doming, regional extension and the old radial and linear Ceraunius Fossae and Tantalus Fossae). Accordingly, intrusive activity was an essential mechanism in the development of the volcanic field of Alba Patera. Moreover, widespread distribution of

the concentric grabens, from the upper to the mid-flanks of the volcano, indicates a vertical intrusion that forms the source of subsidence by cooling. Since the concentricity of the fractures becomes better pronounced with time, the influence of subsidence was active and even enhances incrementally. A small vertical size of the high density core results in a short range of tensile stresses on the surface and necessitates a particularly large horizontal extent similar to the radial distance of the farthest grabens, i.e. up to 300 km. Neither such magma chamber size are known on the Earth nor similar longevity (2000 Mys) of chambers are realistic. Magma chambers on Earth are active just an instant if compared to the long live span of a volcano (cf. Marsh, 2000), even long-lived magma reservoirs are active for time periods on the order of a few kys only.

Alternative mechanism: Previous models of Alba Patera predicted compressive stresses surrounding the concentric grabens at a farther distance from the summit (Scott et al., 2000). These are however not present on the lower flanks neither at the surrounding of the volcano. The models of subsidence predict compression on the summit area which may be in concordance with the wrinkle ridges observed on the summit cone (Fig. 1.3). A cooling intrusive core can well explain the absence of compressive structures on the flanks and also the increase of magma viscosity with time observed in the shortening of lava length (Schneeberger and Pieri, 1991).

Concentric fracturing in volcanic regions has been reported from several areas on Earth and other planets. This geometry however can have various origins. Analogue experiments of the evacuation of an elongated balloon reservoir (Mège et al., 2000) have been suggested to explain the grabens and troughs of Noctis Labyrinthus in central Tharsis (see Fig. 5 of introduction for location). They show the formation of reverse faults bordering a central collapse whose size is inversely proportional to the depth of the reservoir. Numerous normal faults forming the grabens appear parallel to the central sag and are located at greater distances for a more deeply situated reservoir. For a circular chamber, the observed structures are similar but have a concentric shape corresponding to the cavity (Walter and Troll, 2001). This is very similar to the linear and circular troughs associated to a volcanic centre and imaged on Venus (McKenzie and McKenzie, 1992). The concentric dykes, geometrically correlating to ring-dykes (Anderson, 1936), are thought to arise in response of deflation creating circular gaps subsequently filled by new arrival of magma and explaining the intersection of dikes at high angles (Anderson, 1936; McKenzie and McKenzie, 1992).

Other types of forces that would lead to concentric normal faulting can be found. The piston effect is a particular case (McGovern et al., 2001). Numerical models with an elastic half

space show that if upward pressures applied on elements at the same initial depth have identical values over a distance, a simple translation of the crust similar to the push of a piston occurs with deformation concentrated at the boundary of the reservoir and small or even without deformation above it. With this type of subsurface load, correlation of fractures with maximum stresses would be therefore found only for a reservoir size equivalent to the radius of the observed fractures. While the predicted concentric structures fit the observed structures on Alba Patera, the piston behaviour is probably not realistic because of various reasons. First, it's unlikely that the crust undergoes less deformation above the area of maximum external forces. Secondly, this would imply that the reservoir developed identical characteristics over 200-300km radial distance corresponding to the locus of observed grabens, i.e. that the stress field relations within the volcanic edifice must be unusually homogeneous. Third, the structural study that based on surface imaging revealed a long-term incremental change from radial to concentric lineaments, and not a single or short event due to a piston like deformation above a sill. This type of deformation has been thus not further studied. Gravitational spreading and horizontal traction of a plume at the base of the lithosphere are both processes that should lead to concentric normal faulting on the summit and compression at far distance. These can be ruled out, the first due to the low aspect ratio of Alba Patera 7 km high and 1300 km across (Thomas et al., 1990), the second because horizontal traction must be accommodated by significant compression at the periphery which is however not observed around Alba Patera.

The development of Alba Patera after concentric lineament establishment

As seen on mosaic images, during the late stages of concentric fracturing the summit cone formed on Alba Patera (Fig. 3 in the introduction). The summit cone is characterised by a net increase of slope inclination compared to the underlying main shield, implying a slightly different viscosity and/or magma composition. Based on overlapping of fractures and lavas flows, Ivanov and Head (2002) inferred a time relationship with the summit cone which formed during and after the concentric grabens. Scott (2000) suggested the summit cone being a different magmatic source than the main shield, leading to such morphological change.

Combined concentric and radial lineaments have been observed on the Earth, e.g. on the Galapagos Islands of Isabela and Fernandina (McBirney and Williams, 1969). Gently dipping lower flanks, relative steep upper flanks and a flat zone similar to so-called "overturned soup plate" volcanoes are morphologically similar. However, based on crater counts and relative lineament ages, the formation of the circumferential lineaments on Alba Patera established clearly in the later history of the volcanic shield. On the Galapagos volcanoes, concentric and radial dike intrusions emplaced synchronously or in multiple alternating stages (Chadwick

and Dieterich 1995). Thus the mechanisms behind inverted soup bowl volcano shapes can be varied.

The summit cone on Alba Patera indicates a centralised conduit, apparently not influenced by circumferential fractures on the summit rim. The stratovolcanoes somma-Vesuvio in Italy and Pico do Fogo in Cape Verde are illustrative examples of strato-volcanoes forming on a relatively flat and wide shield inside a caldera-like depression. The caldera surrounding Pico do Fogo formed by lateral sector collapse rather than an ash-flow collapse caldera (Day et al. 1999). Contrasting to such cataclysmic events on earth, the caldera of Alba Patera appears to be the result of a smooth change toward higher concentricity with time, in which later the summit cone grew. However morphologically similarly to Fogo and Vesuvius sommas, the cone is characterised by steeper flanks and relatively circular shape. Such adjustment of the volcano architecture may perhaps be associated with a change of magma composition and viscosity. On Alba Patera's summit cone a huge shallow magma chamber existed at time of summit cone formation, as partially preserved by the large caldera depression 140km across on the top.

6. Summary and conclusion

The lineament study of Alba Patera presents a progressive change from radial to increasing concentricity of the fault pattern. This is accompanied by a decrease of the volcanic feeding rate and an augmentation of the erupted lava viscosity with time. Based on the Finite Element models developed in this study, the tectonics and volcanism at Alba Patera in the first stages are well explained by doming and subsequent rifting caused by a hot thermal anomaly. The addition of both regional and local upward movements shows predicted faulting similar to the radial Tantalus Fossae. Subsidence mechanisms have been reproduced using both physical and numerical methods. This can lead to the concentric pattern that characterises the Alba Fossae and Tantalus Fossae on the mid and upper flanks of Alba Patera. Continuity of these structures with radial-linear fractures indicates earlier phases when subsidence and regional extension were processes of similar magnitude. With on-going subsidence, new fractures appeared with a pattern of increasing concentricity.

A general understanding of the processes that gave rise to Alba Patera can be outlined from the forms of volcanism observed in relation to the tectonic structures and from natural examples on the Earth (Fig. 1.19). In early stages flood basalts formed; during hotspot volcanism in the field of Alba Patera intrusions healed the widening crust. The root of the growing volcano was composed increasingly of intruded material, partly still parallel to the

regional rift zone, but gradually more in a concentric fashion around the mid-flanks of Alba Patera. The mechanism of circular fracturing was unlikely a process of short-time intrusive or tectonic varieties. Moreover, this development reflects a long-term mechanism active during several hundreds of Mys, which typically accounts for accumulation or mantle dynamic processes. An increase of the density of the mid and lower crust below Alba Patera may likewise have formed a stress field superposing the regional tectonics, which increased with ongoing magmatic activity. The fact that the steep summit cone represents the final stage of a long volcanic evolution seems plausible in this dynamic concept. A more evolved magmatism often reflects a decrease in magma feeding rates and higher viscosities of the lavas and thus steeper morphologies. Likewise the intrusive activity beneath Alba Patera lessened, otherwise the concentric fracturing must have been active in the younger history of the edifice breaching the summit cone.

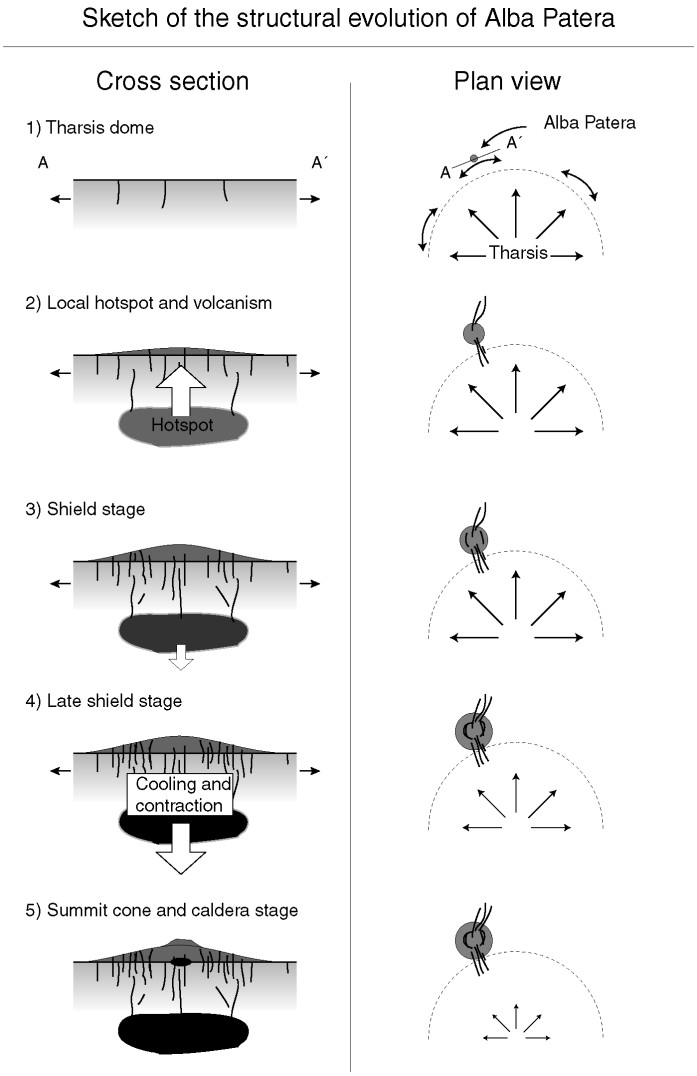

Figure 1.19 – Geodynamic model of Alba Patera.

Part II

Plate flexure on Alba Patera

Absence of bending signatures explained by FE models

Lithospheric flexure on Alba Patera, Mars

Absence of bending signatures explained by FE models

1. Introduction

Lithospheric flexure under volcanic loading has been discussed to explain distinctive concentric grabens, as e.g. visually observed at Nyx Mons, Venus (Rogers and Zuber, 1998), around Elysium Mons (Comer et al., 1985; Hall et al., 1986) and also on Alba Patera on Mars (Turtle and Melosh, 1997; Heller and Janle, 2000). Using more accurate data of the recent Global Surveyor Mission, the loading-induced hypothesis of concentric fracturing can not be proven for Alba Patera (McGovern et al., 2001). Volcanic loading on a thin plate overlying a fluid or viscous mantle causes a downward flexure of the plate under the edifice (Fig. 2.1a). Because of the rigidity of the plate, the downward flexure extends to a certain distance around the volcano, depending on the plate thickness and the volcanic load, creating a moat subsequently filled by sedimentary or volcanic deposits (Fig. 2.2). The flexural depression is again surrounded by a topographic high or bulge. This structure is widely observed on Earth (Moore et al., 1989; Wolfe et al., 1994), and also thought to occur on Mars (Banerdt et al., 1982; Janle et al., 1984; Janle and Meissner, 1986; McGovern and Solomon, 1993) and Venus (McGovern and Solomon, 1997). Globally, in the upper layers of a flat plate, radial stresses are compressive where the lithosphere subsides while they are tensional where the lithosphere uplifts, promoting a restricted extensional regime around large volcanoes (Fig. 2.1b) (Banerdt et al., 1982; Janle et al., 1984; Comer et al., 1985; Janle and Meissner, 1986). Therefore, concentric grabens are likely to form at the bulge.

Although recent MOLA topographic data have now a vertical precision up to 37 cm and a spatial resolution up to 0.23 km, a moat and bulge are not observed around Alba Patera (Smith et al., 2001). Alba Patera has moreover no positive gravity anomalies that would be the expression of bulge and density contrasts along the crust-mantle boundary (Janle and Meissner, 1986; Feighner and Richards, 1994). These are found on other volcanoes on Mars, e.g. around the Tharsis Montes edifices (Zuber et al., 2000). However a few grabens of concentric orientation are observed at the western base of the main Alba Patera shield,

which could be related to volcanic loading (e.g. the Cyane Catenae, the Cyane Fossae (Fig. 1.1)). Most of the concentric lineaments, however, are located on the middle or higher edifice flanks, and thus must have formed by a different mechanism.

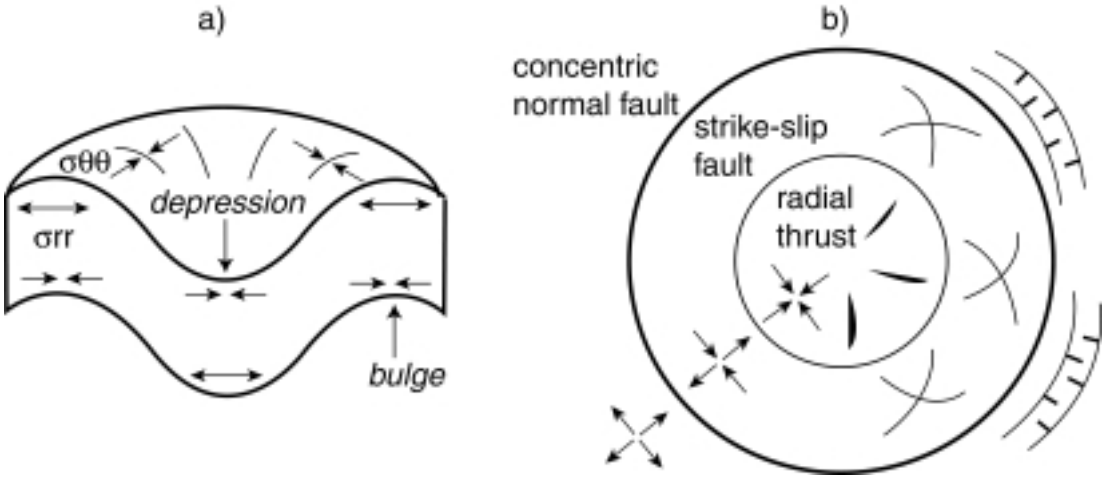

Figure 2.1 – a) Schematic 3D view of plate flexure and stress components due to volcanic loading. Arrows pointing to opposite direction indicate tension, compression otherwise. σrr is the radial stress and σθθ the tangential or hoop stress. b) Plan view of stress orientations on the surface and illustration of corresponding faulting. The volcanic foot is situated approximately at the boundary between strike-slip faults and normal faults. Volcanic loading on a thin plate overlying a fluid or viscous mantle causes a downward flexure of the plate under the edifice. The flexural depression is filled by volcanic material and is surrounded by a bulge. In the upper layers of a flat plate, the radial stresses are compressive and tensional where the lithosphere subsides or uplifts respectively. Therefore, concentric grabens are likely to form at the bulge. Modified from Banerdt et al. (1991) and Melosh (1978).

The aim of this study is to understand the absence of moat and bulge and the small presence of concentric grabens around Alba Patera. Using the Finite Element program TEKTON (Melosh and Raefsky, 1983), the lithospheric flexure induced by the load of Alba Patera is reconstructed to estimate the values of displacements and stresses. The effects of varying the plate thickness, the dimensions of the load, the elastic parameters, and the densities of the crust and mantle are also studied.

Alba Patera has an average radius of 650 km. Whenever a volcano displays a large size in comparison to the planet's radius, the membrane response due to the sphericity of the planet must be added to the bending deformation of the plate (Turcotte et al., 1981; Willeman and Turcotte, 1981, 1982; Janes and Melosh, 1990). The influence of a viscoelastic behaving lithosphere regarding relaxation of stresses is analysed, and a hypothesised support by upward forces at depth (magma chamber, underplating or plume) is considered. The results of the numerical models are compared to the observed structures on Alba

Patera. Based on major similarities between the models and the natural case, constraints can be established on the various parameters used knowing their theoretical effects. This understanding is widely transferable to related processes on Earth and other planets.

2. Geometry and mechanical parameters

The following section describes the geometric and mechanical parameters used in the numerical experiments.

Geometric parameters

The topography is modelled with an axisymmetric cosine form, which represents the smooth shape of Alba Patera better than a cone (Fig. 2.2). The main contributor of the surface load is supposed to be the middle member formation of late Hesperian time (Tanaka et al, 1991), for simplification it will be called the main shield. A maximum elevation of 5 km for the main shield is chosen, which approximates the elevations on the west and east sides. For axisymmetric models, the topographic protuberance on the south of Alba Patera along the Ceraunius Fossae is not considered. Based on the topographic grid from the MOLA data, the diameter of the main shield of Alba Patera is measured about 28° along east-west direction and only 14° in north-south direction. This corresponds to the contour levels 800 m on the west and east along 40° latitude, -500 m on the north and 3500 m on the southern sides along 250° longitude. Most of the models are calculated with the maximum radius, i.e. along E-W direction where grabens due to surface loading are the most expected. Ten degrees being 455 km at 40° latitude for a spherical Mars, this gives a round-off radius of about 650 km for the entire volcanic edifice. The effects of varying the radius and height is shown in the section 5.

Mechanical parameters

To simulate the deformation of the region of Alba Patera, the mechanical variables used are the crust and mantle densities, the Young's Modulus and the Poisson's ratio. Various values of crust and mantle densities are found in the literature: McGovern et al. (2001) uses 2800 kg/m³ and 3300 kg/m³ respectively, Cattermole (1992) 3000kg/m³ and 3800kg/m³, Zuber (2001) and Smith et al. (1999) gave the values of 2900 kg/m³ and 3500 kg/m³ from tracking the motion of the Mars Global surveyor spacecraft. The intermediate and most recent values of densities are chosen (Table 2.1). For terrestrial rocks, the Young's Modulus E is typically in the range of 10 to 100 GPa (Turcotte and Schubert, 1982). These values are determined by axial test loading of small-scale specimens. This is the amount of shortening

or lengthening parallel to the applied stress in uniaxial tests. The lower value is more realistically related to the uppermost kilometres where the crust has been subjected to fractures (Golombek, 1985). The Poisson's ratio ν, a non dimensional constant, quantifies the volumetric distortion of a block with free lateral boundaries (Weijermars, 1997) or the change of length perpendicular to the applied stress in uniaxial test. It is equal to 0.5 for incompressible material where no volume change occurs and has values between 0.25 and 0.33 for most silicates (Twiss and Moores, 1992). Here we begin with a non-fractured and perfect elastic material with a maximum Young's Modulus of 1e11Pa and a Poisson's ratio of 0.25. The viscosity of the lithosphere is the object of the specific section 9.

Young Modulus	Poisson Ratio	Density mantle	Density crust	Gravity Mars
1e11Pa	0.25	3500	2900	3.7067

Table 2.1 Main mechanical parameters used in elastic models

3. Finite Element Modelling

To solve the question of lithosphere bending on Alba Patera, a variety of modelling parameters were performed using different techniques. Since the evaluation methods used for this thesis allow weighting individual parameters, the readers attention is turned to this methodological section. Before describing the results of the models that use various parameters, the numerical method and the exploitation of the output are illustrated.

In a long time scale, the lithosphere is supposed to respond elastically to surface loading, the underlying mantle is inviscid. The fluid mantle is modelled by vertical forces, which counteract the applied surface forces and the consequent bending of the plate (Fig. 2.2). These upward-directed hydrostatic forces $F_{(h)}$ are equivalent to the weight of the removed material [$F_{(h)}=\rho_{(mantle)}gW_{(x)}$] where $W_{(x)}$ is the displacement of the plate, and g the gravity (Turcotte and Schubert, 1982). In these models, the volcanic weight is represented by vertical pressures loading the lithosphere. These are composed of the apparent topography [$-\rho_{(solid)}gH_{(x)}$] and the part filling the depression under the edifice due to plate flexure [$-\rho_{(solid)}gW_{(x)}$]. Because the deflection is not known at the departure, the coefficients depending on the deflection W(x) [$\rho_{(mantle)}-\rho_{(solid)}$] multiplied by the surface of application is entered as Winkler coefficients and these are subtracted to the stiffness matrix in the Finite Element program TEKTON. The load is applied instantaneously (in once) since in elasticity

the principle of superposition states that the sum of displacements and stresses due to incremental forces is equivalent to the displacements and stresses of the total load. Various thicknesses of the elastic plate are tested. Modelling the elastic response of the plate under the edifice's weight gave results that display no importance whether a density within the elastic plate is included or not. The following results present the flexural displacements or stresses at the free surface where the lithostatic stresses, or hydrostatic stresses depending on the choice of equilibrium initial state, are zero.

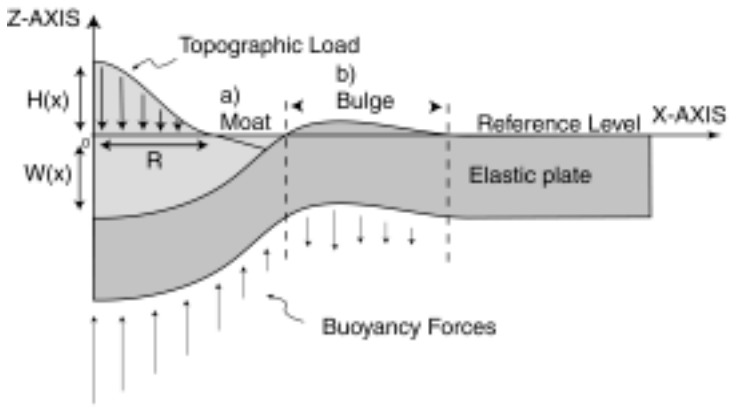

Figure 2.2 - Illustrative axisymmetric model of the lithospheric flexure due to the topography. H(x) is the apparent topography relative to the surroundings, W(x) is the deflection of the elastic plate, R the radius of the apparent surface load. The volcano is surrounded by (a) circumferential depression (moat) commonly filled by volcanic material, and (b) peripheral flexure (bulge). Buoyancy forces are exerted by the underlying fluid mantle, these depend on the gravity, vertical displacements W(x) and of the mantle density W(x)*g*ρ(mantle). Taking the density difference between mantle and crust incorporates the load in the moat filling which is W(x)*g*ρ(crust).

In axisymmetric models, only half of the model is meshed. The left side is the axis of symmetry where no horizontal slip is allowed. The right far boundary is fixed in all directions. The surface and bottom of the plate are free to move in vertical and horizontal directions. Along the x-axis, the element size is constant over a length equivalent to five times the load radius, at greater distances it increases regularly by a factor three to limit the number of nodes and thus the solution time. The total length of the plate is about 7 times the load radius to avoid boundary effects. The element size is small near the surface where the results are of importance, and increases with depth until reaching a limiting value. The elastic plate thickness was varied in individual runs to analyse its effect on deformation and stresses.

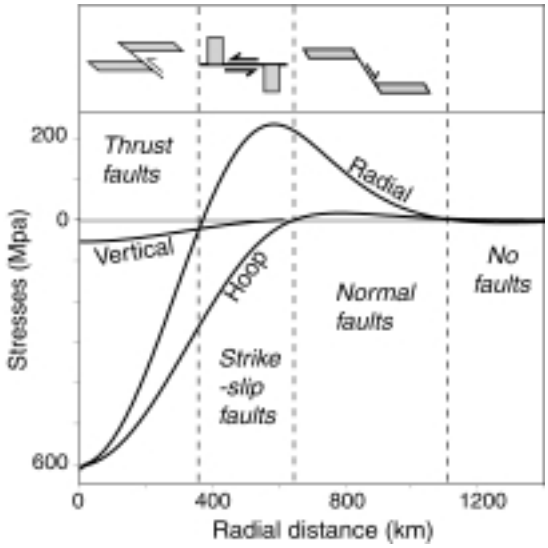

Figure 2.3 - Stresses and the corresponding type of faults using Anderson's theory (1951). Above an illustration of the faults. Strike-slip fault is illustrated horizontally on the surface while for the two other faults are shown along depth. If the vertical stress is greater than the radial and hoop stresses, thrust faults are obtained (here near the axis of symmetry). If the vertical stress has an intermediate value, then strike-slip faults could form. Thirdly, if the vertical stress is minimum, the fault would be normal (here in the volcanoes periphery). The load is 650 km radius and 5 km high, the plate is 50 km thick, the Young Modulus 1e11Pa, the Poisson ratio 0.25.

The numerical results are generally interpreted in three "themes":

- Flexure of the lithosphere
- Types and importance of stresses and their orientation,
- Regions of faulting, fault types and fault orientation.

T denotes the thickness of the elastic lithosphere. Stresses have two characteristic magnitudes. The maximum compressive stress is found at the axis of symmetry where hoop and radial stresses are equal. Note in engineering finite element programs, compressive stresses are by definition negative. At further distance, the maximum tensile (positive) stress corresponds generally to the radial stress in these models of surface loading (Fig. 2.3). The different regions of faulting predicted are determined using Anderson's theory (1951), modified to suit the convention of positive stress for extension. This states when the vertical stress is greater than the radial and hoop stresses, thrust faults form. If the vertical stress has an intermediate value, then strike-slip faults form. Third, if the vertical stress is minimum, normal faults would form. The initiation of fracturing depends on the differential stress ($\sigma 1$-$\sigma 3$) (e.g. Twiss and Moores, 1992). Thus, the difference between the maximum and minimum stresses has been calculated for the lithosphere flexure models. This gives information on the position and type of presumable failure(s), when the position of maximum stress difference is correlated to the different regions of faulting. This could also depend on the maximum tensile stress on the free surface, thus this is also indicated.

4. Plate thickness

The plate thickness on Mars beneath Alba Patera may be an important factor for its tectonic history. Determining lithosphere thickness on earth is difficult, especially the reconstruction of a thickness at a given time in Earth's history has engaged a focused scientific community (e.g. Watts 2001). For the inaccessible terrain on Mars where no ground stations are yet established, this unknown factor of the plate thickness becomes a major variable in for numerical models. This section deals with the effects of varying the elastic plate thickness which has been tested to range from 10km to 130km.

Flexure

Lithosphere flexure can be described by a wave-form. The "wavelength" is the length joining the axis of symmetry to the position of the maximum positive displacement or bulge. With increasing plate thickness, the wavelength of the flexure widens from about 700km to 1600km (Fig. 2.4). The magnitude of the deflection at the axis of symmetry decreases. This means that a volcano situated on a thick plate will cause a wide region to subside. In contrast, the bulge does not follow a regular variation. An increase of the maximum upward displacement, up to 250m at intermediate thickness of 40km, is followed by a decrease. However, larger areas around the volcano undergo upward displacement with increasing plate thickness.

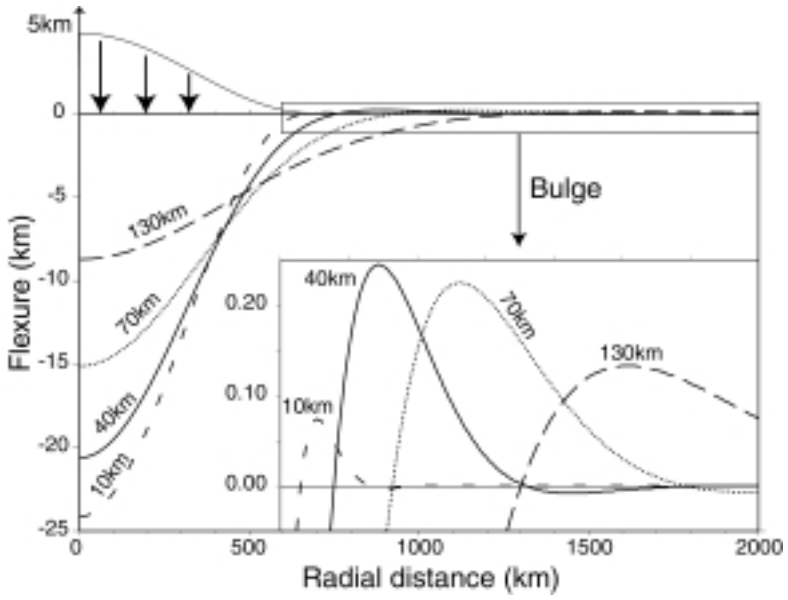

Figure 2.4 – Effects of plate thickness on displacements. By thinning the plate, the deflection increases. The maximum upward displacement augments to a maximum at an intermediate plate thickness. For a very thin plate, stretching reduces the bulge. See Fig 2.5 for stretching definition.

This irregularity observed for the magnitude of bulge is explained by considering stretching in addition to the bending deformation of a thin plate. The length of the line situated at

middle depth in the elastic plate, called neutral line, is normally constant for ideal bending deformation (Fig. 2.5). But with decreasing plate thickness, there is a contribution from stretching, i.e. elongation of the middle line. This means, a volcano situated on a thin plate causes a small region to subside, but at high subsidence rates.

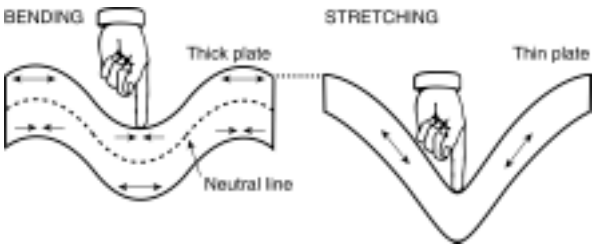

Figure 2.5 – In bending, the middle surface of the plate undergoes no change of length, neither elongation nor shortening. This gives its name of neutral surface. In contrast, in case of very thin plate, stretching occurs with elongation of the whole plate. Stretching induces tensile stress that decreases the compression observed for bending under the load.

Stresses

Due to stretching, the radial stress displays also two trends. By thickening the plate, the radial stresses, both negative and positive, increase first in absolute values until the plate is 50 or 40km thick and then decrease (Fig. 2.6). The position of maximum tension migrates outward from the base of the volcano to about 800km radial distance. The maximum compression is always at the axis of symmetry where radial and hoop stresses are equal. The tensile or positive hoop stresses are much lower than the radial stresses, it does not exceed 25MPa compared to the maximum radial stress of 250Mpa making its role relatively insignificant. The vertical stress corresponds to the applied volcanic load, being an invariant loading factor in the models, independently on the thickness of the elastic plate. The shear stress is zero at the free surface.

Figure 2.6 – Effect of plate thickness on radial and hoop stresses. Stresses first augment in absolute values until the plate is 40km thick. For thicker plates, their absolute magnitudes decrease. These results are explained by a component of stretching combined with bending for very thin plates.

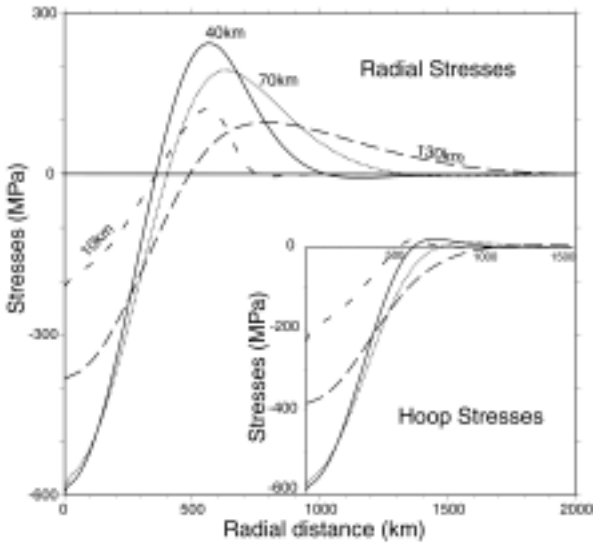

Type of faulting

The regions of faulting are illustrated in figure 2.7 for various plate thickness. According to the type of faulting, three main regions are defined. A zone of thrust faults near the axis of symmetry is surrounded on the flanks by a zone of strike-slip faults. Around the load, the type of faults is normal and concentric, radial stresses being larger than hoop stresses. All three regions widen horizontally for increasing plate thickness. At the far periphery of the load the stresses are negligible, so that no faulting should be observed. The maximum differential stress is situated at the load centre and corresponds to thrust faulting for each plate thickness. Its value increases from 180Mpa to 560Mpa from a plate thickness of 10km to 50km and then decreases down to 330Mpa for T=130 km. A second peak of differential stress is obtained at the lower flanks of the edifice. Its position is relatively localised i.e. within 500-600km compared to the maximum radial tension which moves to 790km for T=130km. Except for very thin plate, i.e. 10-20km, it is situated in the area of strike-slip faulting. Once more, there is a peak of 290Mpa at the intermediate plate thickness 50km. Regarding these first models, strike-slip faulting is thus predicted. For thicknesses less than 50km, a mixed mode could be possible with presence of normal faulting if the position of maximum radial tension is chosen as fracture criterion.

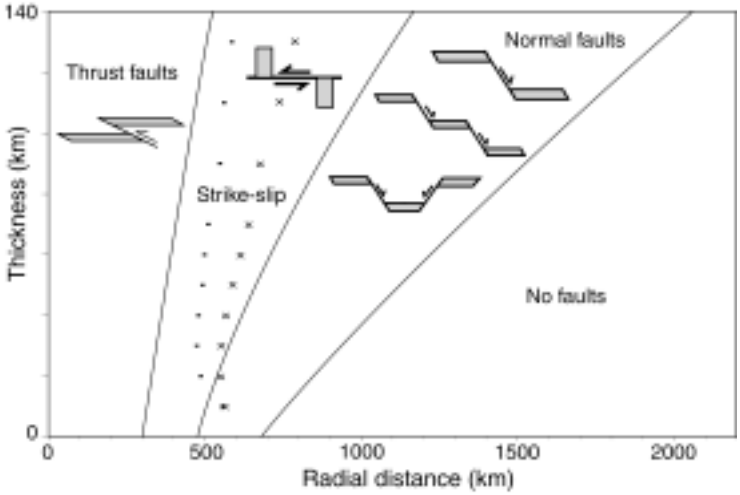

Figure 2.7 – Effect of plate thickness on faulting. The axis of symmetry is at 0 km radial distance. Squares mark the second maximum stress difference, the first being at the axis of symmetry. The cross marks the maximum radial tensile stress.

5. Size and height of the volcano

Edifice height

In this section the height of the volcanic edifice was tested, showing that this parameter is likely of minor (or no) importance for the type and position of faulting. A summary of the

finite element runs performed for various hypothetical heights of Alba Patera models is given in figure 2.8.

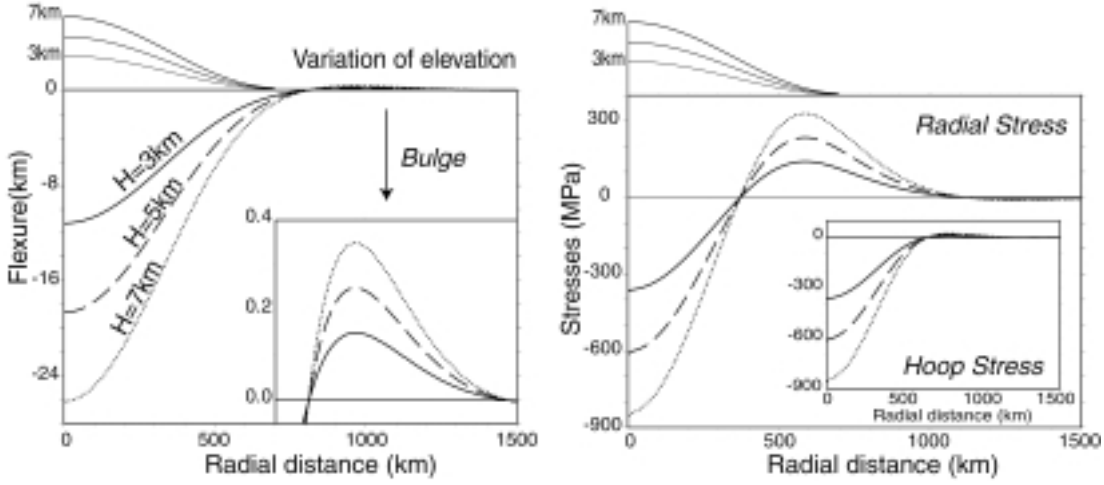

Figure 2.8 – Effect of load height on the magnitudes of flexure and stresses. The positions of the maximum displacements and stresses don't move. The radial position of the bulge is at 1000 km, the position of the second peak of stress difference at 490 km, the position of the maximum radial stress at 590 km. The maximum deflection, maximum compressive stresses and first peak of stress difference are observed at the axis of symmetry. The magnitudes of all these characteristics however decrease linearly with the height. The model has a load of 650 km radius on a 50 km thick elastic plate.

Varying the height H of the volcanic topography, tested from 3 to 7 km in interval of 2km, has, for constant volcanic radii, no effect on the positions of the maximum or minimum flexural displacements, neither on the positions of stress maxima, nor on the position of the differential stress peaks. The ranges of the different faulting and positions of likely failure are thus not modified. However, the magnitude of deflections, the bulge, and stresses decreases linearly with height (Fig. 2.8). The same is observed for different thicknesses of the elastic plate. Thus, the maximum elevation of the cone is not a significant factor for the correlation with the position of observed fractures, but is important for the magnitude of displacement and stresses. An important factor for the fault position is tested in the following sub-section.

Edifice radius

The width of Alba Patera is irregular, being almost twice as wide in E-W as in N-S. The effect of the load width is tested with the radii of 350km, 650km and 500km corresponding to the NS minimum and EW maximum radii and an intermediate width of Alba Patera. The amount of downward deflection and the wavelength of the flexure augment with the width of the load (Fig. 2.9). The peaks of maximum tensile radial stress moves at further radial distance from the volcano and its magnitude increases.

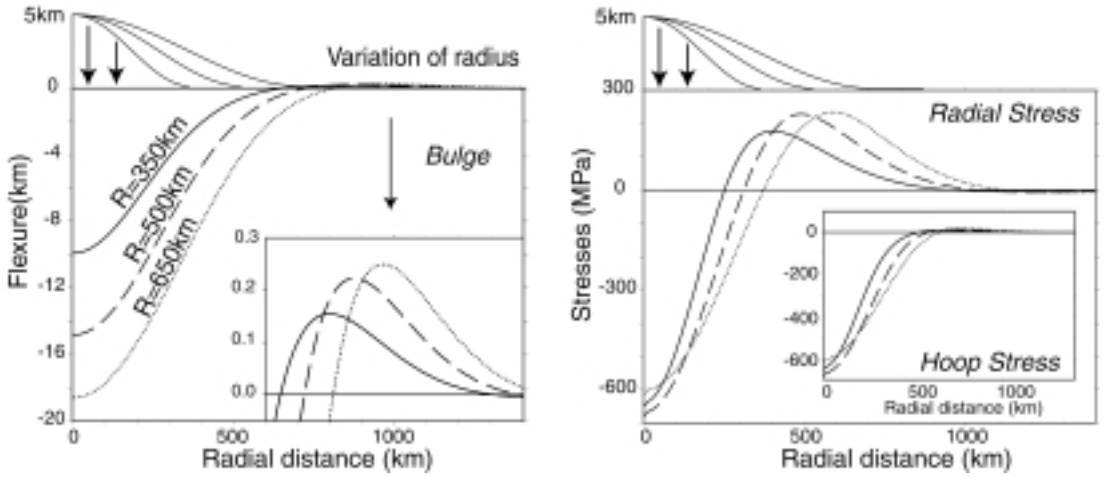

Figure 2.9 – Effect of load radius. Left: flexure; right: hoop and radial stresses. Deflection, bulge and tension are minimum for loads of small radius. Maximum upward displacements and tension are observed at the base of the volcano whatever is its radius. Compression near the axis are lower for the largest load probably by implication of stretching. The model has a 5km high load on a 50km thick plate.

The arrangement of faulting still shows a trisection of faulting for all computed models (Fig. 2.10). However, the importance of each section may vary. At first sight, increasing the load radius widens significantly the region of thrust faulting, whereas the two other regions undergo only slight changes in width. However, the normalisation with the radius of the load shows that the widths of all three zones decrease with larger radius. The wavelength of the flexure, relative to the radius, is reduced by increasing the ratio width/thickness. That means that for smaller cones, the influence of strike-slip faulting on and around the edifice increases.

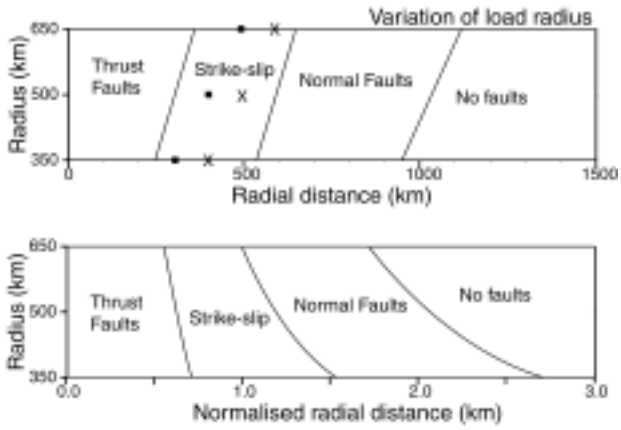

Figure 2.10 - Effect of varying load radius on the repartition of faults. Normalisation is made by dividing the radial distance by the corresponding load radius. Squares indicate the maximum stress difference or the position of possible failure. Crosses show the position of maximum tensile radial stress. The load has a 650km radius and 5km height, on a 50km thick elastic plate.

6. Poisson ratio and Young Modulus

The mechanical values are of major importance for faulting development. For this reason, models were recalculated for a variety of material parameters, spanning the proposed natural values of crustal rocks on Mars and Alba Patera.

Poisson ratio

Under the load, there is an increase of compressive radial or hoop stresses with the Poisson's ratio ν while the tensile radial stresses are similar for the three values (Fig. 2.11). For an element of Poisson's ratio around 0.5 (incompressible), there is no change of volume. When compressed vertically and free to move laterally, the horizontal length of this element would be greater.

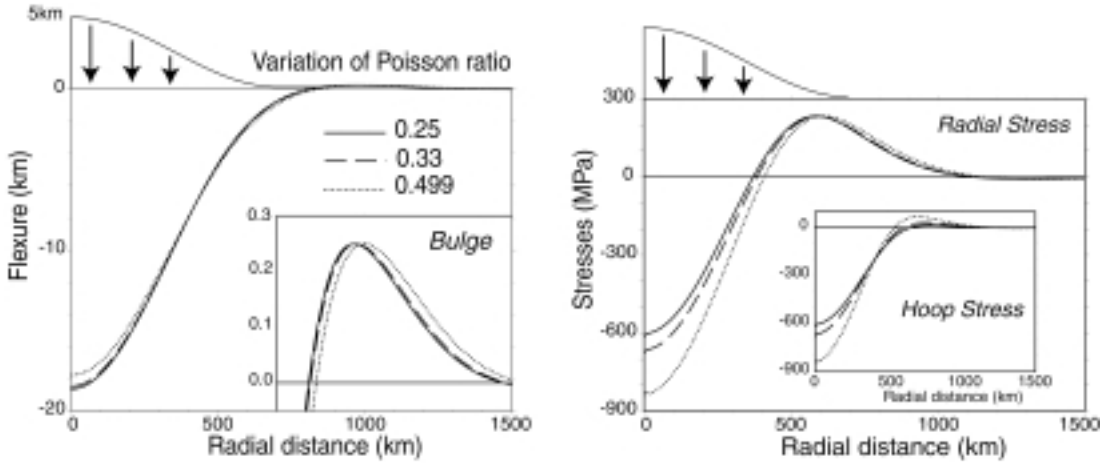

Table 2.11 Flexure and stress for various Poisson ratio. The load has 650km radius, 5km height and the plate 50km thick. The Poisson ratio has relative small effect on displacements and tensile stresses. The maximum deflection at the axis of symmetry is around -18 km for all tested values of Poisson ratio, the maximum upward displacements as well, i.e. 0.250 km.

However, because of the surrounding rocks, it can not expand, thus this element undergoes more compression. In contrast, the element can extend in radial direction outward from the volcano as indicated by the farther position of maximum radial stress. Thus, the magnitude of the radial tension doesn't differ significantly between a compressible or incompressible material. And because of outward motion, the tension in tangential direction or the hoop stress is greater and the area of strike-slip faulting shortens by 100km in favour of normal faulting for nearly incompressible material (Fig. 2.12). In this case, regarding the differential stress, normal faulting is expected for a thin plate up to 50km and strike-slip fault for thicker plates.

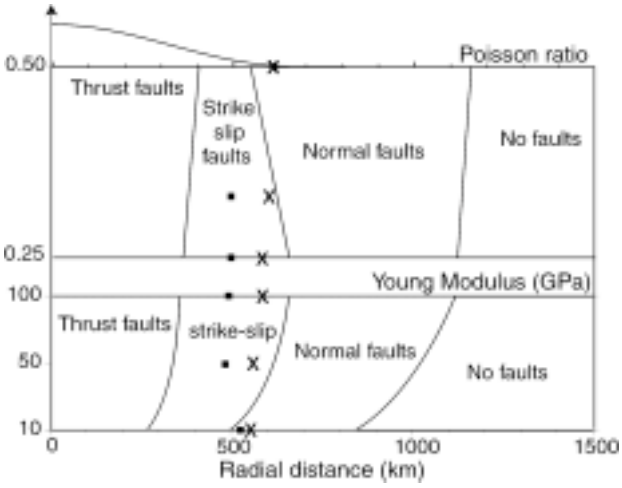

Figure 2.12 - Faulting on the surface for various Poisson ratio and Young Modulus. The squares indicate the position of maximum differential stress, the crosses the position of maximum radial stress. The importance of the strike-slip faulting region decreases for incompressible material, i.e. higher Poisson ratio or for a plate that contains a low strength upper layer, i.e. low Young Modulus. For E=10Gpa, the magnitude of differential stress peak found at the axis of symmetry becomes lower than the peak at the foot of the volcano.

Young Modulus

The presence of a crustal discontinuity between an uppermost layer of highly fractured rock and the underlying layers relatively intact of the lithosphere may considerably reduce the stresses (Golombek, 1985). In absence of seismic measurements, the depth of this possible discontinuity is hard to estimate. Based on fault dips of the Ceraunius Fossae, Plescia (1991) proposed a 2km weak upper layer. This discontinuity could also correspond to the contrast between a brittle upper crust and a more ductile underlying basement. Mège et al. (2000) used an analogy with the East Pacific Rise that has a 2-3km brittle crust.

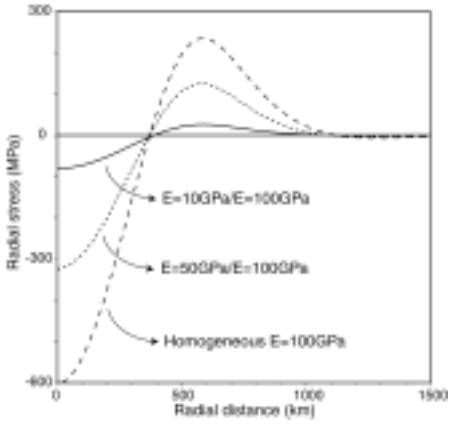

Figure 2.13 – Effect of the Young Modulus on the radial stresses. The plate is composed of an upper 2km layer of low strength, i.e. low Young Modulus that is typical of fractured material. High strength characterised the lower layer. The strength contrast reduces significantly the stresses. The load has 650km radius, 5km height and the plate 50km thick.

The effect of such low-strength surface layer has been studied. The most striking result obtained with an inhomogeneous strength within the plate is the drop of stress magnitudes, while the positions of maximum remain similar (Fig. 2.13). The tensile radial stress diminishes by an order of magnitude between an homogeneous strong plate of 100Gpa Young Modulus and a plate that contains an upper 2km thick layer of 10Gpa strength. The displacements however are not significantly modified. The maximum deflection varies by

1km between these two types of models, the magnitude of the bulge remains around 250m and translate by 30km inward. These results have only small changes by varying the depth of the discontinuity in the range of the values tested 0.5-5km or changing the lower layer from 100Gpa to 50GPa.

7. Crust and mantle densities

The ranges of crust and mantle densities found in the literature range between 2800 and extreme high values of 3500 kg/m³ (Cattermole 1992; Zuber, 2000; McGovern et al. 2001). In order to understand better the influence of the crust/lithosphere density, models are made with the densities 2800kg/m³, 2900kg/m³ and 3000kg/m³. The difference between the mantle density (3300kg/m³) and the crust density, used to calculate the buoyancy forces, varies from 500kg/m³ to 300kg/m³.

Crust density

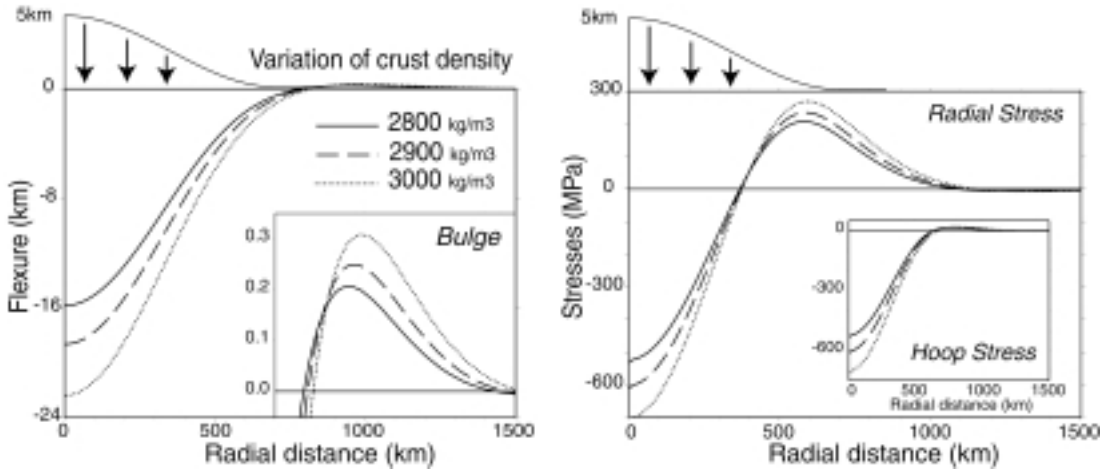

Figure 2.14 – Effect of crustal densities or the surface loading that is proportional to the crustal density. The regions of faulting do not change significantly but this parameter has most effect on the magnitude of displacements and maximum compressive and tensile radial stresses. The load has 650km radius, 5km height and the plate is 50km thick, the mantle density is fixed to 3500kg/m³.

The density of the crust was changed in individual FEM runs. Increasing the load density augments the surface load and lowers the restoring forces due to the fluid mantle. Consequently, higher are the magnitudes of maximum downward and upward displacements and the amount of maximum compressive and tensile radial stresses (Fig. 2.14). The three regions of faulting are slightly larger for a higher load density, while the position of the second maximum differential stress and the position of maximum radial stress does not

change significantly. The changes in the type of faulting due to variations of load density are of negligible importance.

Mantle density

Varying the mantle density affects only the Winkler restoring force coefficient. Increasing the mantle density or the restoring forces causes a net decrease of displacements, flexural wavelength and stresses (Fig. 2.15). It shortens slightly all the regions of faulting. But variations of +/-200kg/m³ have no striking repercussion on the type of faulting as indicated by the constant position of the 2nd maximum differential stress at about 500 km radial distance.

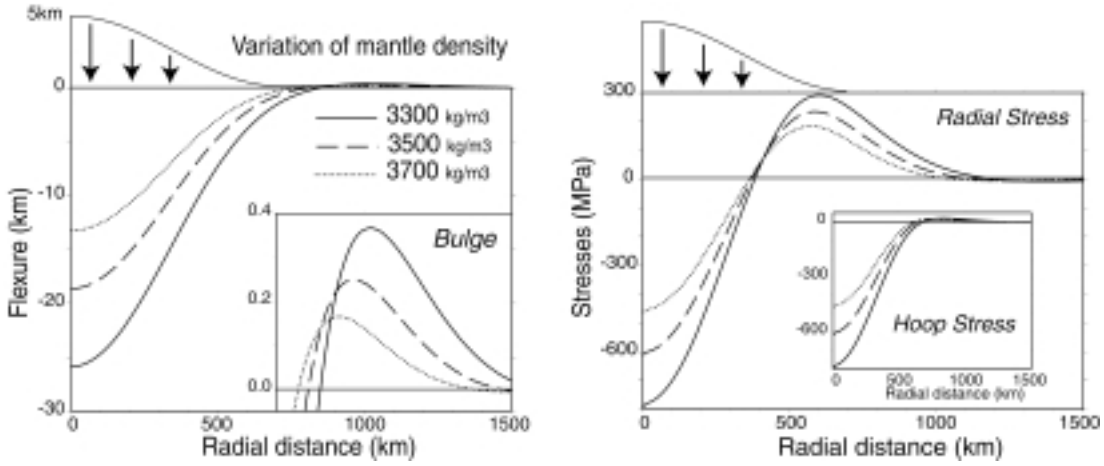

Figure 2.15 - Flexure and stresses for various densities of the mantle. This has effect on the amount of restoring forces from the buoyant mantle as it depends on the density difference between mantle and crust. The regions of faulting do not differ significantly but the magnitudes of displacements and stresses considerably decrease if the restoring forces augment with the mantle density. The density of the crust is fixed to 2900kg/m³. The load has 650km radius, 5km height and the plate is 50km thick.

8. Planet curvature

When the width of the volcano represents a significant portion of the planet circumference, the curvature of the planet must be taken into account (Fig. 2.16). In-plane forces or membrane stresses, uniform across the thickness of the shell, are added to the bending stresses (Banerdt et al, 1991). The in-plane component $\sigma\theta\theta$ is compressive everywhere while the out-plane component $\sigma\phi\phi$ is compressive under the edifice and tensile at the surrounding (Banerdt et al., 1991). σrr is the vertical stress.

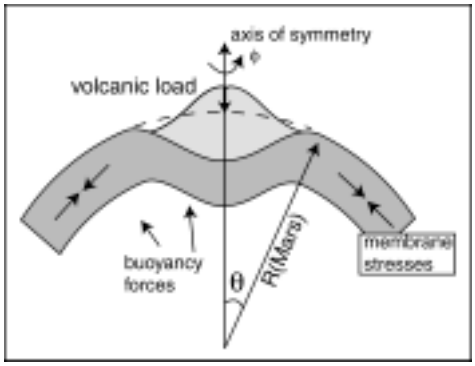

Figure 2.16 – Illustration of planet curvature. For a wide volcano, the planet curvature must be taken into account. Membrane stresses, uniform across the thickness of the shell, are added to the bending stresses. Here is represented the in-plane stress component σθθ that is compressive everywhere. The out-plane component σϕϕ, not shown here is compressive under the edifice and tensile at the surrounding.

The finite element program TEKTON provides the facility to use spherical axisymmetric elements. The nodes are positioned by their radius from the centre of the planet and the angle from the axis of symmetry (Fig. 2.16). The Winkler coefficients, used to apply restoring forces from the buoyant mantle, still depend on the density difference between the mantle (3500kg/m³) and crust (2900kg/m³). To transform pressure values to forces, these also depend on the area of application around the axis of symmetry, adapted to spherical modelling. For simplicity, the results on the free surface have been projected horizontally with x-coordinates equal to R(Mars)*θ, R being the radius of Mars, i.e. 3389.5km. The σϕϕ stress thus corresponds to the hoop stress of the flat case and the σθθ to the radial stress.

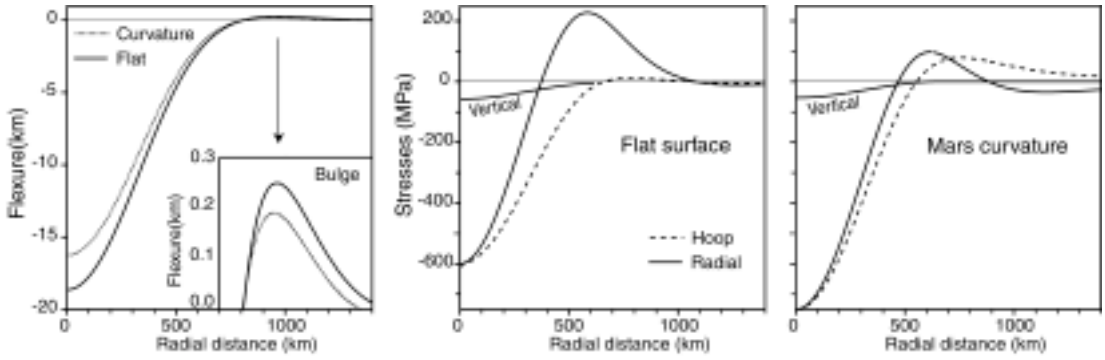

Figure 2.17 – Comparison of surface stresses between a flat plate and shell. More compression is observed with a shell. The radial stress is significantly reduced while the hoop stress augments. The load geometry is 650km radius and 5km high. The plate is 50km thick.

There are no striking modifications of displacements between the models of a plate and the models using a shell. A decrease of 2km is observed in the deflection and 50m for the upward displacements for a 50km thick plate. However, the planet curvature has significant repercussion on the tensile stress results. The radial stress is halved (hoop stress in the spherical geometry) while the positive hoop stress (out-of-plane stress) augments. The region of strike-slip faulting is now confined to a band 100km wide (300km for a plate) in favour of thrust fault and normal fault which grow toward the foot of the volcano (Fig 2.18).

A new remark is the prediction of radial normal faults around the volcano and strike-slip faulting.

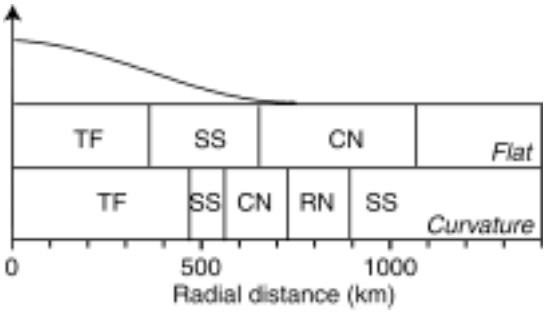

Figure 2.18 - Type of faulting on the surface induced by the flexure of either a plate or a shell under volcanic loading. With a shell, a new region of radial normal faulting is predicted at the surrounding of the volcano and the region of strike-slip fault is significantly reduced. The plate thickness is 50km, the topographic load height 5km and 650km radius. TF for thrust fault, SS for strike-slip faulting, CN concentric normal faulting, RN radial normal faulting.

The factor radius is tested for the minimum value of 350km and a 50km thick lithosphere. Though decreasing, the discrepancy, mainly in the tensile radial stresses, between the flat and curved elastic lithosphere is still significant. The maximum tensile radial stresses are 170Mpa (plate) and 90Mpa (shell) respectively. The importance of planet curvature has been also tested for various plate thicknesses. The differences between plate and shell pass from 230MPa to 140MPa and 25MPa for lithosphere 30km, 50km and 130km thick respectively or from 43% to 6% relative to the stresses on a flat plate. The planet curvature remains important for the stress field at the base of the volcano. The decrease in radial stress using a shell is between 55% (T=30km) and 70% (T=130km). The hoop stress increases from 25MPa to 85MPa for T=30km and from 5Mpa to 35MPa for T=130km. Thus, the curvature of Mars is a primordial parameter to infer the stresses due to the load of Alba Patera.

9. Viscous lithosphere

In previous models, the emplacement of the load was instantaneous, the lithosphere considered to be elastic and the mantle to be an inviscid fluid in long time scale. The focus of this section is to study the effects of two time dependent processes, load emplacement and lithospheric viscosity. The viscous relaxation within the mantle is supposed to be more rapid than the other process (Nadai, 1963; Comer et al., 1985), so that inviscid fluid, simulated by Winkler restoring forces used in previous sections, is still appropriate.

The Finite Element program TEKTON provides a library for viscoelastic elements. The initial response is elastic. At further time, the response is viscous. The method for modelling a viscoelastic response of the lithosphere overlying an inviscid fluid mantle differs little from

the initial models of elastic plate (see Fig. 2.2). The viscous material of the lithosphere is characterised by the Young Modulus 100 GPa when not otherwise specified, and by the Poisson ratio 0.25 and must be completed by the viscosity. The Finite Element estimation of viscous deformation is numerically fulfilled in several time steps, each step covering a certain number of years.

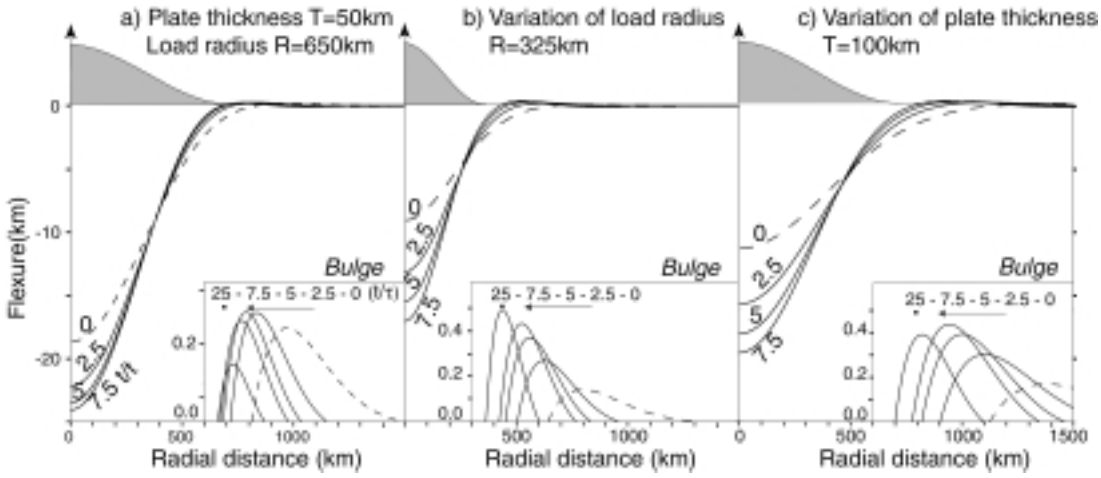

Figure 2.19 – Volcanic loading and flexure of a viscoelastic lithosphere overlying a fluid mantle. Illustrated is the amount of flexure in km versus the radial distance from the volcanoes midpoint. A volcanic load of smaller horizontal extent (b) or a thicker lithosphere (c) slow down the convergence toward isostatic compensation. The maximum deflection for local compensation is 24.1 km for a 5 km high volcano corresponding in all models to a mantle density of 3500 kg/m³ and a crust density of 2900 kg/m³. See text for definition of the Maxwell relaxation time t/τ. Note the very rapid relaxation in these models caused by such large Martian volcano on a relative thin plate. The deflection increases with time while the upward displacement passes by a maximum at intermediate time before decreasing. The bulge translates toward the base of the volcano.

Instantaneous loading models

If the load is applied instantaneously, which means that its emplacement was much more rapid than the relaxation time, the initial response is identical to the models calculated for an elastic plate overlying a fluid mantle. Thus, the initial stresses and upward displacements are in the upper range of the values found previously (section 4). With time, the magnitude of radial stresses and negative hoop stresses decrease (Fig 2.20a). Before decreasing as well, the tensile hoop stress passes by a maximum, that still remains inferior to the corresponding radial stress. The maximum downward displacement increases and the bulge migrates from the surrounding of the volcano to its lower flank (Fig 2.19a). This in accordance with a compensation toward Airy type. The maximum upward displacement displays a peak after about 4000 years for a modelled viscosity of 1e24Pa.s. Subsequently, the displacement

decreases again. The rate of the decrease for the displacements and stresses is not constant but wane with time, i.e. the variations are rapid first but diminish toward convergence.

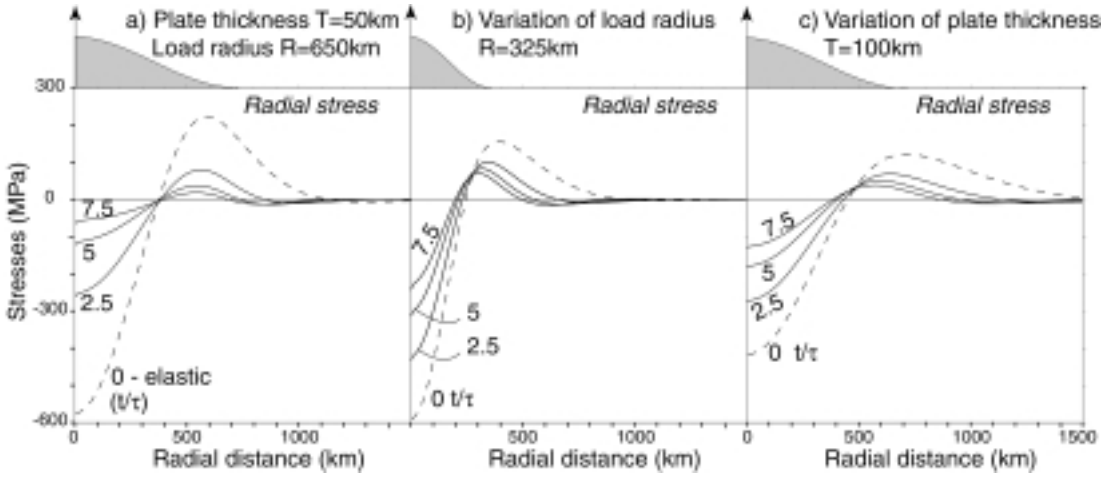

Figure 2.20 - Radial stresses of a viscoelastic lithosphere overlying an inviscid mantle subjected to volcanic loading (compare Fig 2.19). It is shown that the convergence toward isostastic compensation may slow down due to a volcanic load of smaller horizontal extent or a thicker lithosphere. The time indicated is the Maxwell relaxation time (see text for explanation). The positive hoop stresses are much lower than the radial ones and are thus not presented. The hoop stresses display the two phases observed for upward displacements with a peak at intermediate time.

The effects of the parameters viscosity, size of the load, plate thickness, emplacement of loading are explored. The “evolution” of the plate flexure toward Airy compensation has been found identical for the various values of the viscosity. But the time at which a specific value of displacement and stress is obtained augments by the same factor as the change of viscosity. The plots can be thus presented for each ratio of time to the Maxwell relaxation time. This time τ corresponds to the state when elastic strain is equal to viscous strain and depends on the viscosity, Poisson ratio and Young Modulus ($\tau=2(1+\nu)\eta/E$) (McGovern et al., 2001). For these tests, the time step was 1000, 10 000, and 100 000 years for viscosities of 1e24, 1e25 and 1e26Pa.s respectively. The processes were run for a total time increasing by the same factor, i.e. 20 Myrs, 200 Myrs and 2 byrs. The load was applied instantaneously. Secondly, plate thickness and load lateral size affect the rapidity of the convergence toward Airy isostasy (Fig 2.19 and 2.20). For identical viscosity, the compensation of a large load converges faster than for a smaller load. A thick plate slows down this convergence although the initial stresses are lower (Fig. 2.20c).

Incremental loading models

Volcanoes usually grow episodically, that means that higher feeding rates and volcano growth are followed by a less active or inactive phase, an alternating process that is recorded not only from silicic (dormant) explosive volcanoes but also from high productive sites that formed large basaltic shield volcanoes (e.g. Hawaiian Archipelago, Canary Islands, Azores) (Simkin and Siebert, 1994). To understand the influence of such incremental loads based on numerical models, the load is deposited in several units, so that a partial relaxation of older lava units is possible before the occurrence of a new magmatic episode (Fig 2.21).

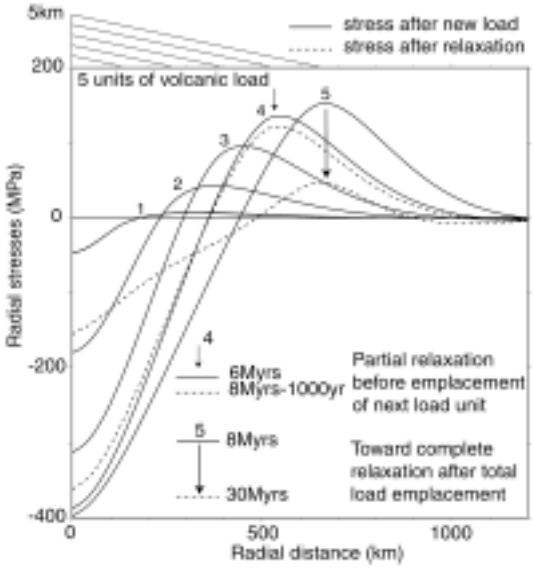

Figure 2.21 - Growing load on a viscoelastic plate. Partial relaxation of lava units is made possible before adding a new lava unit. The duration of total load emplacement, i.e. 8Myrs, is here short relative to the 0.5-1.5byrs emplacement of the main shield of Alba Patera. The viscosity has been chosen an arbitrary value of 1e25Pa.s. An increase of this viscosity by one order increases the time by the same order.

In models, the volcanic load is defined to be in the form of a cone that increases laterally and vertically with time. The vertical pressures simulating the growing cone are applied at different times using the load history factors provided by the finite element software TEKTON. The final geometry is that for a volcano of 650km radius and 5km height. If the loading is applied in 5 units, the initial geometry is 1km high and 130km half-wide. As long as the increments of pressures are applied, the stresses augment if the relaxation under the precedent loading was not complete (Fig 2.21). Once all the pressure units are applied, the flexure displays the behaviour observed for an instantaneous load with rapid subsidence and stress relaxation followed by slow convergence toward Airy compensation.

By increasing the duration of load emplacement by one order of magnitude with respect to the relaxation time, the maximum upward displacement and tensile stresses decreases significantly (Table 2.2). However the results do not significantly differ if the range of time remains in the same order. For example, the maximum radial stress has been found 39.9MPa, 36.3MPa and 35.7MPa for a duration of total load emplacement of 0.5Ga, 1Ga,

1.5Ga in 10 units and with an homogeneous strong viscoelastic plate. The growth of Alba Patera is constrained by the crater counts between 0.5-1.5Ga for the main shield (Tanaka et al., 1991). Thus, a constant intermediate duration of 1Ga has been used all along this study. Finally, the results are sensitive to the number of units as long as the total load is applied in a relative long duration. The emplacement of the load together with the lithospheric relaxation is of primary importance.

time/τ	Instant	Maxwell relaxation time τ						
		0.1	**1.**	**10.**	**100.**	**100.**	**100.**	**100**
Time	Instant	1 Ma	10 Ma	100 Ma	1 ba	1 ba	1 ba	1 ba
Number unit	5	5	5	5	5	10	20	20
Thick. (km)	50	50	50	50	50	50	50	100
Max d (m)	240	240	225	180	165	153	160	150
Position (km)	880	910	880	850	820	810	820	1100
Max σrr (MPa)	175	170	150	85	72	36	20	37
Position (km)	660	660	670	710	740	745	650	785

Table 2.2 - Maximum upward displacement dz and radial stresses σrr for various load emplacement on a viscoelastic flat plate overlying an inviscid mantle. The Maxwell relaxation time τ is equal to $2(1+\nu)\eta/E$, here the value is round-off. The Poisson ratio ν is 0.25, the Young Modulus is 100 GPa. For indication, the time is also given in years that corresponds to a viscosity of 1e25Pa.s. "Number unit" is the number of lava units, "Thick." the thickness of the plate, "Max d" is the maximum upward displacement with radial position indicated, "max σrr" is the maximum radial tensile stress with radial position indicated.

10. Support by subsurface forces

The flexural effects of volcanic loading may be decreased by upward subsurface forces. These forces occur if magma melting, i.e. underplating, ponds the crust, or by the presence of an underlying plume that upwarps the lithosphere. For simplicity, such a loading effect has been tested by adding an area of elliptic form. The process of doming the crust is primarily driven by buoyancy forces, i.e. magmatic material rising due to its lower density relative to the surrounding host rocks. In models, the "magma reservoir" is contained within the elastic plate and subjected to density decrease relative to the surrounding rock. The density contrast is prescribed to be 200kg/m^3.

Without surface loading, doming due to density decrease at depth induces tensile hoop and radial stresses above the "reservoir" with maximum at the axis of symmetry. This corresponds to upward displacement. Beyond the distal part of the reservoir, on the surface, the radial stresses are compressive while the hoop stresses tend toward zero which fits with a small downward displacement. Thus, to decrease the effect of the volcano load, the position of the negative displacements and stresses due to doming must match the area of the bulge and the tension caused by the surface loading at the foot of the volcano. Inflation from a magma reservoir of lateral size smaller than about half the volcano width and centred under the volcano is thus an unlikely process for a significant decrease of bulge and stress. In other extreme cases, forces that are applied from the axis beyond the horizontal extent of the volcano decrease the compression due to the volcano but increase the effects of surface loading at the base of the volcano because this area is now situated in the tensile part of the doming. Thus such large process are also ruled out to explain the absence of bulge and moat and the limited presence of grabens in Alba Patera's surroundings.

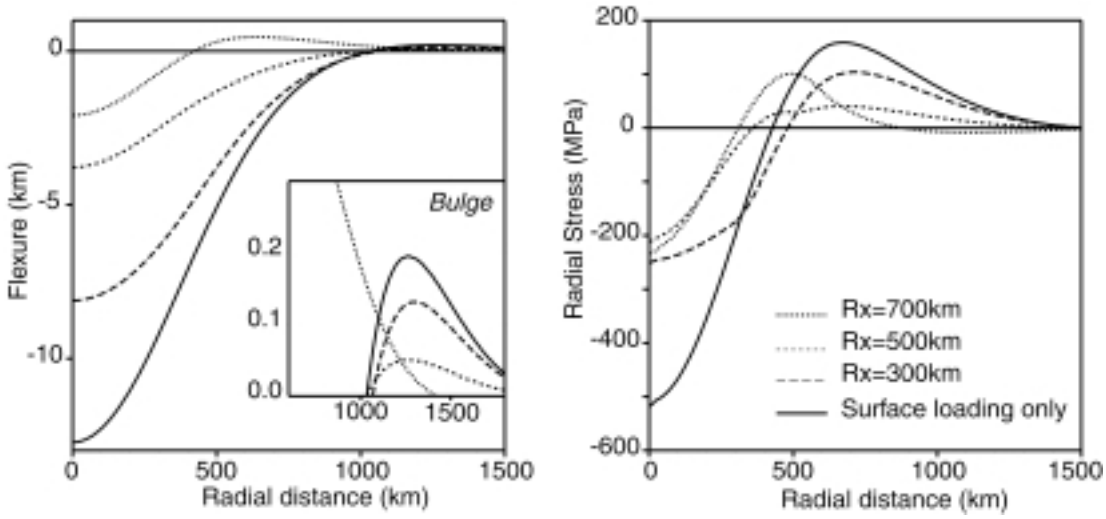

Figure 2.22 – Partial support of surface loading by upward subsurface forces. The parameters are 650km volcanic load radius, 5km load height, 90km plate thickness, 20km vertical radius of subsurface load, 10km depth to its top. The radial tension passes to 100MPa and the bulge to 140/116m with 10km z-radius and 400-600km x-radius and 10km depth from the surface to its top, the plate being 90km thick.

The area of density contrast must be broadly in the range of 300-700km horizontal radius to decrease the effect of the volcanic loading (Fig. 2.22). The best decrease has been found for example for a 500km lateral half-size of reservoir in case of a 90km thick plate. For larger x-radius, the compression near the axis doesn't drop significantly in contrast to the deflection, an increase is even observed between 700km and 500km x-radii. By increasing the x-radius while keeping the z-radius constant, the deformation due to doming tends toward a piston-

like effect with a major vertical upward displacement and little outward horizontal displacement that can not relax the compression caused by the surface loading. A 700km x-radius is not a favourable case for our study because of the high predicted bulge and the particularly low deflection that contrasts with the crustal thickening observed by gravity anomalies.

A smaller vertical radius leads to less compressive stresses to decrease the tensile stresses induced by surface loading, while doming tends to be a dominant process if the vertical radius is larger. The results are relatively insensitive to the depth of application of the area of subsurface density contrast in the range 10-130km studied, as long as the lateral sizes of the subsurface loading are much larger than the depth of its application. This has been tested in a 200km thick plate that allows to vary further the depth. The results do depend on depth for a 100km x-radius tested at 30km and 160km depth to the top but not for a 300km x-radius. Similar tests have been done with an elastic half-space, the choice of plate bottom as a free surface only subjected to restoring forces reduces the effect of the depth for a large load, so that depth can not be exactly inferred using this method.

In the case of an inhomogeneous plate with an upper layer of low strength, i.e. low Young Modulus, the stresses due to doming only are lowered while the displacements remain similar to those of an homogeneous strong plate in the same way as for surface loading (see section 6). Thus, the effects of the subsurface load relative to the surface loading do not depart from the above remarks.

11. Discussion

The main purpose of this study is to better understand the absence of moat, bulge and concentric grabens (normal faults) around Alba Patera that normally arise by plate flexure under volcano loading. The numerically determined magnitudes of the bulge and tensile stresses that may form at the foot of the edifice, and the predicted regions and types of deformations need to be considered to understand the dynamics of the volcano of Alba Patera.

The geometrical and mechanical values used in the numerical models represent the key players in the structural evolution of Alba Patera. Although geometric parameters can be prescribed accurately, the mechanical values assumed for Martian materials are quite uncertain, which may bias the interpretation of the models.

As summarised in table 2.3, the general effects of the geometric and mechanical parameters and of the Mars curvature have a complex interplay. We seek parameters that decrease the

radial stresses below the order of a few megapascals to avoid fracturing at the base of the volcano. It should be remarked that the upper crust is unable to sustain tensile stresses of the order of 200-300MPa without ejecta debris (Wilson and Mouginis-Mark, 2002). Fracturing and thus stress relaxation are supposed to occur before such magnitudes are reached. A predicted upward displacement that doesn't exceed the order of cm or dm may be a sufficient upper bound to explain absence of bulge and moat, coincident with limited coverage by filling. The most significant parameters for decreasing stresses to prevent fracturing around Alba Patera are the Young Modulus, the planet curvature and the viscosity. However, only a change of viscosity may significantly lower the flexural bulge. A combination of Young Modulus and planet curvature could explain the absence of normal faulting at the base of the volcano but not the absence of bulge and moat unless subsequent filling of the moat up to the bulge was preponderant.

Parameters	**Range parameters**	**Range bulge**	**Range radial stress**
Plate thickness	10-130km	75-250m	100-240MPa
Radius of volcano	350-650km	150-250m	180-235MPa
Height of volcano	3-7km	150-250m	140-330MPa
Poisson ratio	0.25-0.499	250m	230MPa
Young Modulus	10-100GPa *	170-250m	40-230MPa
Crust density	2800-3000 kg/m³	200-300m	210-270MPa
Density mantle	3300-3700 kg/m³	165-370m	290-180MPa
Planet curvature	T=20-130km **	80-190m	30-120MPa
Lithosphere viscosity	η =<1e25Pa.s	240-150m	20-175MPa

Table 2.3 – Variations of maximum displacements and maximum radial stresses found for the various parameters tested in this study. The underlined parameters are found to be the primary factors to explain the absence of concentric grabens at the base of the volcano. With lithosphere viscosity, the upward displacements and radial stresses, presented in this table, are the calculated maximum. In long-time scale, they converge both toward zero. Low or zero upward displacements can thus explain the absence of bulge today. When not specified, the tests are fulfilled for an intermediate plate 50km thick and the mechanical parameters of Table 2.1. (*) Young Modulus of the 2km upper layer, (**) T thickness of elastic shell.

Mechanical parameters

The viscosity of the mantle enforces a time interval between volcano growth and its isostatic compensation, as well as it regulates the type of deformation to some extent. On Earth, the volcano loading is limited by plate drift above a partially melted zone on the upper mantle, whereas on Mars loading may continue for billions of years. In absence of plate tectonics on

Mars, the formation of a volcano is fixed above the magma feeding source and thus potentially of long duration. This explains partly the great size of Martian volcanoes compared to the volcanoes on the Earth – and points up the time-dependent viscous behaviour of the lithosphere. The history of Alba Patera may have lasted as long as 2 byrs, as inferred by crater counts (Tanaka et al., 1991). The time formation for the main shield (middle member) probably spanned in the range of 0.5-1.5 byrs, to be compared to the order of <1-10 Myrs on Earth. This duration of load emplacement inferred by crater counts and the absence of grabens at the base of the volcano can give a bound on the viscosity of the lithosphere.

Due to the large size of Alba Patera, viscous processes were probably of primary importance to relax the bending stresses of the lithosphere caused by the surface loading. Indeed, for a wide volcano, the equilibrium passes more rapidly from regional flexure to Airy compensation in geological time (Fig. 2.19) (Watts, 2001). However, for understanding the presence or absence of fractures, the viscosity is not a relevant parameter if the emplacement of the whole volcanic load is rapid or instantaneous. Maximum stresses are obtained at the time of application of the entire load and do not differ from the flexural stresses of an elastic plate. Thus, the growth of the load must be also taken into account.

The plate or shell is modelled with an homogeneous viscosity which does not consider possible variations of viscosity with depth (Watts and Zhong, 2000). Thus, the values correspond to an effective viscosity. The table 2.2 presented the results for an homogeneous strong plate. An upper layer of 50Gpa and 10GPa low strength reduces the tensile stresses by about a half up to one order of magnitude respectively (section 6). The tensile stresses are also halved by considering the planet curvature (section 8). Thus, if the plate is flat, the strength must be around 10Gpa and the emplacement of the load in 20 episodes at least. Using a more likely intermediate crustal strength of 50GPa, fracturing should not occur with an effective viscosity of 1e25Pa.s at most, a load that grows in more than 20 eruptive events during 1byrs, on a shell 50km thick. If the viscosity is lowered by one order of magnitude, the total duration of load emplacement could decrease by the same order. Higher viscosity doesn't allow sufficient relaxation between load units to reduce the stresses even if the number of units is elevated. The time of load emplacement must be in such case one order higher to have similar results as for a viscosity of 1e25Pa.s which disagrees with the time span of Alba Patera's construction. Thus, constraints can be obtained for the effective viscosity and strength of the lithosphere from the absence of concentric grabens around Alba Patera, the planet curvature being a invariant parameter.

Whatever the modelled parameters, the maximum upward displacement at the periphery, i.e. the bulge, was always predicted to be on the order of hundred of meters, unless it is

supported at depth. Because Alba Patera is characterised by a low-slope angle, material filling by landslide debris can not have been a significant process on the volcano unlike on the Tharsis shields or Olympus Mons that rise up to 25km elevation (Lopes et al., 1980; Zimbelman and Edgett, 1992). A low magnitude positive displacement could be found at long-time scales when the lithospheric relaxation is complete. A significant bulge may have been present at earlier time. Owing to the protracted and early time of the volcano emplacement, lithospheric relaxation may be a significant process to reduce this topographic expression of bending. This could well compete the hypothesis of filling by lava flows to account for the absence of moat and bulge around volcanoes and may influence, for example, the estimation of magmatic flux from the amounts of extrusive lava on Venusian volcanoes (McGovern and Solomon, 1997). In contrast, high magnitude stresses at the time of the last units emplacement leaves irreversible marks such as fracturing. It's possible however that fracturing arose during the growth of the volcano and was subsequently covered by younger lava flows but the stresses after the time of the last lava unit should be low.

Geometrical and loading parameters

Size of volcano: The influence of the volcano size coupled to subsidence and graben formation is debated. Comer et al. (1985) found that during the growth of a volcano, new grabens form at greater distance from the load centre. This contrasts with the results from analogue models (Williams and Zuber, 1995), modelled by a granular load (lead shot) on an "elastic plate" (sand, gelatine and agar) overlying a viscous "mantle" (syrup). In these experiments, new grabens form nearer to the axis, though still around the simulated edifice. The first results are explained by the modelling of a growing load in three instantaneous loads which does not properly reproduce a true growing load and doesn't take into account the formation of pre-existing cracks. The analogue models indicate that pre-existing structures induced during the growth of the load can not be responsible for the concentric grabens well above on the upper and mid-flanks of Alba Patera. The next section shows that growing load has an important implication in association with the relaxation by viscous processes.

Plate thickness: Older lava units are subjected to loading by more recent units, so that the plate should appear more rigid than predicted in models using vertical pressures. The decrease of displacement for very thin plate may not occur in reality as the thickening by volcanic construction reduces the stretching. Moreover, higher tensile stresses are generally estimated for vertical pressure models in comparison to those where the whole edifice is meshed and subjected to body forces. However, the maximum difference between the two

methods has been found to be roughly 30MPa corresponding to a radial stress of 240MPa value (vertical pressure) and a plate 40km thick, while we seek parameters that induce stresses one order of magnitude lower.

In this context, the three-dimensional shape of a “plate” is a common simplified assumption. Complex relief at the base of the plate would likely be more realistic. Detailed data with adequate resolution on this hidden geometry are, however, hardly available on Earth – and fiction on Mars. Thus, the effect of an inhomogeneous plate thickness has not been demonstrated in the models provided herein. It has been shown in studies of mascon loading, i.e. volcanism associated with large impact craters, that the results are not significantly modified, as long as the lateral extent of a thinned area is much smaller than the load width (Pullan and Lambeck, 1981; Freed et al., 2002). The results are similar to those given by an intermediate plate thickness if the thinned extent is similar to the volcano width. Thus, the stresses for an inhomogeneous plate thickness remain in the order of the stresses found for a constant plate thickness.

The elastic thickness on Mars was estimated from the radial distances of concentric grabens, supposed to result from volcanic loading, or from the absence of graben around a known load (Comer et al., 1985). In this study, plate thickness is not a primary parameter to explain the absence of bulge and grabens at the base of Alba Patera, making difficult to discriminate its magnitude. Zuber et al. (2000) found that a 50km elastic plate best fits topography and gravity anomalies. McGovern et al. (2001) calculated an elastic thickness higher than 50km from flexure of surface loading and gravity data and found a higher bound of 75km with a partial support at depth.

Support: The flexure of a plate subjected to surface loading may be modified by subvolcanic processes. This has been for example seen beneath the Hawaiian Ridge where underplating exerts an upward uplift and thus decreases the downward flexure of the crust due to Hawaiian volcanoes (Watts et al., 1985). Bottom loading has been used to explain the absence of depression around volcanoes on Venus or Mars (McGovern et al, 1998). It is proposed by those workers, that the rising mantle material counteracts significant flexuring of the crust. The radial Tantalus Fossae in the north of Alba Patera indicate the presence of a hotspot (see part I). Such wide uplift of 1000km would emphasise the stresses from surface loading. This is, however, incompatible with the absence of concentric grabens around Alba Patera. Thus, it is likely that such large subsurface processes waned at the time of main shield emplacement. Moreover, the radial Tantalus Fossae that cut the more recent flanks of the main shield on Alba Patera may imply another process, i.e. either doming of an extent smaller than the volcano size or reactivation of pre-existing faults by subsidence due to the density increase of a volcanic core (see Part I). If these radial structures are the result

of doming of size equivalent or smaller than the volcano size, the forces from uplift must not drop before the stresses from surface loading have relaxed. Otherwise concentric structures would be probably observed on the lower flanks. In all cases, this must be accompanied with stress relaxation as any support probably waned with time.

Structural parameters and their implications

Absence of strike-slip faults: The types of predicted faulting comprise a region of strike-slip faulting on the lower flanks of the edifice on which the maximum differential stress and the maximum tensile radial stress are generally found. Strike-slip faulting is however not observed on Alba Patera. Two main parameters could explain this absence, in accordance with the detailed study of Freed et al. (2001) on this problem. The planet curvature diminishes the extent of this region by one third (Fig. 2.18) and the viscosity of the lithosphere allows significant relaxation of the stresses, so that they may be no longer sufficient to cause such type of faulting - the absence of grabens at further radial distance can be explained in the same way (section 9). The absence of strike-slip faulting has been predicted in other studies but also not observed (Tanaka et al., 1991; McGovern and Solomon, 1993; Williams and Zuber, 1995; Roger and Zuber, 1998). They might have been inhibited by the initial formation of tension cracks or normal cracks which were reactivated (Tanaka et al., 1991; McGovern and Solomon, 1993) when for example the volcano radius was smaller, or may also be buried by younger lava flows (McGovern and Solomon, 1993). The presence of a highly fractured upper layer 1-3km thick like the megaregolith as on the Moon, where faults may initiate, reduces significantly the prediction for strike-slip faulting (Golombek, 1985). Knowing that the minimum level for creation of strike-slip faulting is twice the stress necessary for normal fracturing (Weijermars, 1997), the absence of strike-slip faulting is in accordance with the absence or limited presence of normal faulting. Finally, Freed et al. (2001) advanced that the Anderson's theory of faulting doesn't take into account the regions of mixed mode of faulting which would lead to a region of pure strike-slip faulting half the width predicted by Anderson (1951).

Thrust faulting: Another argument in favour of significant lithospheric relaxation is the presence of the concentric grabens on the mid flanks of Alba Patera, i.e. the Alba Fossae and concentric Tantalus Fossae. It has been shown in the part I that these structures are well explained by the subsidence probably associated with the density increase of a volcanic core that has a lateral extent much less than the volcano. It has been also demonstrated that the compression due to the volcanic loading would sweep out the tensile effect of the subsidence on the mid-flanks. This suggests that the stresses due to volcanic loading were not significant at the time of graben formation. In most of the models developed in this

study, except in those using a viscous lithosphere, the magnitude of the compressive stress exceeds the magnitude of tensile stresses needed for normal faulting of the flanks. Radial ridges interpreted as wrinkle ridges are found on the summit cone. These could relate to continuing subsidence of the volcanic core (part I). Alternatively, this could be the result of the cone load because the relaxation of a short-wavelength load is less rapid than for wider load. But, if the flexural stresses due to volcanic loading must be absent at the time of flank graben formation, these can be not be responsible for the wrinkle ridges because their formation postdates most of the concentric grabens.

Catenae: Alba Patera is characterised by two sets of grabens, termed Catenae, that enclose chains of pit craters (see also Part I for map and description). On the eastern side, there are the parallel Tractus Catenae, Archeron Catenae and the Phlegeton Catenae that transect the lower and upper flanks (Fig. 1.1). On the western lower flanks, the Cyane Catenae are coupled with the Cyane Fossae. The Catenae indicate a volcanic origin that contrasts with the other grabens observed on the main shield of Alba Patera. They are mostly related to giant dike formation that source has been situated within the northern flanks of Ascraeus Mons (Tanaka and Golombek, 1989) or farther south within the Tharsis Province (Scott et al., 2002).

The Catenae on the eastern side of Alba Patera display NE-SW linear trends that do not follow the predicted volcanic loading stress field of Alba Patera. They show similarities with the structures within the neighboured region of Tempe Terra, also associated with a Tharsis dike swarm (Mège and Masson, 1996; McGovern et al., 2001; Hauber and Kronberg, 2001). The orientation of these Catenae clearly departs from the trend of the concentric grabens on the upper flanks of Alba Patera. This suggests dissimilar mechanisms and/or stress fields during their formation. Based on crosscutting relative ages, the eastern Catenae likely formed before the process of subsidence that caused the concentric grabens (part I).

Similar to the Catenae on the eastern side of Alba Patera, the Catenae on the western lower flanks of the edifice show pit craters that suggest underlying dike intrusions. However, their orientations are distinctive (as also pointed out by Scott et al., 2002). The western Catenae are confined to the lower flanks of Alba Patera and present a concentric pattern that may have been influenced by the formation of the volcano (cf. Jager et al., 2000). There is no clear cross-cutting relationship of faulting that could give a time of formation, but the Viking images show partial coverage by lava flows from the main edifice of Alba Patera. However, pit craters align north-south at 114.5°W between 36°N and 34°N (Alba Catenae), similarly oriented as grabens in prolongation to the north. These N-S grabens are cut by concentric

grabens (37.6°N/114.5°W). Assuming the similarly oriented grabens and pit chains are of similar age, and contemporaneous with the western Catenae on the lower flanks, the pit craters on the SW flank formed also prior to concentric fracturing of Alba Patera.
Dikes intrude pre-existing planes of weakness or, if driven by excess of magma pressure, they have the tendency to follow the orientation of least compressive stress (Anderson 1937). The western Catenae bear also a concentric trend, similar to the Alba Fossae on the upper flanks. Thus, it is not ruled out that subsidence of the volcanic core influenced the orientation of these regional structures.

12. Conclusion

In order to better understand the absence of bulge, moat and concentric grabens surrounding the volcano Alba Patera, load conditions and lithospheric flexure were simulated numerically. In order to get an idea about the subsurface forces within the mantle that may counteract the subsidence forces and the deformation process, the effects of support by upward subsurface forces was also explored. The variations of the parameters used for modelling show that the lithospheric viscosity together with load emplacement, the planet curvature and the Young Modulus are the primary factors that can reduce the stress magnitude below the level for fracturing around Alba Patera. Based on our knowledge of flexure, a best-fit model was scrutinised for Alba Patera, helping to better elucidate the processes involved in deforming this colossal volcano. The best fit model is found to have an effective viscosity of the lithospheric thin shell of 1e25Pa.s and an intermediate and homogeneous 50GPa strength of the elasto-viscous lithosphere. This allows stress relaxation in 1Ga, in concordance with the construction time of the main shield that ranges from 0.5-1.5byrs. Although the three primary factors significantly reduce tension at the base of the volcano, the maximum upward displacements, that characterise the bulge, were still found of the order of 100m. A bulge might have been present at earlier time but has subsequently disappeared due to lithospheric relaxation. This is favoured by the long duration and early time of the volcano's formation.

References

Anderson, E.M. (1936) The dynamics of faulting of the formation of Cone sheets, ring-dykes and cauldron-subsidence. Proceedings of the Royal Society of Edinburgh, 56, p128.

Anderson, E.M. (1951) The dynamics of faulting and dyke formation. Oliver and Boyd, Edinburgh, 206pp.

Anderson, R.C.; Dohm, J.M. (2000) Magmatic-tectonic evolution of Tharsis. Proc. Lunar. Planet. Sci. Conf. 31th, p1607.

Anderson, R.C.; Dohm, J.M.; Golombek, M.P.; Hadelmann, A.F.C.; Franklin, B.J.; Tanaka, K.L.; Lias, J.; Peer, B. (2001) Primary centres and secondary concentrations of tectonic activity through time in the western hemisphere of Mars. J. Geophys. Res. Vol106, N09, p20563-20585.

Banerdt, W.B.; Phillips, R.J.; Sleep, N.H. (1982) Thick shell tectonics on one-plate planets: application to Mars. J. Geophys. Res., 87, p9723-9733.

Banerdt. W.B.; Golombek, M.P.; Tanaka, K.L. (1992) Stress and Tectonics on Mars. In Mars, edited by Kieffer. H.H.; B.M. Jakosky.; C.W. Snyder.; Matthews, M.S.. University of Arizona Press, Tucson. p249-297.

Banerdt, W.B.; Golombek, M.P. (2000) Tectonics of the Tharsis region of Mars: insights from the MGS topography and gravity. Proc. Lunar. Planet. Sci. Conf 31th, p2038.

Banerdt, D.N.; Nimmo, F. (2002) Strength of faults on Mars from MOLA topography. Icarus, 157, 34-42.

Borgia, A.; Ferrari, L.; Pasquare, G. (1992) Importance of gravitational spreading in the tectonic and volcanic evolution of Mount Etna. Nature, 357.

Cathles, L.M. (1975) The viscosity of the Earth mantle: Princeton, Princeton University 386pp.

Cattermole, P.; Reid, C. (1984) The summit calderas of Alba Patera, Mars. Proc. Lunar. Planet. Sci. Conf. 15th, p783.

Cattermole, P. (1986) Linear volcanic features at Alba Patera, Mars – Probable spatter ridges. J. Geophys. Res., 91, B13, pE159-E165.

Cattermole, P. (1987) Sequence, rheological properties, and effusion rates of volcanic flows at Alba Patera, Mars. J. Geophys. Res., 92, B4, pE553-E560.

Cattermole, P. (1992) Mars: The Story of the Red Planet (Chapman Hall, 1992).

Cattermole, P. (1996) Planetary Volcanism. A Study of Volcanic Activity in the Solar System. 2nd Ed. New Edition Prentice Hall.

Chadwick, W.W., and J.H. Dieterich (1995) Mechanical modelling of circumferential and radial dike intrusion on Galapagos volcanoes. J. Volcanol. Geothermal Res., 66, p37-52.

Cobbold, P.R., Castro, L. (1999) Fluid pressure and effective stress in sand-box models. Tectonophysics 301:1-19.

Comer, R. P.; Solomon, S. C.; Head, J. W. (1985) Mars: Thickness of the lithosphere from the tectonic response to volcanic loads. Reviews of Geophysics, 23, p61-92.

Day, S. J.; Heleno da Silva, S. I. N. e; Fonseca, J. F. B. D. (1999) A past giant lateral collapse and present-day flank instability of Fogo, Cape Verde Islands. J. Volcanol. Geotherm. Res., 94, p191-218

Ernst, R. E.; Grosfils, E.B.; Mege, D. (2001) Giant Dyke Swarms: Earth, Venus and Mars. Ann. Rev. Earth Planet. Sci., 29, p489-534.

Fahrig, W.F. (1987) The tectonic setting of continental mafic dyke swarms: failed arm and early passive margin, in mafic dyke swarms, edited by H.C. Halls and W.F. Fahrig, Geol. Assoc. Can. Spec. Pap., 34, p331-348.

Feighner, M.A.; Richards, M.A (1994) Lithospheric structure and compensation mechanisms of the Galapagos Archipelago. J. Geophys. Res., 99, B4, p6711-6729.

Freed, A.M., Melosh, H.J. and Solomon, S.C.. (2001) Tectonics of mascon loading: resolution of the strike-slip faulting paradox. J. Geophys. Res., 106, p20602-20620.

Glen, M.G.J. and Ponce, D.A (2002) Large-scale fractures related to the inception of the Yellowstone hotspot. Geology, vol30, n7, p647-650.

Golombek, M.P. (1985) Fault type predictions from stress distributions on planetary surfaces: importance of fault initiation depth. J. Geophys. Res., 90, B4, p3065-3074.

Golombek, M.P. and Anderson, F.S; Zuber, M.T. (2001) Martian wrinkle ridge topography: Evidence for subsurface fault from MOLA. J. Geophys. Res., 106, p23811-23821.

Hall, J.L.; Solomon, S.C.; Head, J.W. (1986) Elysium Region, Mars: test of lithospheric loading models for the formation of tectonic features. J. Geophys. Res., 91, B11, p11377-11392.

Hamblin, W.K; Christiansen, E.H. (1990) Exploring the Planets. Macmillan Publishing company, New York.

Harder, H. (2000) Mantle convection and the dynamic geoid of Mars. Geophys. Res. Lett. Vol. 27 , No. 3, p. 301.

Hartmann, W. K., and Neukum, G. (2001) Cratering chronology and evolution of Mars, in Chronology and Evolution of Mars, Eds. R. Kallenbach, J. Geiss, and W. K. Hartmann. (Bern: International Space Science Institute; also Space Sci. Rev., 96), pp. 165-194.

Hauber, E; Kronberg, P. (2001) Tempe Fossae, Mars: A planetary analogue to a terrestrial continental rift. J. Geophys. Res., 106, N9, p20587.

Heller, A.; Janle, P. (2000) Lineament analysis and geophysical modelling of the Alba Patera Region on Mars. Earth, Moon and Planets, 84, p1-22.

Ivanov, M.A.; Head, J.W. (2002) Alba Patera, Mars: assessment of its evolution with MOLA and MOC data. Proc. Lunar. Planet. Sci. Conf. 33th, p1349.

Jager, K.M.; Head, J.W.; Thomson, B.; McGovern, P.J.; Solomon, S.C. (2000) Alba Patera, Mars: characterisation using Mars Orbiter Laser Altimeter (Mola) data and comparison with other volcanic edifices. Proc. Lunar. Planet. Sci. Conf. 30th, p1915.

Janes, D.M.; Melosh, H.J. (1990) Tectonics of Planetary Loading: a general model and results. J. Geophys. Res., 95, B13, p21345-21355.

Janle, P; Meissner, R. (1986) Structure and evolution of the terrestrial planets. Surveys in Geophysics, 8, p107-186.

Janle, P.; Roth, F.; Voss, J. (1984) Limits of the lithospheric thickness of the Elysium Area on Mars from correlation of surface stresses with the lineament system. Proc. Lunar. Planet. Sci. Conf. 15th, p401-402.

Janle, P.; Erkul, E. (1991) Gravity Studies of the Tharsis Area on Mars. Earth, Moon, and Planets, 53, p217-232.

Lipman, P.W. (1997) Subsidence of ash flow calderas: relation to caldera size and magma-chamber geometry. Bull. Volcanol., 59, p198-218.

Lopes, M.C., Guest, J.E., Wilson, C.J. (1980) Origin of the Olympus Mons aureole and perimeter scarp. Moon and Planets, 22, 221-234.

Marsh, B. D. (2000) Magma Chambers. Encyclopedia of Volcanoes. Academic Press, 191-206.

McBirney, A. R., and Williams, H. (1969) Geology and petrology of the Galapagos Islands, Geol. Soc. Amer. Mem., 118, p197.

McBirney,A.R. (1984) Igneous petrology, Freeman, Cooper&Co., San Fransisco.

McBirney,A.R. (1990) An historical note on the origin of calderas. J. Volcanol. Geotherm. Res., 42, 303-306.

McGovern, P.J; Solomon, S.C (1993) State of stress, faulting and eruption characteristics of large volcanoes on Mars. J. Geophys. Res., 98, 23, p23553-23579.

McGovern, P.J; Solomon, S.C (1997) Filling of flexural moats around large volacnoes on Venus: implications for volcano structure and global magmatic flux. J. Geophys. Res., 102, noE7, p16303-16318.

McGovern, P.J; Solomon, S.C (1998) Growth of large volcanoes on Venus: mechanical models and implications for structural evolution. J. Geophys. Res., 103, p11071-11101.

McGovern, P.J; Solomon, S.C; Head, J.W.; Smith, D.E.; Zuber, M.T.; Neumann, G.A. (2001) Extension and uplift at Alba Patera: insights from the MOLA observations and loading models. J.Geophys. Res. Vol106, NE10, pp.23769-23809.

McKenzie, D.; McKenzie, J.M. (1992) Dike emplacement on Venus and on Earth. J. Geophys. Res., 97, E10, p15977-15990.

Mege,D.; Masson, P. (1996) A plume tectonics model for the Tharsis province, Mars. Planetary and Space Science, 44, p1499-1546.

Mege,D. and Masson,P. (1997) An actually hot tectonic model for the Tharsis hotspot. Proc. Lunar. Planet. Sci. Conf. 28th. 1247.

Mege, D.; Lagabrielle, Y.; Garel, E.; Cormier, M.H.; Cook, A.C (2000) Collapse features and narrow grabens on Mars and Venus: dike emplacement and deflation of underlying magma chamber. Proc. Lunar. Planet. Sci. Conf. 31th, p1854.

Mege, D. and Ernst, R.E., (2001) Contractional effects of mantle plumes on Earth, Mars and Venus. In R. E. Ernst and K. L. Buchan (Eds), Mantle Plumes: Their Identification Through Time, Geol. Soc. Am. Spec. Pap. 352, 103-140.

Melosh, H.J. (1978) The tectonics of mascon loading. Proc. Lunar. Planet. Sci. Conf. 9th. P3513-3525.

Melosh, H.J. and Raefsky, A. (1983) Anelastic response of the Earth to a dip slip earthquake, J. Geophys. Res., 88, 515-526.

Montesi, J.G.J. (1999) Concentric dike swarm and internal structure of Pavonis Mons (Mars) Proc. Lunar. Planet. Sci. Conf. 30th., p1251.

Moore, J.G.; Clague, D.A.; Holcomb, R.T.; Lipman, P.W.; Normark, W.R.; Torresan, M.E. (1989) Prodigious submarine landslides on the Hawaiian Ridge. J. Geophys. Res., 94, p17465-17484.

Mouginis-Mark, P.J.; Wilson, L.; Zimbelman, J.R. (1988) Polygenic eruptions on Alba Patera. Bull. Volcanol., 50, p361-379.

Mouginis-Mark, P.J; Rowland, S.K. (2001) The geomorphology of planetary calderas. Geomorphology 37, p201-223.

Muller, O.H.; Pollard, D.D. (1977) The state of stress near Spanish Peaks, Colorado, determined from a dike pattern. Pure Appl. Geophys., 115, p69-86.

Munro, D.C.; Rowland, S.K. (1993) Structural influences on the distribution of eruptive vents on the western Galapagos. Abstract Vol. IAVCEI General Assembly (Canberra), p77.

Nadai, A. (1963) Theory of flows and Fracture in solids: New York, McGraw-Hill, 705pp.

Phillips, R.J.; Zuber, M.T.; Solomon, S.C.; Golombek, M.P.; Jakosky, B.M.; Banerdt, W.B; Williams, R.M.E.; Hynek, B.M.; Aharonson, O.; Hauck, S.A. (2001) Ancient geodynamics and global-scale hydrology on Mars, Science, 291, p2587-2591.

Plescia, J.B.; Saunders, R.S. (1982) Tectonic history of the Tharsis region, Mars. J. Geophys. Res., 87, p9775-9791.

Plescia, J.B. (1991) Graben and extension in northern Tharsis, Mars. J. Geophys. Res., 96, p18883-18895.

Pruis, M.J.; Tanaka, K.L. (1995) The Martian Northern Plains did not result from Plate Tectonics. Proc. Lunar. Planet. Sci. Conf. 26th, p1147.

Pullan, S.; Lambeck, K. (1981) Mascons and loading of the lunar lithosphere. Proc. Lunar. Planet. Sci. Conf., 12th, p853-865.

Ramberg, H. (1981) Deformation structures in theory and experiments. Geol. Soc. Sweden, 131pp.

Richards, M.A.; Duncan, R.A.; Courtillot, V.E. (1989) Flood basalt and hot track: plume heads and tails. Science, v246, p103-107.

Rogers, P.G; Zuber, M.T. (1998) Tectonic evolution of Bell Regio, Venus: regional stress, lithospheric flexure, and edifice stresses. J. Geophys. Res., 103, E7, p16841-16853.

Schneeberger, D.M; Pieri, D.C (1991) Geomorphology of Alba Patera, Mars. J. Geophys. Res., 96, B2, p1907-1930.

Schultz, R.A. (1996) Relative scale and the strength and deformability of rock masses. J. Struct. Geol., 18, p1139-1149.

Scott, D.H.; Tanaka, K.L. (1980) Mars Tharsis region: volcanotectonic events in the stratigraphic record. Proc. Lunar. Planet. Sci. Conf. 11th, p2403-2421.

Scott, D.H.; Tanaka, K.L.; Greely, R.; Guest, J.E. (1986) Geologic map of the western equatorial region of Mars, scale 1:15,000,000, U.S. Geol. Surv. Misc. Invest. Ser. Map, I-1802-A.

Scott, E.D. (2000) Sub-lithospheric 'subduction' on Mars: convective removal of a lithospheric root. II: Alba Patera. Proc. Lunar. Planet. Sci. Conf. 31th, p1329.

Scott, E.; Wilson, L.; Head, J.W. (2002) Emplacement of giant radial diskes in the northern Tharsis region of Mars. J. Geophys. Res., Vol.107, NoE4.

Simkin, T. and Siebert, L. (1994) Volcanoes of the World, 2nd edition: Geoscience Press in association with the Smithsonian Institution Global Volcanism Program, Tucson AZ, 368 pp.

Smith, R.L.; Bailey, R.A. (1968) Resurgent cauldrons. Geol. Soc. Am. Mem., 116, p83-104.

Smith, D.E.; Zuber, M.T.; Frey, H.V.; Garvin, J.B. Head, J.H.; Muhleman, D.O.; Pettengill, G.H.; Phillips, R.J.; Solomon, S.C.; Zwally, H.J.; Banerdt, W.B.; Duxbury, T.C.; Golombek, M.P.; Lemoine, F.G.; Neumann, G.A.; Rowlands, D.D.; Aharonson, O.; Ford, P.G.; Ivanov, A.B.; Johnson, C.L.; McGovern, P.J.; Abshire, J.B.; Afzal, R.S. and Sun, X. (2001) Mars Orbiter Laser Altimeter: Experiment summary after the first year of global mapping of Mars. J. Geophys. Res., Vol106, E10, p23689-23722.

Solomon, S.C.; Head, J.W. (1982) Evolution of the Tharsis province on Mars: the importance of heterogeneous lithospheric thickness and volcanic construction. J. Geophys. Res., 87, p9755-9774.

Stofan, E.R; Bindschadler, D.L; Head, J.W; MarcParmentier, E. (1991) Corona structures on Venus: model of origin. J. Geophys. Res., 96, E4, p20933-20946.

Tait, S., Wörner, G., Bogaard, P.V.D.; Schmincke, H.U. (1989) Cumulate nodules as evidence for convective fractionation in magma chambers. J. Volcanol. Geotherm. Res., 37, p21-37.

Tanaka, L.K. (1990) Tectonic history of the Alba Patera-Ceraunius Fossae region of Mars. Proc. Lunar. Planet. Sci. Conf., 20th, p515-523.

Tanaka, L.K.; Davis, P.A. (1988) Tectonic history of the Syria Planum province of Mars, J. Geophys. Res., 95, 14893-14917.

Tanaka, K. L., Davis, P.A., and Golombek, M. P. (1989) Development of grabens, tension cracks, and pits southeast of Alba Patera, Mars (expanded abstract): Abstracts for the MEVTV Workshop, Tectonic Features on Mars, Richland, Washington, April 20-21, 1989, Lunar and Planetary Institute, p. 31-33; also in MEVTV Workshop on Tectonic Features on Mars (T. R. Watters and M. P. Golombek, eds.), LPI Tech. Rep.89-06, p. 57-59, 1989.

Tanaka, K.L. and Golombek, M.P. (1989) Martian tension fractures and the formation of grabens and collapse features at Valles Marineris, Lunar. Planet. Sci. Conf., 19th, p383- 396.

Tanaka, L.K.; Golombek, M.P.; Banerdt, W.B. (1991) Reconciliation of stress and structural histories of the Tharsis region of Mars. J. Geophys. Res., 96, E1, p15617-15633.

Tanaka, L.K.; MacKinnon, D.J. (2000) Pseudokarst origin for Valles Marineris, Lunar. Planet. Sci. Conf., 31th, p1780.

Thomas, P.J.; Squyres, S.W; Carr, M.H (1990) Flanks tectonics of Martian Volcanoes. J. Geophys. Res., 95, B9, p14345-14355.

Turcotte, D.L.; Willeman, R.J.; Haxby, W.F.; Norberry, J. (1981) Role of membrane stresses in the support of planetary topography. J. Geophys. Res., 86, p3951-3959.

Turcotte, D.L., and S. Schubert, (1982): Geodynamics: application of continuum physics to geological problem. Jhon Wiley, N.Y., 450 pp.

Turtle, E.P; Melosh, H.J. (1997) Stress and Flexural Modeling of the Martian Lithopsheric Response to Alba Patera. Icarus 126, p197-211.

Twiss, R.J. and Moores, E.M. (1992) Structural Geology. W.H. Freeman and Co., 532pp.

Van Wyk de Vries, B. and Merle, O. (1996) The effect of volcanic constructs on rift fault patterns. Geology, v24, no7, p643-646.

Walker, G.P.L. (1987) The dike complex of Koolau Volcano, Oahu: Internal structure of a Hawaiian rift zone. In: R.W. Decker, T.L. Wright, and P.H. Stauffer (Editors), volcanism in Hawaii. U.S. Geological Survey Professional Paper 1350, p961-996.

Walker, G.P.L. (1992) “Coherent intrusive complexes” in large basaltic volcanoes – a new structural model. J. volcanol. Geotherm. Res., 50, p41-54.

Walter T.R. and Troll V.R. (2001) Formation of caldera periphery faults, an experimental study. Bulletin of Volcanology, 63, p191-203.

Watts, A.B.; Ten Brink, U.; Buhl, P.; Brocher, T. (1985) A multichannel seismic study of lithospheric flexure across the Hawaiian-Emperor seamount chain. Nature, v.315, pp. 105-111.

Watts, A.B. and Zhong, S. (2000) Observations of flexure and the rheology of oceanic lithosphere. Geophys. J. Int. 142, p855-875.

Watts, A.B. (2001) Isostasy and Flexure of the Lithosphere. Cambridge University Press. 472 pp.

Weijmars, R. (1997) Principles of Rock Mechanics. Alboran Science Publishing, 360pp.

Willemann, R.J.; Turcotte, D.L. (1981) Support of topographic and other loads on the moon and on the terrestrial planets. Proc. Lunar. Planet. Sci. Conf. 12th, p837-851.

Willemann, R.J.; Turcotte, D.L. (1982) The role of lithospheric stress in the support of the Tharsis rise. J. Geophys. Res., 87, 9793-9801.

Williams, H.; McBirney, A.R (1979) Volcanology. San Francisco, CA: Freeman, Cooper.

Williams, K.K; Zuber, M.T. (1995) An experimental study of incremental surface loading of an elastic plate: application to volcano tectonics. Geophys. Res. Lett., 22, No15, p1981-1984.

Wilson, L. and Mouginis-Mark, P.J. (2002a) The formation of Hrad Vallis, Mars, and its associated deposits by an explosive sill-cryoshpere interaction. Proc. Lunar. Planet. Sci. Conf. 33th, p1273.

Wilson, L.; Head, J.W. (2002) Tharsis-radial graben systems as the surface manifestation of plume-related dike intrusion complexes: Models and implications. J. Geophys. Res., 10-1029/2001 JE001593.

Wise, D.U. (1976) Faulting and stress trajectories near Alba Volcano, Northern ridge of Mars. Geol.Romana 15, p430-433.

Wise, D.U; Golombek, M.P, McGill, G.E. (1979) Tharsis province of Mars: geologic sequence, geometry and a deformation mechanism. Icarus, 38, p456-472.

Wolfe, C.J.; McNutt, M.K.; Detrick, R.S. (1994) The Marquesas archipelagic apron: seismic stratigraphy and implications for volcano growth, mass wasting and crustal underplating. J. Geophys. Res., 99, p13591-13608.

Zimbelman, J.R. and Edgett, K.S. (1992) The Tharsis Montes, Mars: Comparison of volcanic and modified landforms. Proc. Lunar. Planet. Sci. Conf., 22th, 31-44.

Zuber, M.T; Mouginis-Mark, P.J (1992) Caldera subsidence and magma chamber depth of the Olympus Mons Volcano, Mars. J. Geophys. Res.,97, p18295-18307.

Zuber, M.T.; Solomon, S.C.; Phillips, R.J.; Smith, D.E.; Tyler, G.L.; Aharonson, O.; Balmino, G.; Banerdt, W.B.; Head, J.W.; Johnson, C.L.; Lemoine, F.G.; McGovern, P.J.; Neumann, G.A.; Rowlands, D.D.; Zhong, S. (2000) Internal structure and early thermal evolution of Mars from Mars Global Surveyor topography and gravity. Science, 287, p1788-1793.

Zuber, M.T. (2001) The crust and mantle of Mars, Nature, 412, 220-227.

ACKNOWLEDGMENTS

Many thanks go to Prof. Peter Janle for initiating the project and giving me the freedom to conduct my work, for his patience and comments on this report. Warm thanks to Thomas Walter for the enthusiastic discussions, also for providing access to his laboratory and experimental set-ups and the initiation to analogue experiments. For providing promptly the mosaic of Viking images, I thank Ernst Hauber from DLR. For the computer facilities and help, I'm very grateful to Ruediger Kunze. I also thank Willy Weinrebe, Martin Kordowski and Gerd March from the computer centre of Geomar. For advice in the first and last stages of this project, thanks to Matthias Hort and Jason Morgan. I thank Axel Mohr for the introduction to the FE program NISA, Lars Rüpke, Sebastian Krastel and Matthias Haeckel. Thanks to Angelika Finke and Barbara Wolf for facilitating the literature research. I'm thankful to Peter Janle and Bernd Milkereit for financial support. My gratitude goes to Gerhard Bohrmann for giving me the opportunity to participate out of the frame of this PhD to the cruises SO144-1b/2.

Affectionate thinks and thanks for all members of the GK-cocoon: Volker Karpen for relaxing talks and the studious ambience while opening some days a lively consulting room in our office, our private and kind administrator Alexander Heuser for solving computer hard- and software problems, also for coping with the financial organisation of GK the last year, Michael Abratis for his engagement in the GK organisation for 2 years and also Alexander Schimanski, Barbara Teichert, Sandra Bollwerk, Britta Lissina, Jenny Kandiano, Richard Heath, Stefan Purkl, Sylke Hlawatsch and Christel Van den Bogaard. Un grand merci est adressé à Véro, Cathy et Guyguy pour leur soutien amical de toujours et toute ma reconnaissance à ma famille pour leur tendre affection. Merci, Thomas, pour ton soutien affectif, tes encouragements constants et ta patience.

This support was funded by the « Deutsche Forschungsgemeinschaft » through a grant in the graduate school "Dynamik global Kreisläufe im System Erde" (GRD171).